NON-CONVENTIONAL METHODS FOR ENERGY EXTRACTION FROM HIGH VOLTAGE TRANSMISSION LINES

Dan Valentin NICOLAE

Thesis submitted in fulfillment of the requirements for the degree of

DOCTORIS TECHNOLOGIAE : ELECTRICAL ENGINEERING

in the Department of Applied Electronics and Electronic
Communications, Faculty of Engineering,

VAAL UNIVERSITY OF TECHNOLOGY
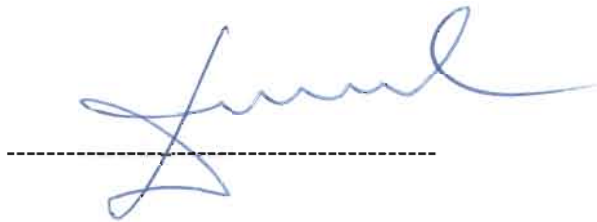
Promoter : **Prof. Dr. M.J. Case**

June 2004

DECLARATION

The thesis is the result of my own independent work, except where otherwise stated. Other sources are acknowledged by giving explicit references. A bibliography is appended.

The thesis is being submitted in fulfillment of the requirements for the degree of Doctoris Technologie Electrical Engineering in the Department of Applied Electronics and Electronic Communications, Faculty of Engineering, Vaal University of Technology. It has not been submitted before for any qualification or examination at any educational institution.

Dan Valentin NICOLAE

June 21st, 2004.

ACKNOWLEDGEMENTS

- To Prof. Dr. M.J. Case for his enormous encouragement, guidance and friendship during the past years.
- To Dr. H.J. de Jager, Dean of Engineering Faculty, for the support he gave me in this endeavour.
- To Dr. H.C. van Zyl Pienaar and the personnel of the Department of Applied Electronics and Electronic Communication for their encouragement and support.
- To Dr. J.J. Walker and the personnel of Power Systems Department for help and support.
- To Mr. J.F. Janse van Rensburg for helping me in achieving the experimental work and for his friendship.
- To all who believed in me.

DEDICATION

Like father like son

My father gave to me the enjoyment of studying

I hope, one day, my son will feel the same

ABSTRACT

A comprehensive study upon "Non-conventional methods for energy extraction from the high voltage transmission lines" was addressed in this thesis. As defined in this study, a non-conventional method to extract energy is one that does not touch the conductors of the line.

The theoretical framework which originated in the Maxwell's equations was presented as a base for discussion of all the methods and the conditions for the extraction to be possible.

This study presents various methods such as capacitive and inductive to extract energy from high voltage alternating current transmission lines (HVAC). Although in theory, for high voltage direct current transmission lines (HVDC), the conditions for extraction are not matched, there remain some methods that could still attract interest.

The centre point of this thesis is the new power application of the Rogowski coil. This method is analysed in full extent starting from theoretical modelling, computer simulations, design of the actual Rogowski coil and power electronics associated with it, and experimental results on a reduced scale model. In doing this, strong mathematical tools and computer software such Matlab 6, Quick Field and MathCAD were used.

At the end of this thesis, some conclusions are presented together with new ideas for further research in the field.

TABLE OF CONTENTS

LIST OF FIGURES

LIST OF TABLES

Glossary of abbreviations

A

ac – alternating current
a – dimension (length)

B

B – magnetic flux density
b – dimension (length)

C

CT – current transformer
C – capacitance
C_s – snubber capacitor
C_f – filter capacitor
C_p – parasite capacitor
C_c – compensation capacitor
$\mathbf{C}$ – capacitive coefficients, matrices

D

dc – direct current
$\boldsymbol{D}$ – electric flux density
D – distance
d – distance
d_1 – diameter 1
d_2 – diameter 2
δ – duty-cycle

E

$\boldsymbol{E}$ – electric field
ε – permittivity
emf – electromotive force
$\mathcal{E}$ – amplitude of emf
$\mathcal{E}$ – emf phasor
$\mathcal{E}_{rms}$ – rms value of emf

F

F – Farad

G

GMR – geometrical mean radius

H

HV – high voltage
$\boldsymbol{H}$ – magnetic field
H – Henry

I

I – current, amplitude
$\boldsymbol{I}$ – current, phasor

$\hat{I}_2$ – peak current through the switch
I_{rr} – reverse recovery current
IGBT – insulated gate bipolar transistor

J

$\boldsymbol{J}$ – current density
J – Joule

K

K_c – compensator gain
K_{vo} – static error constant

L

L – length
L_1 – inductance 1
L_2 – inductance 2
L_{in} – internal inductance
L_s – series inductance
L_r – resonant inductance
LC – inductance capacitance

M

M – mutual inductance
μ – permeability

N

N_c – number of conductors
N_t – number of turns

P

P – active power
P_e – power in electric field
P_m – power in electric field
PWM – pulse width modulation
P_d – diode power loss
P_t – transistor power loss
P_D – power dissipated
$\mathbf{P}$ – matrices of potential coefficients

Q

$\mathbf{Q}$ – matrices of charges

R

RCPA – Rogowski coil power application
ρ – specific (electric) resistivity
ρ_v – volume charge density

r_o – radius
r_1 – radius 1
r_2 – radius 2
R_s – snubber resistor
$R_{th\text{-}jc}$ – thermal resistance junction to case
$R_{th\text{-}cs}$ – thermal resistance case to sink
$R_{th\text{-}sa}$ – thermal resistance sink to air
R – resistance
$\mathcal{R}$ – ratio

S

s – Laplace operator
S – apparent power
ShW – shield wire

T

Tr. – transformer
t_f – the falling switching time of the transistor
T_j – junction temperature
T_a – ambient temperature

U

U_e – energy in electric field
U_m – energy in magnetic field

V

V – voltage, amplitude
$\boldsymbol{V}$ – voltage, phasor
$\mathbf{V}$ – potential matrices
V_d – operating voltage
V_1 – primary voltage
V_2 – secondary voltage
V_s – switched voltage
V_o – output voltage
V_r – ripple voltage

W

W – Watt

X

x – coordinate

Y

y – coordinate

Z

z – coordinate

1. INTRODUCTION

Nowadays, nobody can imagine normal life without electricity. The access to electricity has become a normal human right in modern society. Although this is recognized world-wide, there are still places where people cannot access electricity. Some reasons for this inequity in South Africa are the size of the country and the impossibility of building small economical distribution systems in remote areas.

In South Africa a problem has arisen in areas that have high voltage networks of high power rating yet do not have the population density which justifies the installation of standard power supply systems. One of the main focus areas of our government is to bring electricity to all people.

Another problem in these areas is the supply of power to the telecommunications establishments, a problem that is presently being addressed mainly by means of solar power generation. A power supply of several kW would meet many of the needs.

1.1 Preview

To provide electric power to users situated far from high population density or industrial sites such as mines, a rural grid must be constructed from an existing substation to the location of the user. Such a rural grid costs several thousand Rand per kilometre and for every doubling of the power rating the cost increases four-fold. This puts electric power out of range for many rural dwellers in southern Africa on economic grounds alone.

In many countries electric power is consumed at a great distance from the generating station. The position of the power station is dependent on an abundant source of energy (water, coal, gas, oil or nuclear) for driving the turbine. The usage of electrical energy takes place in areas in which sufficient economic activity (such as

mining, manufacturing, intensive farming, import/export of raw materials and manufactured goods) is taking place. The position of the electric power station and the place where the electric power is used, is therefore not necessarily in the same geographic location. This leads to long transmission lines of high voltage to minimize losses due to I^2R losses in the lines. These high voltage grid lines are constructed over vast distances along which major transport routes also run. The telecommunication industry has repeater stations (cells) all along these routes and relies for power for the repeaters mostly on solar panels which are expensive, have a short life span, are easily vandalized or stolen and also require periodic maintenance.

A general solution to address the problem is the use of renewable energy such as solar and wind. There are already solutions to bring electricity to the people in remote areas, based on this type of energy under research or development.

1.1.1 Requirements for small power tapping

In recent years, other solutions to address the electric energy supply in remote areas have been approached. The aim of these new energy-tapping solutions is to supply several kW output at 50 Hz 230 V from a high voltage (HV) transmission line, that would meet the needs of the repeater stations as previously stated and also unlock potential for bringing more users into the electric fold which otherwise would not be economically justifiable. These methods of connecting to the high voltage transmission line will eliminate the need for the conventional rural grid from a conventional substation to the rural user.

As presented by other authors (Ekstrom & Lamell 1991: 126, Aghaebrahimi & Menzies 1997: 1697) the requirements for a small power tapping station should be:

- The power extracted from the transmission line should be less than 10 percent of the main system (Bahrman et al 1995:1699).
- The tap must have a negligible impact on the reliability of the main transmission along either alternating current (HVAC) or direct current HVDC lines.

2

- The tap control should not interfere with the main system control, i.e. the tap control has to be strictly local (Aghaebrahimi & Menzies 1997: 1698).
- Any fault in the local ac network must not disturb the operation of the main transmission line.

1.1.2 Definition of "non-conventional method of extracting energy"

A "non-conventional method" of tapping small amounts of electric power from the high voltage transmission line, either HVAC or HVDC, according to this study has to comply with the above mentioned requirements and must not be in direct contact with the conductors of the main line. In this way of non-contact, all the above requirements are strictly achieved.

1.1.3 Current situation in the field of low power tapping

There are at present experimental capacitive coupling systems using passive series compensation in South Africa where a several kilometre long section of the overhead shield wire is insulated and used to extract power:

The first, with a power rating of 17 kVA, was built under supervision of Leigh Stubbs near ESKOM's Apollo substation on the Kendal Minerva transmission line in 1992 (Stubbs 1994: 10, 24, 31).

The second (50 kVA), using standard components, was built under supervision of Rikus Lategan in the Northern Cape a few years later (Lategan & Swart 2002: 220). The Research Institute of Hydro Quebec (I.R.E.Q.) have developed and implemented systems using capacitive coupling with varying degrees of success in Canada and in Peru.

There are also solutions to extract small amounts of power from HVDC transmission lines such as those presented by Ekstrom & Lamell (1991: 126), Aghaebrahimi &

Menzies (1997: 1697) and Bahrman et al. (1995:1699) with some of them already implemented in Canada, Brazil or Corsica with power tapped up to 50 MW.

But the majority of the abovementioned applications have a direct contact between the main lines and tapping system that create the hazard of local fault-influence.

1.2   Problem statement

The problem to be solved is the design and development of a current-to-voltage power converter as a new Rogowsky Coil Power Application (RCPA) of sufficient power rating in order to provide 230V 50Hz to a load.

1.3   Solution proposed by this research

A comprehensive study of non-conventional methods of tapping energy from high voltage transmission line will be presented.

The design and experiments of Rogowski Coil Power application to extract electric energy from a HVAC transmission line will be presented. Extraction of power from an HVAC line by means of this proposed method has previously neither been developed nor implemented. The solution consists of a Rogowski Coil of sufficient power rating inductively coupled with the transmission line; the output is pulse-width modulated in order to provide a regulated 230V 50Hz supply for a load, without any storage element.

1.4   Research fields

1.4.1   Main theme of this research ◡

The field of this research is in the general area of electrical engineering which is usually subdivided into electronic engineering, power engineering as well as, these days, computer engineering.   Power engineering is usually subdivided into two

4

fields, i.e. the provision of electrical power and the consumption of electrical power. On the provision, usually three divisions co-exist, i.e. Generation, Transmission and Distribution as shown in Figure 1.
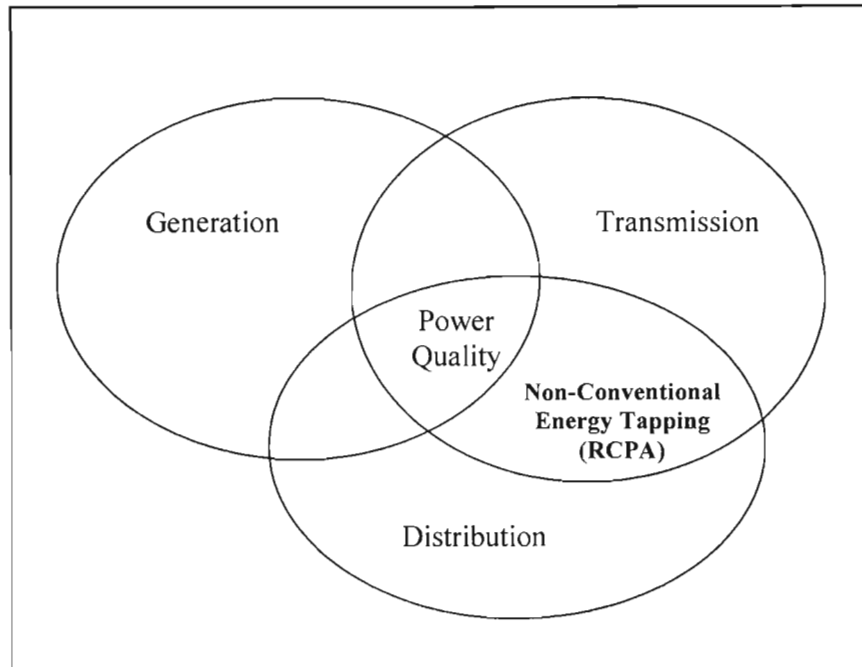
Figure 1 Position of non-conventional methods in power engineering

The RCPA system can be placed in the intersection between Transmission and Distribution since it provides a means to extract power from the transmission line, which is above 133 kV and provide it on the distribution side, which is lower than 33 kV.

Another aspect that is impacted by the application of the RCPA is its influence on the transmission line. Power quality is an aspect that has become very important in electrical engineering as a whole. The International Electrical Commission Standard IEC-555-3 and IEEE-519-1992 regulate the industry and have as an aim clean ac line currents and a power factor close to unity (Agrawal 2001: 439).

Power quality can therefore be placed at the intersection of Generation, Transmission and Distribution, since all three areas involved in the provision of electrical energy must make sure that power quality is not compromised. In a three-phase system an imbalance in the voltages will impact negatively on the power quality delivered to the clients. Since the RCPA is placed on the transmission line between the generator and the user, its effect will have to be analyzed and its impact on power quality assessed.

1.4.2 Power electronics and RCPA

Figure 2 shows the fields of power electronics addressed during the design of RCPA. The power electronics areas, having direct impact upon in the RCPA, are that of:

- AC-to-AC conversion
- Control
- Power quality
- Protection

Although many more areas can be added under power electronics in Figure 2, only those that help to illustrate the fields touched on in this research have been included.
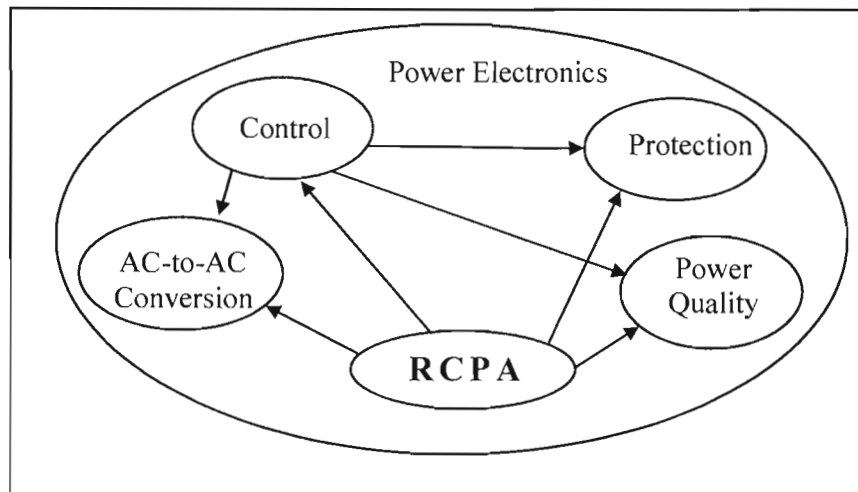
Figure 2 Power electronics and RCPA

1.4.3 Component design

Since the Rogowski Coil, as a power conversion device, is central to the successful application of the proposed solutions, the component design must also be included in the field of research.

1.5   Research method

Figure 3 shows the visual modeling of the research methods used in this study.
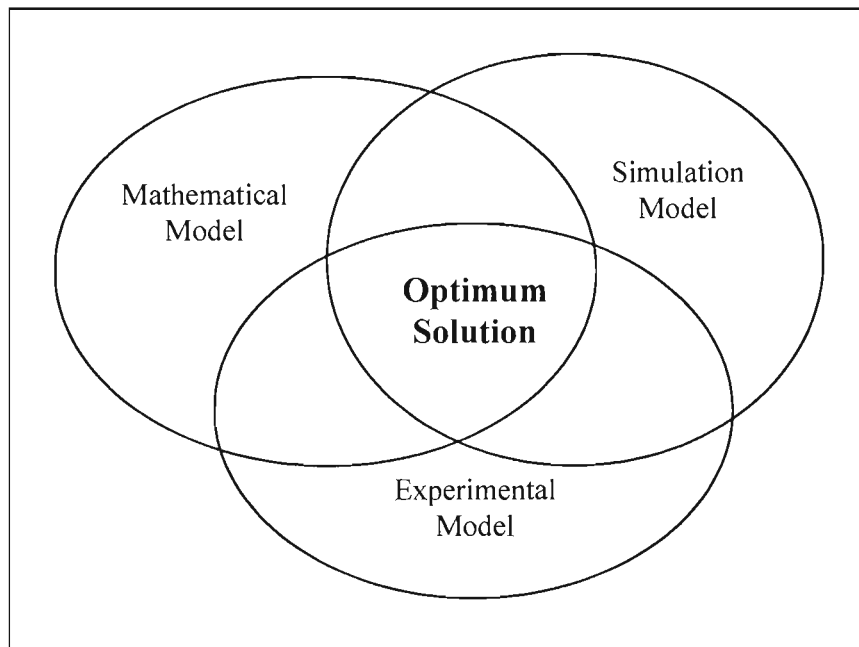
Figure 3 Illustration of research method

The research was done by setting up three models:

- At first, a comprehensive theoretical analysis of extraction concepts and a critical evaluation of the solutions were approached. A mathematical model to prove feasibility of the proposed solution was derived.

- A simulation model was then developed. Critical evaluation of the results from these two models had to show a great deal of overlap (illustrated by the intersection between the two circles representing the mathematical and

7

simulation models) before an experimental model was designed, built and tested.

- The experimental model was refined until there was acceptable correlation between the physical measurements, the simulation model and the calculations of the mathematical model.

At the intersection of the three models the optimal solution for the proposed tapping device should be found. The entire research process should be a reiterative one, that is when any step fails to give reasonable results then at least one of the previous steps must be reviewed.

Once the research has provided the optimal solution, then all work should be presented as a thesis and at least one paper presented at national and international level (Nicolae 2004).

2. THEORETICAL FRAMEWORK

The study of non-conventional methods for energy extraction from the high voltage transmission lines should start with the review of the electromagnetic theory and, especially, to find the energy stored in the electromagnetic field.

2.1 Energy stored in the electromagnetic field

In order to determine the energy stored in an electromagnetic field we have to start with Maxwell's equations. He put the existing knowledge (at that time) about electrostatics and electromagnetism in a time-varying form and had included the basic parameters of electromagnetic field (E, D, H, B, ρ and J) into a system of equations.

The **first** of Maxwell's equations is Gauss's law concerning the electric field through a closed surface and this is, in fact, a generalization of Faraday's experiments with concentric spheres: "the electric field through any closed surface is equal to total charge enclosed by that surface" (Hayt 1989: 56). In the integral form this could be written as:

$$\oint_S \boldsymbol{D} \cdot \boldsymbol{ds} = \int_{vol} \rho_v \cdot dv \tag{2.1}$$

or:

$$\int_S \boldsymbol{D} \cdot \boldsymbol{ds} = \int_{vol} \rho_v \cdot dv \tag{2.2}$$

If, using the divergence theorem (Annexure A: A.20), the surface integral from (2.1) is converted into a volume integral such as:

9

$$\int_3 \nabla \cdot \boldsymbol{D} dv = \int_3 \rho_v \cdot dv \qquad (2.3)$$

From equation (2.3), the differential form of Gauss's law that is the **first** Maxwell equation can be written:

$$\nabla \cdot \boldsymbol{D} = \rho_v \qquad (2.4)$$

The **second** Maxwell equation is that the magnetic field through any closed surface is zero (Marshall et al. 1996:183). This is also evident in the Biot-Savart law that in a differential form states that "at any point P the magnitude of the magnetic field intensity produced by a differential element (dH) is proportional to the product of the current (I), magnitude of the differential length (dL), and the sine of the angle lying between the conductor element and the line connecting it to the point P at distance r where the field is desired" (Hayt 1989: 217):

$$dH = \frac{I \cdot r}{4 \cdot \pi \cdot r^3} dL \qquad (2.5)$$

The integral expression of the magnetic flux through a closed surface can be written (Marshall et al. 1996: 183):

$$\oint_S B(r)ds = 0 \qquad (2.6)$$

The differential form of equation (2.6) is the second Maxwell equation:

$$\nabla \cdot \boldsymbol{B} = 0 \qquad (2.7)$$

The **third** Maxwell equation is a time-varying generalization of Ampere's circuital law that can be written in integral form (Hayt 1989: 320):

10

$$\oint_l HdL = I + \int_2 \frac{\partial D}{\partial t} dS \qquad (2.8)$$

The point form of the third Maxwell equation is (Hayt 1989: 319, Hoole & Hoole 1996: 313):

$$\nabla \times H = J + \frac{\partial D}{\partial t} \qquad (2.9)$$

The term $\partial D / \partial t$ has the dimensions of current density, and it exists in any region where the electric flux density D is changing in time. This term is called displacement current density.

The **fourth** Maxwell equation is, in fact, the Faraday Law that shows that a time-varying magnetic field produces an electric field (Hayt 1989: 318). In integral form this can be written:

$$\oint_l Edl = -\int_2 \frac{\partial B}{\partial t} dS \qquad (2.10)$$

And in point form:

$$\nabla \times E = -\frac{\partial B}{\partial t} \qquad (2.11)$$

Summarizing the abovementioned, it can be written:

$$\nabla \cdot D = \rho_v \qquad (2.12)$$

$$\nabla \cdot B = 0 \qquad (2.13)$$

$$\nabla \times H = J + \frac{\partial D}{\partial t} \qquad (2.14)$$

$$\nabla \times E = -\frac{\partial B}{\partial t} \tag{2.15}$$

Now, using electrostatic, magnetostatic and Maxwell's equations, the energy stored into the electric field can be written:

$$U_e = \int_3 \frac{1}{2} D \cdot E dv \tag{2.16}$$

and into the magnetic field:

$$U_m = \int_3 \frac{1}{2} B \cdot H dv \tag{2.17}$$

Poynting noticed the relation between the time derivative of energy, power and the form of Maxwell's equation (Hoole & Hoole 1996: 318). The power associated with the electric field:

$$P_e = \frac{\partial U_e}{\partial t} = \int_3 \frac{1}{2} \left(\frac{\partial D}{\partial t} E + \frac{\partial E}{\partial t} D \right) dv = \int_3 \left(\frac{\partial D}{\partial t} E \right) dv \tag{2.18}$$

and for power associated with the magnetic field:

$$P_m = \frac{\partial U_m}{\partial t} = \int_3 \frac{1}{2} \left(\frac{\partial B}{\partial t} H + \frac{\partial H}{\partial t} B \right) dv = \int_3 \left(\frac{\partial B}{\partial t} H \right) dv \tag{2.19}$$

The expressions for the power associated with electric and magnetic fields could be derived from Maxwell's equations (2.14) and (2.15). If the equation (2.15) is multiplied by H, then:

$$H \cdot \nabla \times E = -\frac{\partial B}{\partial t} H \tag{2.20}$$

12

If equation (2.14) is multiplied by E, then:

$$E \cdot \nabla \times H = E \cdot J + E \cdot \frac{\partial D}{\partial t} \qquad (2.21)$$

Subtracting equation (2.21) from (2.20), then:

$$H \cdot \nabla \times E - E \cdot \nabla \times H = -H \cdot \frac{\partial B}{\partial t} - E \cdot \frac{\partial D}{\partial t} - E \cdot J \qquad (2.22)$$

Using identity (Annexure A: A.13) for the lefthand term of the equation (2.22), it can be written:

$$\nabla \cdot (E \times H) = -H \cdot \frac{\partial B}{\partial t} - E \cdot \frac{\partial D}{\partial t} - E \cdot J \qquad (2.23)$$

The volume integral of the equation (2.23) is:

$$\int_3 \nabla \cdot (E \times H) \cdot dv = -\int_3 \left(H \cdot \frac{\partial B}{\partial t} + E \cdot \frac{\partial D}{\partial t} \right) dv - \int_3 E \cdot J dv \qquad (2.24)$$

Applying the Stokes's theorem (Annexure A: A.21) for the lefthand term and assuming that the constitutive equations $B = \mu H$ and $D = \varepsilon E$ are linear, the expression for energy conversion by Poynting can be written:

$$\int_2 (E \times H) \cdot ds = -\int_3 \left[\frac{\partial}{\partial t} \left(\frac{1}{2} \mu H^2 \right) + \frac{\partial}{\partial t} \left(\frac{1}{2} \mu H^2 \right) \right] dv - \int_3 E \cdot J dv$$

$$\int_2 (E \times H) \cdot ds = -\frac{\partial}{\partial t} \int_3 \left[\frac{1}{2} \left(\mu H^2 + \varepsilon E^2 \right) dv \right] - \int_3 E \cdot J dv \qquad (2.25)$$

Equation (2.25) represents the general expression for the electromagnetic energy/power (all terms have Watts as their unit). In the electrostatic case the energy stored in the field is $0,5 \cdot \varepsilon E^2$ ($J \cdot m^{-3}$) and in the magnetostatic case it is $0,5 \cdot \mu H^2$ ($J \cdot m^{-3}$). Therefore the first term after the equality sign is the rate of decrease (since it is $-\partial / \partial t$) of the sum of the electric and magnetic field energies. The last term represents the total energy loss in the system.

2.2 General form of power density for a transmission line

Let us consider a cylindrical conductor of radius r_o, length L and carrying a current I (Figure 4). This analysis should start from the Maxwell equation (2.15). In this particular case:

$$\frac{\partial B_\theta}{\partial t} = \frac{\mu}{2\pi r} \frac{dI}{dt} \tag{2.26}$$
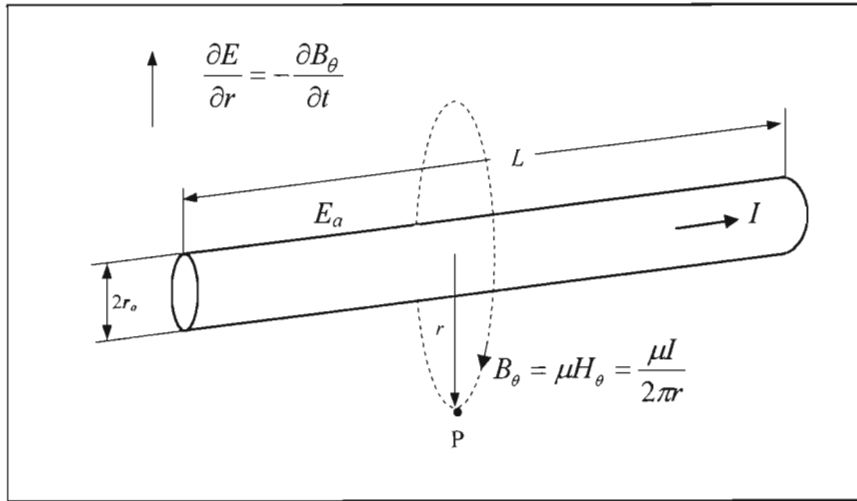
Figure 4 Interpretation of the Poynting vector for a conductor

The curl in cylindrical coordinates is:

$$\nabla \times \boldsymbol{E} = \vec{u}_r \left(\frac{1}{r} \frac{\partial E_z}{\partial \theta} - \frac{\partial E_\theta}{\partial z} \right) + \vec{u}_\theta \left(\frac{\partial E_r}{\partial z} - \frac{\partial E_z}{\partial r} \right) + \vec{u}_z \frac{1}{r} \left[\frac{\partial}{\partial r} \left(r E_\theta \right) - \frac{\partial E_r}{\partial \theta} \right] \qquad (2.27)$$

Note that for a long straight conductor (in cylindrical coordinates): $\partial / \partial \theta = 0$ and $\partial / \partial z = 0$, so that curl of $\boldsymbol{E}$ involves only $\partial / \partial r$. Substituting (2.26) into (2.15) and proceeding to integrate from the conductor surface out to r, and then the electric field is:

$$E_r = E_a + \frac{\mu}{2\pi} \cdot \frac{dI}{dt} \cdot \ln \frac{r}{r_o} \qquad (2.28)$$

where E_a is electric field along the surface of the conductor.

The energy in a length L of the conductor is stored into magnetic field and is given by:

$$U_m = \int_3 \frac{1}{2} \boldsymbol{B} \cdot \boldsymbol{H} dv \qquad (2.29)$$

If the volume element dv is replaced in cylindrical coordinates by $dz \cdot d\theta \cdot r \cdot dr$, then:

$$U_m = \frac{\mu}{2} \int_{z=0}^{L} \int_{\theta=0}^{2\pi} \int_{r=r_o}^{r} H^2 dz \cdot d\theta \cdot r \cdot dr \qquad (2.30)$$

$$U_m = \frac{\mu}{2} \left(\int_{z=0}^{L} dz \right) \left(\int_{\theta=0}^{2\pi} d\theta \right) \left[\int_{r=r_o}^{r} \left(\frac{I}{2 \cdot \pi \cdot r} \right)^2 r \cdot dr \right]$$

$$U_m = \frac{\mu I^2 L}{8\pi^2} \left(\ln \frac{r}{r_o} \right) (2\pi)$$

$$U_m = \frac{\mu I^2 L}{4\pi} \ln \frac{r}{r_o} \qquad (2.31)$$

The power associated with the magnetic field (2.19) is given by:

$$P_m = \frac{\partial}{\partial t} U_m = \frac{\mu I \cdot L}{2\pi} \left(\ln \frac{r}{r_o} \right) \frac{dI}{dt} \tag{2.32}$$

The last term from the equation (2.25) can also be evaluated:

$$\int_3 E \cdot J \cdot dv = \int_3 E_a \cdot J \cdot dv \tag{2.33}$$

If volume element dv is replaced with $dz \cdot d\theta \cdot r \cdot dr$ and the current density J with $I / \pi r_o^2$ then:

$$\int_3 E \cdot J \cdot dv = \int_{z=0}^{L} \int_{\theta=0}^{2\pi} \int_{r=0}^{r_o} E_a \left(\frac{I}{\pi r_o^2} \right) \cdot dz \cdot d\theta \cdot r \cdot dr$$

$$\int_3 E \cdot J \cdot dv = \frac{E_a I}{\pi r_o^2} \left(\int_{z=0}^{L} dz \right) \left(\int_{\theta=0}^{2\pi} d\theta \right) \left(\int_{r=0}^{r_o} r \cdot dr \right)$$

$$\int_3 E \cdot J \cdot dv = \frac{E_a I}{\pi r_o^2} (L)(2\pi) \left(\frac{r_o^2}{2} \right)$$

$$\int_3 EJdv = E_a \cdot I \cdot L \tag{2.34}$$

Now, disregard the current through the conductor and consider the potential V applied to this conductor. According to Maxwell's law (2.9), when the conductor has a variable potential V, then a displacement current appears:

$$J_d = \varepsilon \frac{\partial E}{\partial t} \tag{2.35}$$

For a brief look into this matter, consider a transmission voltage being applied between the line and the ground and h the distance between line and ground that is much greater than the radius of the conductor. At a specific moment, the electrostatic situation can be considered as:

$$V = \int_{r=r_o}^{r=h} \frac{q}{2\pi\varepsilon_0 r} dr \tag{2.36}$$

where q is the charge density per length.

$$V = \frac{q}{2\pi\varepsilon_0} \ln \frac{h}{r_o} \tag{2.37}$$

The electric field at point P situated at distance r from the conductor is given by:

$$E = \frac{q}{2\pi r} \tag{2.38}$$

Taking q from equation (2.37) and substituting into (2.38), the expression for the field can be written as:

$$E = \frac{\varepsilon_0 V}{2r \ln (h/r_o)} \tag{2.39}$$

According to equation (2.25), the term $0{,}5 \cdot \varepsilon E^2$ ($J \cdot m^{-3}$) is the energy stored in the electric field and:

$$P_e = -\frac{\partial}{\partial t} \int_3 0{,}5 \cdot \varepsilon_0 \cdot E^2 dv \tag{2.40}$$

In this situation there is a cylindrical symmetry and the volume element dv can be replaced with $dz \cdot d\theta \cdot r \cdot dr$.

$$P_e = -\frac{\partial}{\partial t} \int_{z=0}^{z=L} \int_{\theta=0}^{\theta=2\pi} \int_{r=r_o}^{r=h} 0,5 \cdot \varepsilon_0 \cdot \left(\frac{\varepsilon_0 V}{2r \ln(h/r_o)} \right)^2 dz \cdot d\theta \cdot r \cdot dr \qquad (2.41)$$

$$P_e = -\frac{\partial}{\partial t} \left[\left(\int_{z=0}^{L} dz \right) \left(\int_{\theta=0}^{2\pi} d\theta \right) \left[\int_{r=r_o}^{h} \left(\frac{\varepsilon_0^3 \cdot V^2}{8 \cdot r^2 \cdot \ln^2(h/r_o)} \right) r \cdot dr \right] \right]$$

$$P_e = -\frac{\partial}{\partial t} \left[L \cdot 2\pi \cdot \frac{\varepsilon_0^3 \cdot V^2}{8 \cdot \ln^2(h/r_o)} \int_{r=r_o}^{h} \frac{dr}{r} \right]$$

$$P_e = -\frac{\pi \cdot \varepsilon_0^3 \cdot L \cdot V}{2 \cdot \ln(h/r_o)} \cdot \frac{dV}{dt} \qquad (2.42)$$

2.3   Non-conventional methods for energy extraction from HV transmission lines

A non-conventional method for extracting energy from an HV transmission line as defined in this study is such that the transmission line is not in direct contact with the tapping device (see paragraph 1.1.2), which means capacitive or inductive coupling.

As presented in paragraph 2.2 and in equations 2.16 and 2.17, there is energy stored in an electromagnetic field. But to extract power from the electromagnetic field of the transmission line, equations (2.32) and (2.42) should be non-zero; in other words it is possible to tap energy when there is a variation of current or voltage. The conclusion is that it is possible to extract energy from HVAC transmission lines.

The methods of tapping power from HVAC transmission lines could be classified into capacitive and inductive coupling.

The capacitive coupling methods that will be discussed in Chapter 3 are:
- Resonant methods.
- Non-resonant methods.

The inductive coupling methods that will be presented in Chapter 4 are:
- Current transformer tapping.
- Rogowski coil power application.

Although, by definition the high voltage direct current does not have any cyclic variation in voltage or current, some methods to tap energy from the HVDC transmission line will still be proposed and discussed in Chapter 5. They are:
- Capacitance modulation methods.
- Inductive methods.
- Resonant methods.

3. HVAC CAPACITIVE COUPLING METHODS

Any capacitive coupling method of tapping energy (CAPTAP) from high voltage transmission lines is based on the capacitance created between the conductors of the line and an auxiliary (shield) wire parallel with the line. Therefore, the analysis of HVAC capacitive coupling methods must start with determination of the coupling capacitance.

3.1   Coupling capacitance

3.1.1   Capacitance of a two-wire system

Figure 5 shows a two-wire system with conductors each having a different radius. The assumption of uniform charge density along the conductors is considered.
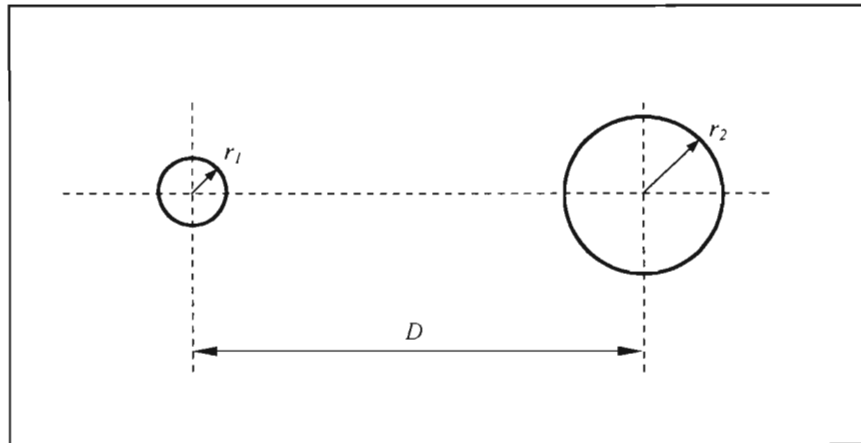
Figure 5 Two-wire capacitance system

The capacitance of this system (Hallen 1962:55) is:

$$C = \frac{2 \cdot \pi \cdot \varepsilon_o}{\ln\left(\gamma + \sqrt{\gamma^2 - 1}\right)} \quad \text{F·m}^{-1} \tag{3.1}$$

where:

$$\gamma = \frac{D^2 - r_1^2 - r_2^2}{2 \cdot r_1 \cdot r_2} \tag{3.2}$$

When $D \gg r_1 \cdot r_2$ equation (3.2) can be simplified (Grainger & Stevenson 1994:175) as:

$$C = \frac{2 \cdot \pi \cdot \varepsilon_0}{\ln\left(\frac{D^2}{r_1 \cdot r_2}\right)} \quad \text{F·m}^{-1} \tag{3.3}$$

But the influence of the earth should also be taken in consideration. Figure 6 shows a two-wire system in presence of earth; the image method is considered.

D_{12} = the distance between the two conductors

H_{11} = the distance on vertical between the first conductor and its image

H_{22} = the distance on vertical between the second conductor and its image

H_{12} = the distance on vertical between the first conductor and the image of the second one

H_{21} = the distance on vertical between the second conductor and the image of the first one
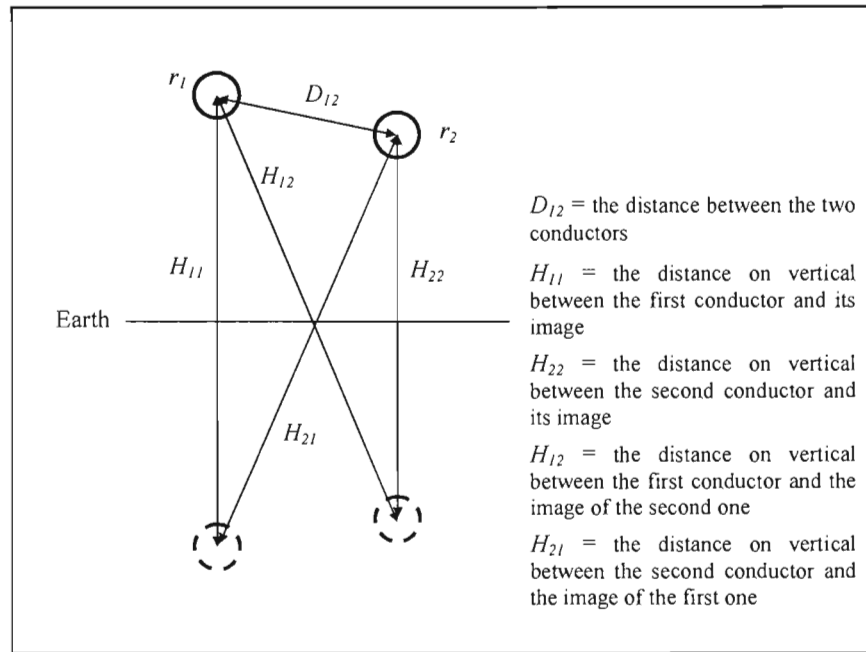
Figure 6 Earth influence on two-wire capacitance system

In this situation, the capacitance of the system could be written (Hallen 1962:55) as:

$$\frac{1}{C} = \frac{\ln\left(H_{11}/r_1\right)}{2\cdot\pi\cdot\varepsilon_0} + \frac{\ln\left(H_{22}/r_{12}\right)}{2\cdot\pi\cdot\varepsilon_0} - 2\frac{\ln\left(H_{12}/D_{12}\right)}{2\cdot\pi\cdot\varepsilon_0} \tag{3.4}$$

$$C = \frac{2\cdot\pi\cdot\varepsilon_0}{\ln\left(\dfrac{D_{12}^2}{r_1\cdot r_2}\cdot\dfrac{H_{11}\cdot H_{22}}{H_{12}^2}\right)} \quad \text{F·m}^{-1} \tag{3.5}$$

When the earth is far enough from the two-wire system, then equation (3.5) becomes the same as equation (3.3).

3.1.2 Capacitance of a multi-wire system

In practice, the system has more than two wires. Therefore, a multi-wire system of N_c conductors presented in the Figure 7 should be considered.
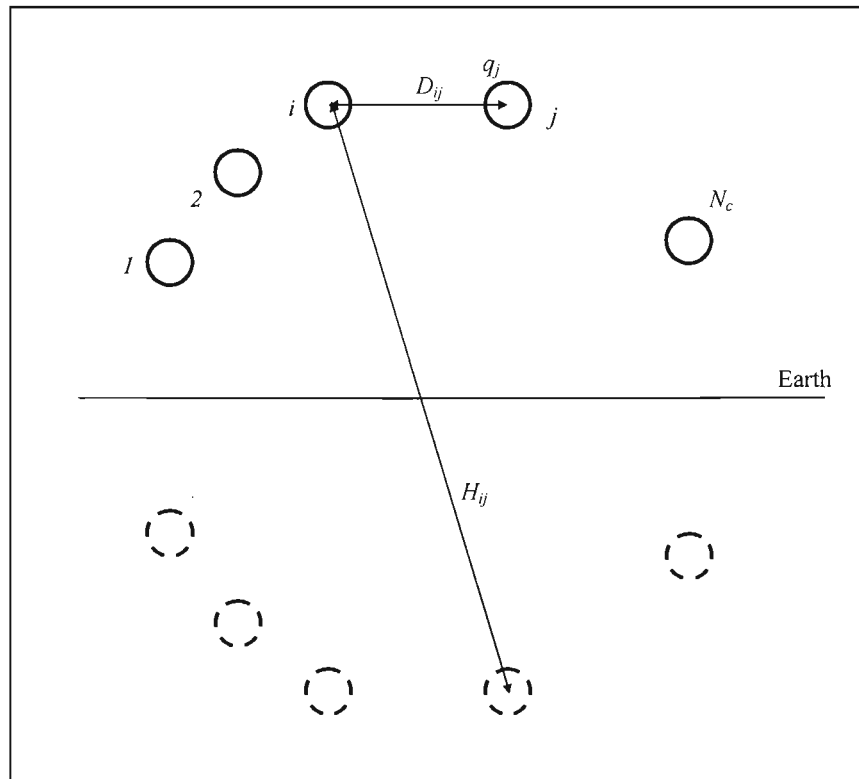
Figure 7 Multi-wire capacitance system

Assuming that each conductor j has an ac charge q_j ($C \cdot m^{-1}$) uniformly distributed along the conductor, then the voltage V_i between i^{th} conductor and earth due to all charges q_j in the system is:

$$V_i = \frac{1}{2 \cdot \pi \cdot \varepsilon_0} \sum_{j=1}^{N_c} q_j \ln \frac{D_{ij}}{H_{ij}}$$
(3.6)

where:

D_{ij} = the distance between conductors i and j
H_{ij} = the distance between conductor i and the image of conductor j

Equation (3.6) can be written in matrix format:

$$
\begin{bmatrix} V_1 \\ V_2 \\ \vdots \\ V_i \\ \vdots \\ V_{N_c} \end{bmatrix}
=
\begin{bmatrix}
p_{11} & p_{12} & \cdots & p_{1j} & \cdots & p_{1N_c} \\
p_{21} & p_{22} & & & & p_{2N_c} \\
\vdots & & \ddots & & & \vdots \\
p_{i1} & p_{i2} & & p_{ij} & & p_{iN_c} \\
\vdots & & & & \ddots & \vdots \\
p_{N_c1} & p_{N_c2} & \cdots & p_{N_cj} & \cdots & p_{N_cN_c}
\end{bmatrix}
\cdot
\begin{bmatrix} q_1 \\ q_2 \\ \vdots \\ q_i \\ \vdots \\ q_{N_c} \end{bmatrix}
$$
(3.7)

$\quad\quad$ **V** $\quad\quad\quad\quad\quad\quad\quad\quad$ **P** $\quad\quad\quad\quad\quad\quad$ **Q**

or:

V = P·Q
(3.8)

where $p_{ij} = q_{ij} \ln(D_{ij}/H_{ij})$ are potential coefficients.

The system could also be described by the following:

$$
\begin{cases}
q_1 = c_{11}V_1 + c_{12}V_2 + \cdots + c_{1N_c}V_{N_c} \\
q_2 = c_{21}V_1 + c_{22}V_2 + \cdots + c_{2N_c}V_{N_c} \\
\vdots \\
q_{N_c} = c_{N_c 1}V_1 + c_{N_c 2}V_2 + \cdots + c_{N_c N_c}V_{N_c}
\end{cases}
\tag{3.9}
$$

In the matrix format the system can be written as:

$$
\underbrace{\begin{bmatrix} q_1 \\ q_2 \\ \vdots \\ q_i \\ \vdots \\ q_{N_c} \end{bmatrix}}_{\mathbf{Q}}
=
\underbrace{\begin{bmatrix}
c_{11} & c_{12} & \cdots & c_{1j} & \cdots & c_{1N_c} \\
c_{21} & c_{22} & & & & c_{2N_c} \\
\vdots & & \ddots & & & \vdots \\
c_{i1} & c_{i2} & \cdots & c_{ij} & \cdots & c_{iN_c} \\
\vdots & & & & \ddots & \vdots \\
c_{N_c 1} & c_{N_c 2} & \cdots & c_{N_c j} & \cdots & c_{N_c N_c}
\end{bmatrix}}_{\mathbf{C}}
\cdot
\underbrace{\begin{bmatrix} V_1 \\ V_2 \\ \vdots \\ V_i \\ \vdots \\ V_{N_c} \end{bmatrix}}_{\mathbf{V}}
\tag{3.10}
$$

or:

$$
\mathbf{Q} = \mathbf{C \cdot V}
\tag{3.11}
$$

The coefficients c_{ij} are purely geometrical quantities, depending on the size, shape, orientation and position of each conductor. The c_{ii} is called coefficient of capacitance and c_{ij} *(i≠j)* is called coefficient of electrostatic induction.

An interpretation of the last system of equations may be undertaken with reference to the first of these equations. The total charge q_1 has a component $c_{11}V_1$ that may be attributed to a capacitance c_{11} between the first conductor and ground, since V_1 is the potential to ground. Additionally, there is a charge $c_{12}V_2$ residing on the first conductor, which may be attributed to a capacitance c_{12} between the first and the second conductor, and electrostatic induced due to V_2.

Thus the entire set of (the last) equations may be interpreted in terms of capacitance c_{ii} between the ith conductor and ground, and c_{ij} between the ith conductor and each other conductor in the system. These capacitances are purely geometrical quantities.

An example of the calculation of the multi-wire system applied for shield-wire source parameters was presented by Gururaj and Nandagopal in 1970. At that time, the method made use of graphs and it may have been useful in times when computing capabilities to the designer as they are now, were not available. Now, at I.R.E.Q. Canada, there is software to calculate such parameters (Bolduc 2002).

In brief, the voltage induced in the shield wire is greatly influenced by the position of it in relation to the phase conductors. The diameter of the shield wire has a great influence upon the equivalent source impedance.

An example of multi-wire/capacitance system using an isolated shield wire is presented in the Figure 8. Using this system a power of 5 to 6 kW·km^{-1} can be extracted (Stubbs 1994:23, Bolduc 2002).
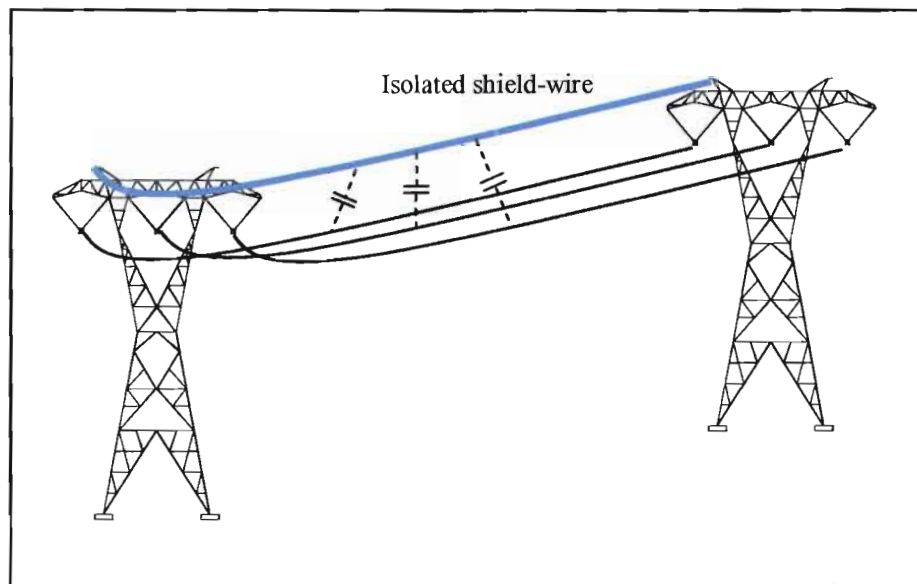
Figure 8 Isolated shield-wire system

25

3.2   Isolated shield-wire non-resonant method

In this method, the shield wire is connected directly to a step-down transformer as in Figure 9.
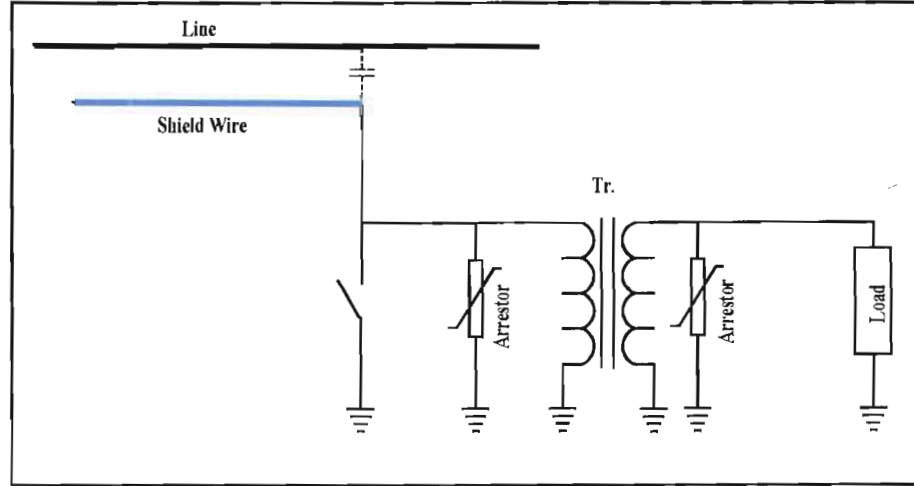
Figure 9 Non-resonant method

Using Matlab 6 with Power System Blockset, the influence of the variation of coupling capacitance from 57 nF (the value found by Stubbs 1994:23 for 9,6 km long isolated shield wire) to 50 nF and load was studied. The results of the influence in the output voltage due to 14 percent change in coupling capacitance are presented in Figure 10a and the influence of 400 percent change in the load current is shown in Figure 10b.

a) Coupling-capacitance step   b) Load-current step
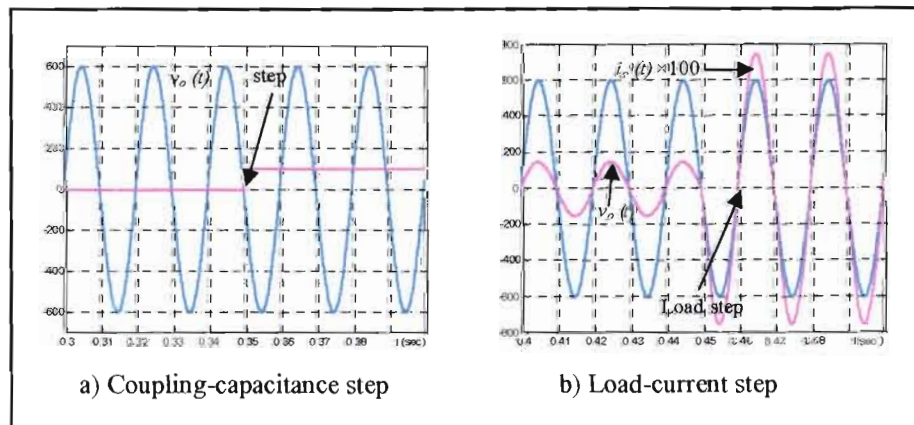
Figure 10 Output parameters of non-resonant method

3.3 Isolated shield-wire resonant methods

The resonant methods are based on introduction of an inductor in series between the coupling capacitor and step-down transformer and tuning the circuit on the industrial frequency that could be 50 or 60 Hz, depending on the standard frequency.

3.3.1 Passive method

The passive method studied by Stubbs (1994) is presented in Figure 11. In this solution the value of the series inductor and other elements of the system should be implemented very closely compared to the calculated values; any change in parameters can shift the system from resonance.
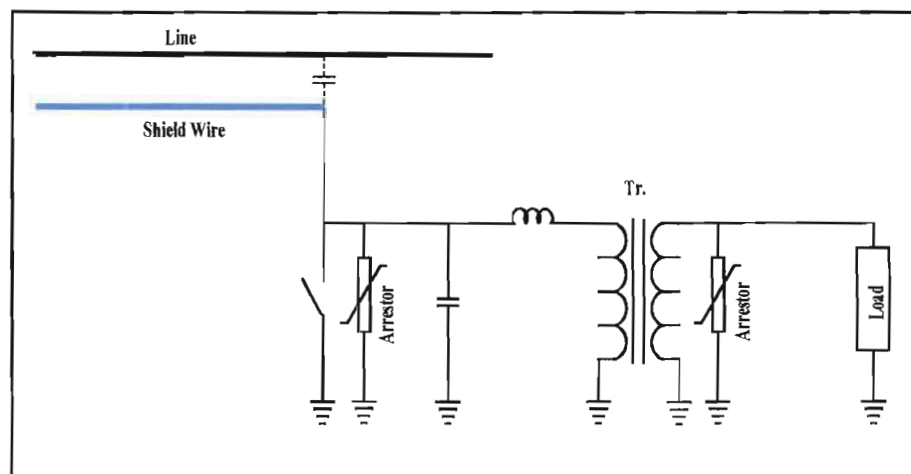
Figure 11 Passive resonant method

This method was further studied and improved by Lategan & Swart (2002) introducing a three-phase induction motor to run in background; in this way, the variation of the load is reduced and accordingly the tuning conditions are fairly constant.

3.3.2 Active method

The passive method presented some problems such as resonant frequency shift, ferroresonant oscillations and voltage regulation. In this new method developed at I.R.E.Q. Canada (Bolduc 2002), the initial series inductor + transformer was replaced by a "self-regulated reactor with air gap" presented in Figure 12; the controller keeps the system tuned to the desired frequency (60 Hz in this case) and in this way the output voltage is identical in shape with line voltage and in phase with it.
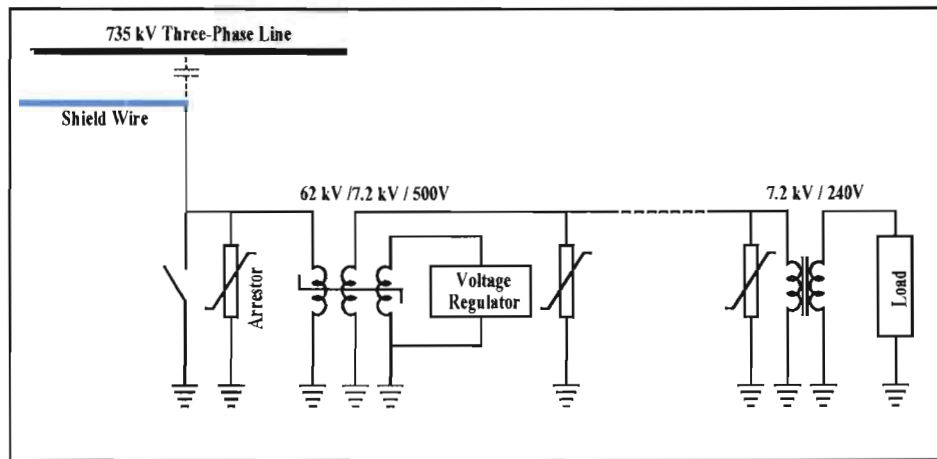
Figure 12 Active method, isolated shield wire

3.4 Other capacitive methods

There are some other capacitive-coupling methods that do not necessarily fall under the initial definition (given in paragraph 2.3) of non-conventional methods of energy tapping but do not use a classical high voltage step-down transformer.

3.4.1 Antenna method

In this method, an antenna-wire is attached to a live conductor of the line. Using isolation spacers, the wire is fixed at a certain distance. For example: a 16 m long antenna mounted 0,30 m below a 120 kV conductor line can supply a 30 W load (Bolduc 2002). The load could be a radio transmitter, receiver or a neon light. The

last application is widely used by EDF in France to light transmission lines (Bolduc 2002).

3.4.2 Capacitive divider method

The capacitor divider has been known for quite a while but using this technology to transform high voltage to medium voltage for delivering power is more recent. In this method, a bank of capacitors is connected directly to the conductor line via a high voltage protective device as presented in Figure 13.
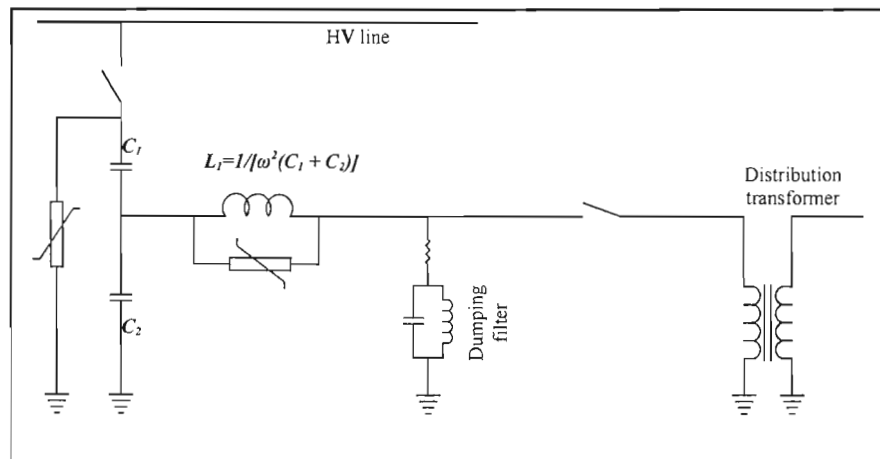
Figure 13 Capacitive divider system

This system is used on transmission lines from 120 kV up to 345 kV and delivers power between 1,5 MVA and 4 MVA (Bolduc 2002). The capacitive solution is also under development in South Africa (Raphalalani et al. 2001).

3.5 Comments about capacitive methods

The capacitive methods represent a big class of solutions of extracting energy from HVAC. They are based on a straightforward principle that allows good design. The range of power extracted could be from tens of watts up to megawatts.

29

The methods based on an isolated shield wire present the inconvenience of a very long distance in order to get relatively high power.

In the higher range of power is the capacitive divider. But this method requires a direct contact with the conductors of the line. It should be mentioned that this method presents another major advantage: if placed somewhere between two classic inductive substations, the capacitive divider substation serves not only to feed loads but, in addition, acts as a reactive compensator thus improving the voltage regulation of the line.

4. HVAC INDUCTIVE COUPLING METHODS

4.1 Energy stored in magnetic field

As mentioned before, the energy stored in the magnetic field is:

$$U_m = \int_3 0,5 \cdot \boldsymbol{B} \cdot \boldsymbol{H} dv \tag{4.1}$$

And the power density due to the magnetic field in the vicinity of a conductor is:

$$P_m = \frac{\partial}{\partial t} U_m = \frac{\mu I \cdot L}{2\pi} \frac{dI}{dt} \ln \frac{r}{r_o} \tag{4.2}$$

But all the methods involved in extracting energy from the magnetic field are based on Faraday's Law:

$$\nabla \times \boldsymbol{E} = -\frac{\partial \boldsymbol{B}}{\partial t} \tag{4.3}$$

Or, the most known expression:

$$emf = -\frac{d\Phi}{dt} \tag{4.4}$$

That can also be expressed as:

$$emf = -K \frac{di}{dt} \tag{4.5}$$

where K is a constant that depends on geometry and *di/dt* is the variation of the current through the transmission line.

4.2   Rogowski coil power application

If a loop is placed in the vicinity of a conductor/line carrying a variable current, then according to Faraday's Law, an electromotive force (emf) will be induced in that loop. Based on this principle, the Rogowski coil is used to measure currents. In this research, a new power application of the Rogowski coil is used to extract power from the HVAC transmission lines.

4.2.1   Single-phase application

In Figure 14 a Rogowski coil is shown placed under a single-phase line.
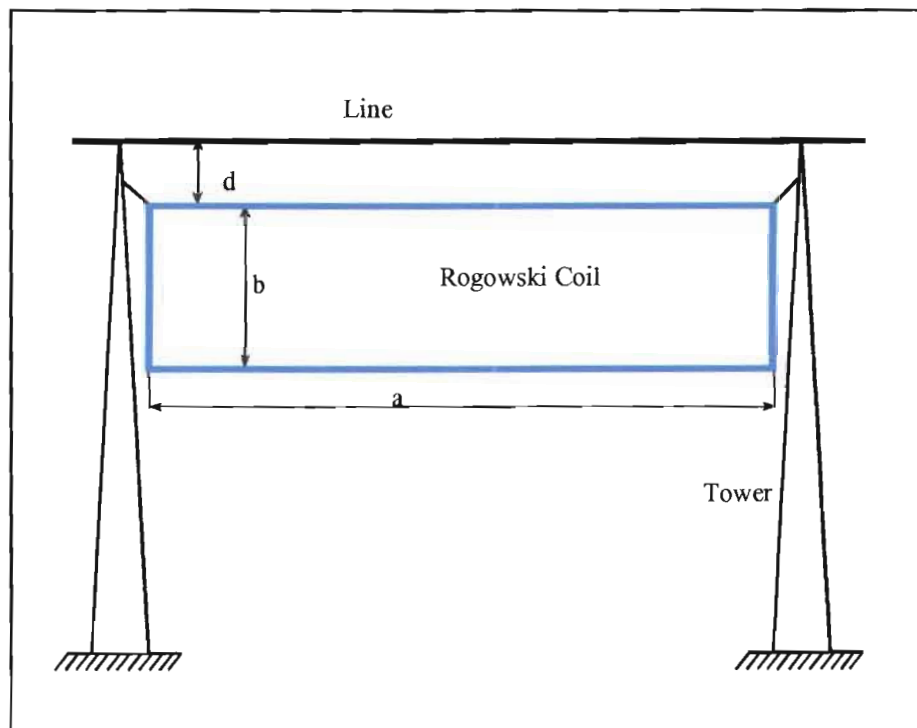
Figure 14 Single-phase Rogowski coil power application

4.2.1.1 Induced emf evaluation

A more general geometric position of the Rogowski coil relative to the line is presented in the Figure 15.
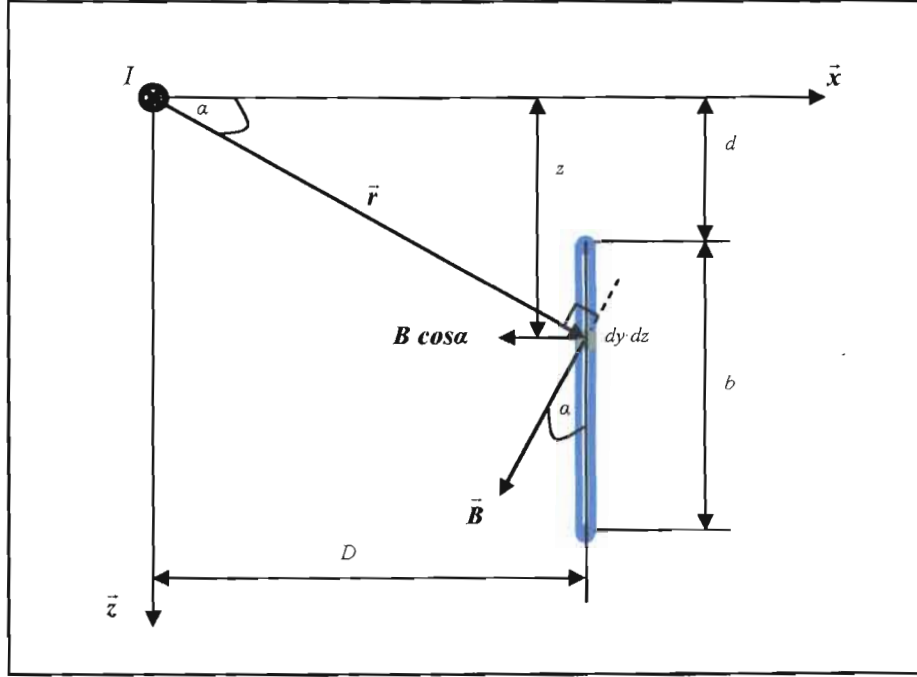
Figure 15 General position of Rogowski coil in relation to the line

In order to find the emf induced in the coil by the current I, the following assumptions should be considered:

- The loop is rectangular (width = b and length = a), has N_t turns and is parallel with the line and with the y axis.
- The influence of the round corners and the sag is neglected.
- The line current is: $i(t) = I \sin(\omega t)$

As mentioned previously, the emf induced is given by (4.2). The magnetic flux created by the current I is:

$$\Phi_{\mathrm{m}} = N_t \int_S \vec{B} \cdot d\vec{A} = N_t \int_S B \cdot \cos\alpha \cdot dy \cdot dz \tag{4.6}$$

33

where S is the surface of the coil. Because there is no variation of the induction on y axis and the conductor can be considered infinite long, the equation for B is:

$$B = \frac{\mu_o \cdot i(t)}{2 \cdot \pi \cdot r} \tag{4.7}$$

$$r = \sqrt{z^2 + D^2} \tag{4.8}$$

$$\cos \alpha = \frac{z}{\sqrt{z^2 + D^2}} \tag{4.9}$$

Substituting (4.7), (4.8) and (4.9) in (4.6) the result is:

$$\Phi_m = \iint \frac{\mu_o \cdot i(t) \cdot N_t \cdot z}{2\pi \left[z^2 + D^2 \right]} dy \cdot dz \tag{4.10}$$

With $z \in [d, \, d+b]$ \hfill (4.11)

$$y \in [0, \, a] \tag{4.12}$$

$$\Phi_m = \left(\int_0^a dy \right) \cdot \left\{ \int_d^{d+b} \frac{\mu_o \cdot i(t) \cdot N_t \cdot z}{2\pi \left[z^2 + D^2 \right]} dz \right\} \tag{4.13}$$

$$\Phi_m = \frac{\mu_o \cdot i(t) \cdot N_t \cdot a}{4\pi} \ln \frac{D^2 + (d+b)^2}{D^2 + d^2} \tag{4.14}$$

$$e(t) = -\frac{\partial}{\partial t} \left[\frac{\mu_o \cdot i(t) \cdot N_t \cdot a}{4\pi} \ln \frac{D^2 + (d+b)^2}{D^2 + d^2} \right] \tag{4.15}$$

34

$$e(t) = -\left[\omega \cdot I \cdot N_t \cdot a \cdot 10^{-7} \cdot \ln \frac{D^2 + (d+b)^2}{D^2 + d^2}\right] \cos(\omega t) \tag{4.16}$$

If:

$$\mathcal{E} = \omega \cdot I \cdot N_t \cdot a \cdot 10^{-7} \cdot \ln \frac{D^2 + (d+b)^2}{D^2 + d^2} \tag{4.17}$$

Then:

$e(t) = - \mathcal{E} \cdot \cos(\omega t)$

$e(t) = - \mathcal{E} \cdot \sin(\omega t + 90^0)$ (4.18)

4.2.1.2 Characteristics of the induced emf

- As shown in (4.17), the induced emf is directly proportional to the current through the main line; it also depends non-linearly on geometry of the system.
- The induced emf is directly influenced by the distortions of the current flowing through the line.

If the current contains harmonics, then it could be written as:

$$i(t) = \sum_{n=1}^{\infty} I_n \sin(n \cdot \omega t + \varphi_n) \tag{4.19}$$

where n is the rank of the harmonic.

Applying (4.5) results:

$$e(t) = \sum_{n=1}^{\infty} (-K \cdot n \cdot \omega \cdot I_n) \cdot \cos(n \cdot \omega t + \varphi_n) \qquad (4.20)$$

Then:

$$\frac{\mathcal{E}_n}{\mathcal{E}_1} = n \frac{I_n}{I_1} \qquad (4.21)$$

Equation (4.21) shows that any distortion of the main current is magnified in the induced emf.

4.2.1.3 Basic model of single-phase application

The basic equivalent model of the single-phase Rogowski coil power application is presented in Figure 16 where I is the main current, M is the mutual inductance that couples the line with the Rogowski coil, Z_{in} (R_{in} and L_{in}) is the internal impedance, $\mathcal{E}$ is the emf induced and V_o is the output voltage.

a) Air-core transformer   b) Equivalent diagram

Figure 16 RCPA basic model

36
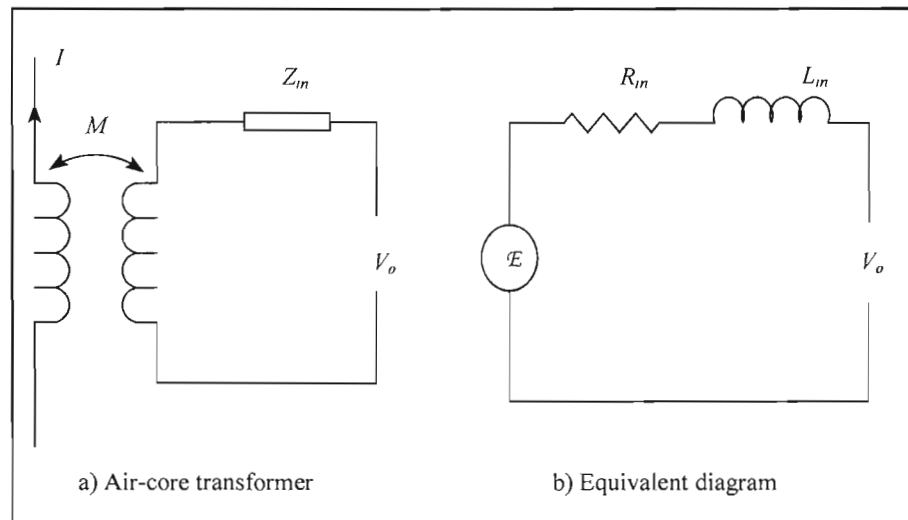
Internal resistance depends on the dimensions of the coil (a, b and r_o – radius of the wire used), resistivity of the material used for wire (ρ) and number of turns (N_t):

$$R_{in} = \frac{2 \cdot (a+b) \cdot N_t \cdot \rho}{\pi \cdot r_o^2} \tag{4.22}$$

According to Babani (1945: 114), the self-inductance of a rectangular inductor of round wire for low frequency is:

$$L_{in} = 4 \cdot 10^{-7} N_t^2 \left[a \ln \frac{2ab}{r_o \left(a + \sqrt{a^2 + b^2} \right)} + 2\sqrt{a^2 + b^2} + b \ln \frac{2ab}{r_o \left(b + \sqrt{a^2 + b^2} \right)} - \frac{7}{4}(a+b) \right] \tag{4.23}$$

where $a, b >> r_o$ $\hspace{3cm}$ (4.24)

With a careful choice of the number of turns (N_t), geometrical parameters (a, b, d, D and r_o) and material (ρ), the desired power (1-3kW) can be achieved.

The result of the simulation of this model, using Matlab 6, is presented in Figure 17. The input parameters used for this simulation are those for the reduced scale model that will be presented on Chapter 7.
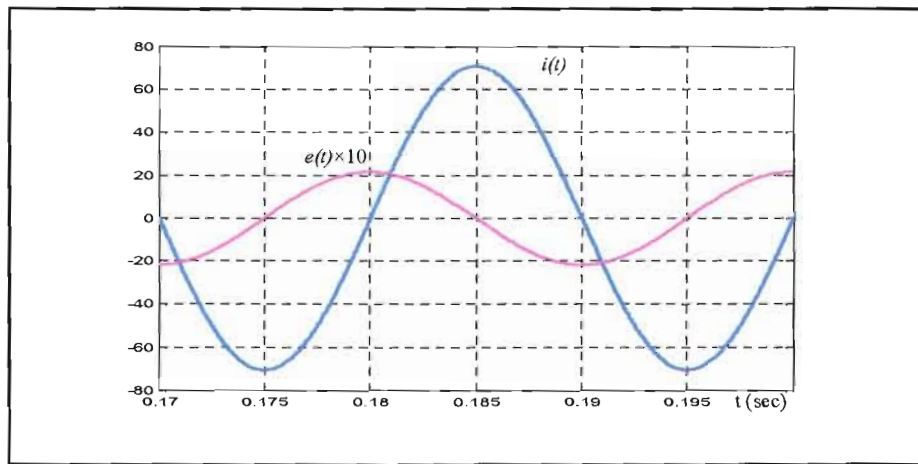
Figure 17 Simulation results for single-phase basic system

4.2.2 Three-phase application

In practice, the most used configuration for transmission lines is three-phase, therefore it is necessary to find the emf induced into the Rogowski coil in this situation (Figure 18).
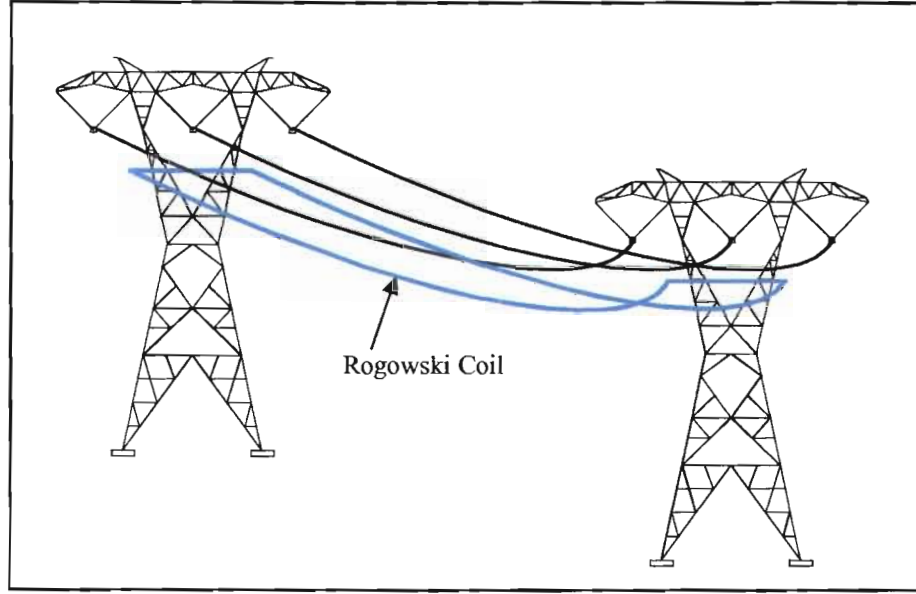
Figure 18 RCPA Three-phase system illustration

4.2.2.1 Emf evaluation

Let us consider a cross-section of the above configuration, presented in Figure 19, where D_L is the distance between phases, D is the distance between the lines plane and the coil plane (the coordinate y is not shown).

Let us consider a convenient three-phase current system:

$$i_1(t) = I \sin\left(\omega t - 120^0\right) \tag{4.25}$$

$$i_2(t) = I \sin\left(\omega t\right) \tag{4.26}$$

$$i_3(t) = I \sin\left(\omega t + 120^0\right) \tag{4.27}$$
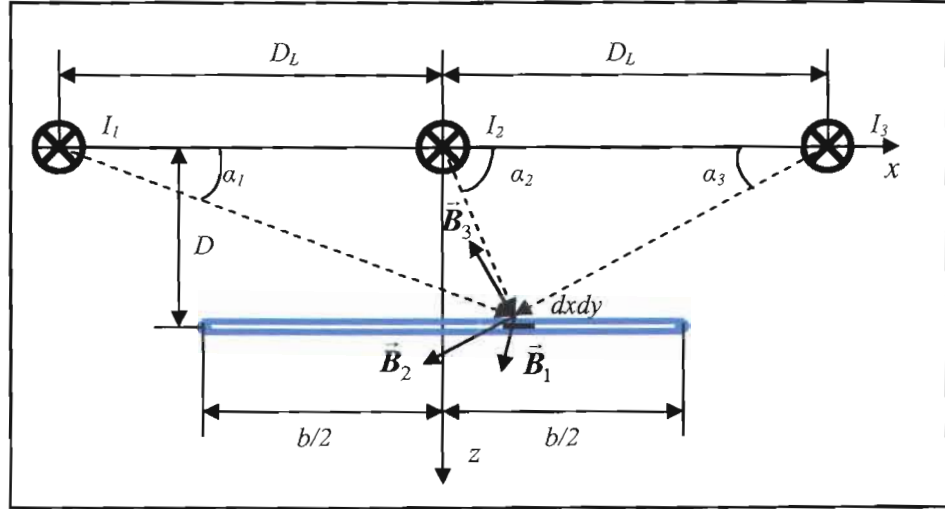
Figure 19 RCPA Three-phase system: cross-section

According to the superposition principle, each current will induce an emf in the Rogowski coil and the result will be the sum of all:

$$e(t) = e_1(t) + e_2(t) - e_3(t) \tag{4.28}$$

The emfs $e_1(t)$ and $e_3(t)$ can be derived in the same way as for single-phase (4.18) and:

$$e_1(t) = -\mathcal{E} \cdot \cos(\omega t - 120^0) \tag{4.29}$$

$$e_3(t) = -\mathcal{E} \cdot \cos(\omega t + 120^0) \tag{4.30}$$

The amplitude $\mathcal{E}$ can be derived using (4.17) and applying the coordinate system as in Figure 19:

$$\mathcal{E} = \omega \cdot I \cdot N_t \cdot a \cdot 10^{-7} \ln \frac{(D_L + b/2)^2 + D^2}{(D_L - b/2)^2 + D^2} \tag{4.31}$$

$$e_2(t) = -\mu_0 \cdot a \cdot N_t \left[\frac{di(t)}{dt} \right] \cdot \left| \int_0^{b/2} \frac{x \cdot dx}{\sqrt{x^2 + D^2}} + \int_0^{b/2} \frac{-x \cdot dx}{\sqrt{x^2 + D^2}} \right| = 0 \tag{4.32}$$

Then:

$$e(t) = -\mathcal{E}\cos(\omega t - 120^0) + \mathcal{E}\cos(\omega t + 120^0) \qquad (4.33)$$

$$e(t) = \sqrt{3} \cdot \mathcal{E}\sin(\omega t) \qquad (4.34)$$

From (4.34), it is possible to conclude that the emf induced for the three-phase system is $\sqrt{3}$ greater than that for single phase and the power extracted could be 3 times bigger for the same geometry of the system.

The simulation results using the parameters of the basic model are presented in Figure 20.
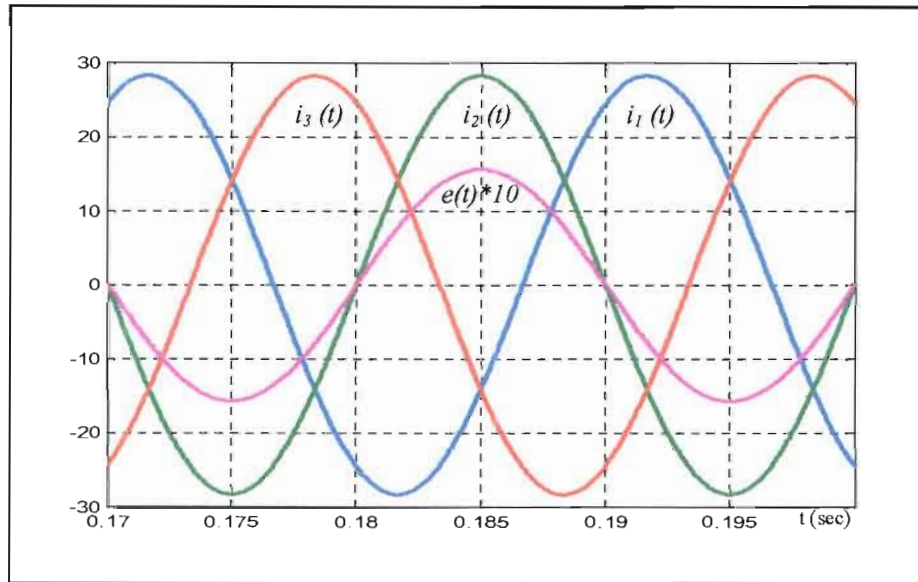
Figure 20 Three-phase system: simulation results – basic model

Regarding to equation (4.31), it should be mentioned that the amplitude $\mathcal{E}$ is maximum when $b = D_L$.

4.2.2.2 Estimated emf / turn

Next the emf induced in one turn is estimated if a nearly ideal situation is considered:

- The Rogowski coil is in the same plane as the conductors: $D = 0$ m
- The distance between two towers is $a = 250$ m
- The distance between line conductors is $D_L = 8,5$ m
- The width is such that the long sides of the coil, parallel to the lines, do not come closer than 4 m to the lines, resulting in: $b = 9$ m
- The amplitude of the main current is $I \approx 1500$ A

With these assumptions, the emf induced is:

$$\mathcal{E} = \sqrt{3} \cdot \omega \cdot I \cdot a \cdot 10^{-7} \ln \frac{\left(D_L + b/2\right)^2 + D^2}{\left(D_L - b/2\right)^2 + D^2} \tag{4.35}$$

$$\mathcal{E} = \sqrt{3} \cdot 2 \cdot \pi \cdot 50 \cdot 1500 \cdot 250 \cdot 10^{-7} \ln \frac{\left(8,5 + 4,5\right)^2 + 0^2}{\left(8,5 - 4,5\right)^2 + 0^2} = 48,1 \ \text{V/turn} \tag{4.36}$$

$$\mathcal{E}_{rms} = 34 \ \text{V/turn} \tag{4.37}$$

By adding a number of turns a reasonable power could be achieved. An in-depth analysis of the power extracted will be presented in Chapter 6.

4.3 Current transformer tapping methods

Another class of methods to extract energy from HVAC is based on the current transformer (CT). Normally, the current transformer is designed to be used for measuring currents.

Basically, the CT is an iron-core transformer and its function is based on Faraday's Law. With a different approach for design, the CT can handle a reasonable output power. The basic model is presented in Figure 21.
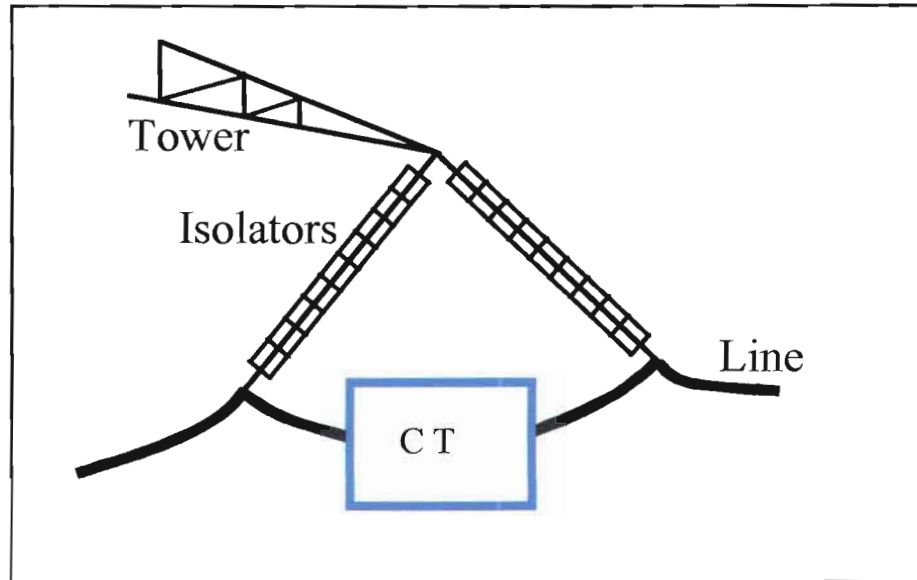
Figure 21 Illustration of the basic model for CT-based methods

4.3.1 Current-to-current power application

In this situation, the CT could be used as a normal but more powerful device that feeds a load directly. This method has the following disadvantages:

- It can feed only a single-phase load.
- It requires a load that accepts current feeding.
- There is no control over the output.

4.3.2 Current-to-voltage conversion with dc storage

In this method (Janse van Rensburg & Case 2002: 181), the input current that feeds a CT is converted into voltage via a boost converter and by means of using a PWM switching technique, a constant DC voltage is generated. This voltage supplies a

single/three-phase inverter to create the 50Hz AC voltage and deliver a power of 1-3 kW. The basic diagram of this method is presented in Figure 22.
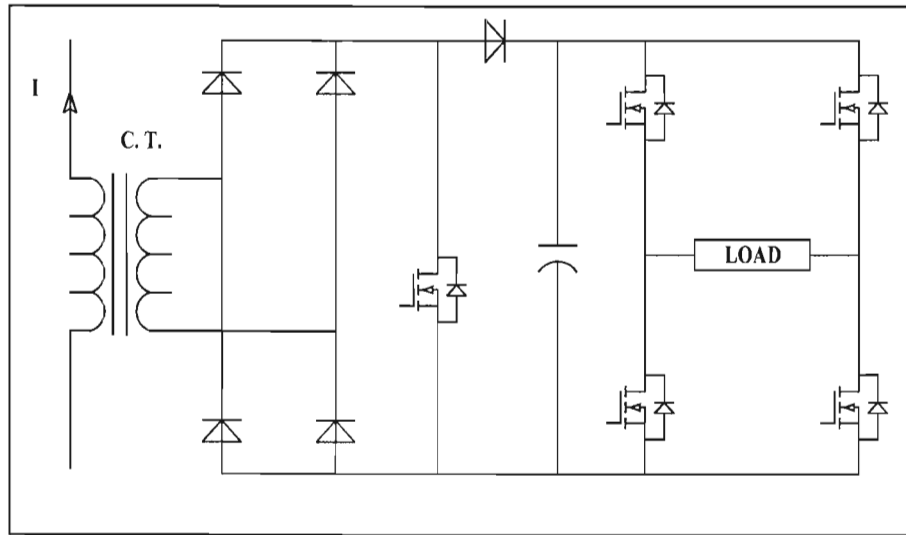
Figure 22 Basic diagram of current-to-voltage with dc storage – CT-based tapping method

This method addresses all the disadvantages presented by the previous method:

- It can feed single or three-phase loads.
- It is equivalent to voltage source that is suitable for almost all AC loads.
- It has good control facilities.

4.3.3 Direct alternating current to alternating voltage conversion

In this method, developed by Janse van Rensburg (Janse van Rensburg & Nicolae 2004), a new design of the power CT permits a direct conversion of alternating current into alternating voltage using an additional secondary, that by means of PWM switching modulates the magnetic flux and thus the output voltage of the main secondary coupled to the load via a low-pass filter.

This method is still under research.

4.4   Comments about inductive methods

The inductive methods of extracting energy from HVAC transmission lines represent a viable alternative to the capacitive (CAPTAP). They are recommended for a power range of several kilowatts.

Compared to the capacitive methods, the inductive method does not require a very long distance: for the methods based on CT intervention to only one tower is necessary, while for the Rogowski coil power application the coupling device should be installed between two, or eventually more towers.

The influence of the CT-based methods on the transmission is dependent on the ratio of the current transformer. If one takes into consideration a ratio of 1:100 and a level of load current of 10 to 30 A, then what is seen in the primary is below 1 A. If this small input current is compared with the main current through the line that very well exceeds 1000 A, then the conclusion is that there is practically no influence. The Rogowski coil power application also exerts a very small influence on the transmission line due to the air-core coupling.

5. HVDC ENERGY TAPPING METHODS

The non-conventional methods for tapping energy from HVDC lines are based on energy stored into electric field on one hand but also on imperfections of the parameters of the DC current and voltage. The solutions that are already presented in literature and implemented are based on physical contact between the HVDC line and the tapping system (Ekstrom & Lamell 1991: 126, Aghaebrahimi & Menzies 1997: 1697, Bahrman et al. 1995:1699 and Chetty et al. 2004).

5.1 Energy stored in electric field

As mentioned before, the energy stored into an electric field is as in (2.16) and the power density associated with electric field as in (2.42). Let us put these equations into a form that could show ideas of tapping energy:

$$U_e = \frac{1}{2} C \cdot V^2 \quad \text{J}$$
(5.1)

In (5.1), if the voltage is considered constant, then by making the capacitance variable the power related to the electric field is:

$$P_e = \frac{1}{2} V^2 \frac{\partial C}{\partial t} \quad \text{W}$$
(5.2)

5.2 Capacitance modulation methods

The basic model of capacitive methods for energy extraction from HVDC transmission lines is similar to that used for HVAC lines. It consists of an isolated wire installed parallel to the main line. Then using various methods, the capacitance created between the main line and this auxiliary conductor can be varied in time

45

(modulated). If this variable capacitance is connected in series with a transformer, then a certain amount of energy could be transferred to the load. In Figure 23 is shown the basic model and in Figure 24, the equivalent diagram.
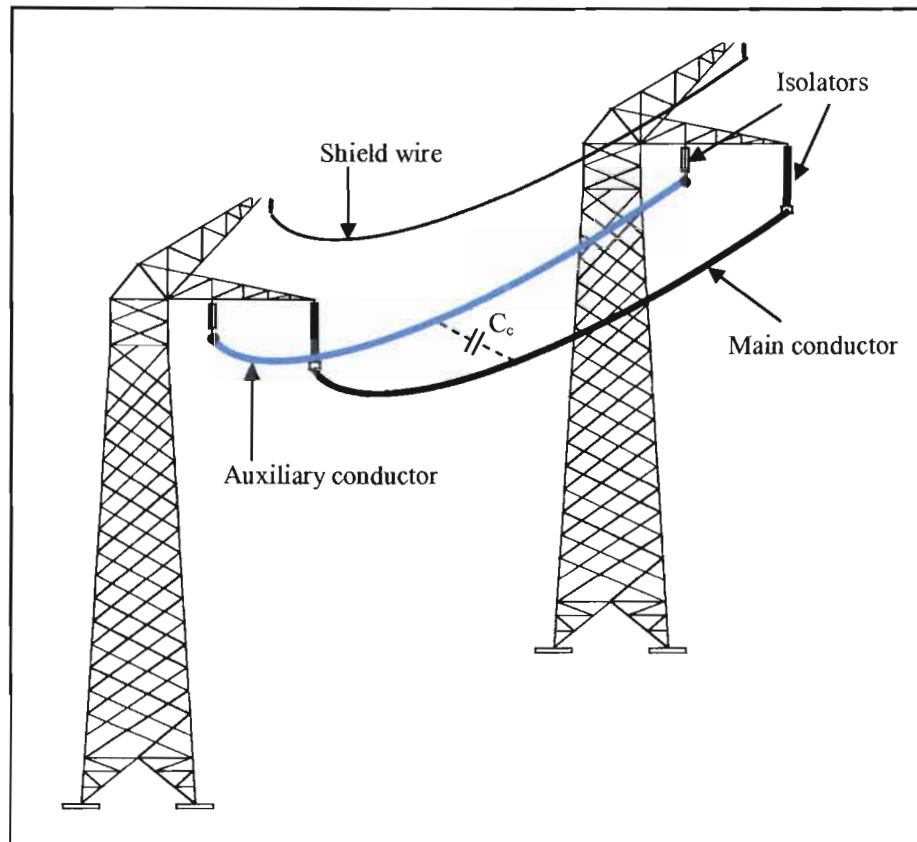
Figure 23 Capacitive methods: basic model illustration
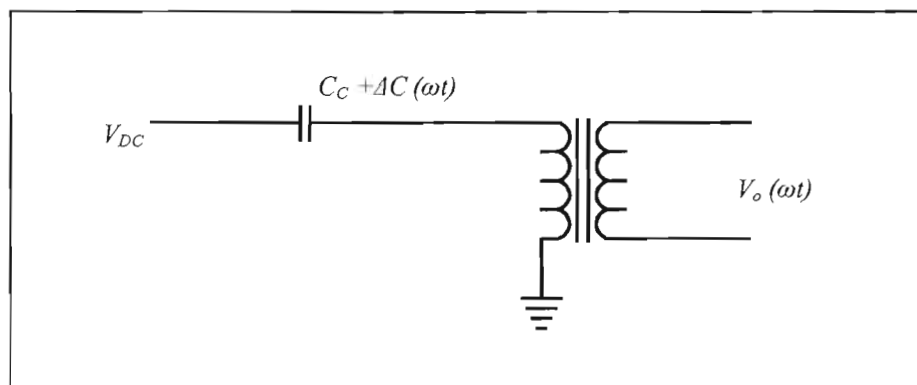
Figure 24 Capacitive methods: equivalent diagram

5.2.1 Mechanical modulation

A simple solution in order to get a variable coupling capacitance is to make the auxiliary wire oscillate mechanically. This idea represents only a theoretical interest. In order to be able to have a reasonable energy transfer, the auxiliary wire must oscillate with a reasonable frequency; a heavy mechanical system usually does not oscillate with a frequency higher than 10 Hz therefore the induction in the transformer is very weak.

If one makes a balance between the mechanical power used to move the auxiliary wire and the electric energy generated, then the immediate conclusion is that this method does not extract energy. If the cost of this method is considered, then this solution is not economical.

5.2.2 Static modulation

A static modulation could be obtained if a semiconductor or ceramic device is inserted between coupling capacitor (C_c) and the output transformer. The basic phenomenon could be similar to that of the varicap diode.

By all means, if a static modulation can be obtained, then the ratio between output power and the power used to drive the modulation process could be greater than unity.

This new idea conceived by the author does not have sufficient technological support. It opens new fields in theoretical and technological research. It is also envisaged that high frequency techniques should be involved in order to reduce volume and increase the efficiency of inductive transfer.

5.3   Inductive methods

These methods are based on the imperfections of the DC parameters: voltage and current.

5.3.1   Characteristics of the dc line parameters

It is general knowledge that HVDC is obtained via twelve pulse three-phase converters as the most usual solution. As a result, the output DC voltage and, consequently, the current have ripple. It is also known that filtering of high voltage and high current is very difficult and therefore the output parameters will always contain ripple. In Figure 25, a simulation graph of the voltage and current of the same characteristics as those of the Cabora Bassa Apollo HVDC transmission line are presented; an inductor of 0,83 H / 1800 A is used to smooth the output (Raynham & Goosen 1979). In this figure: V_o (kV) is the ac-to-dc converter output voltage, V_l (kV) is the line voltage after smoothing and I_l (A) is the line current.
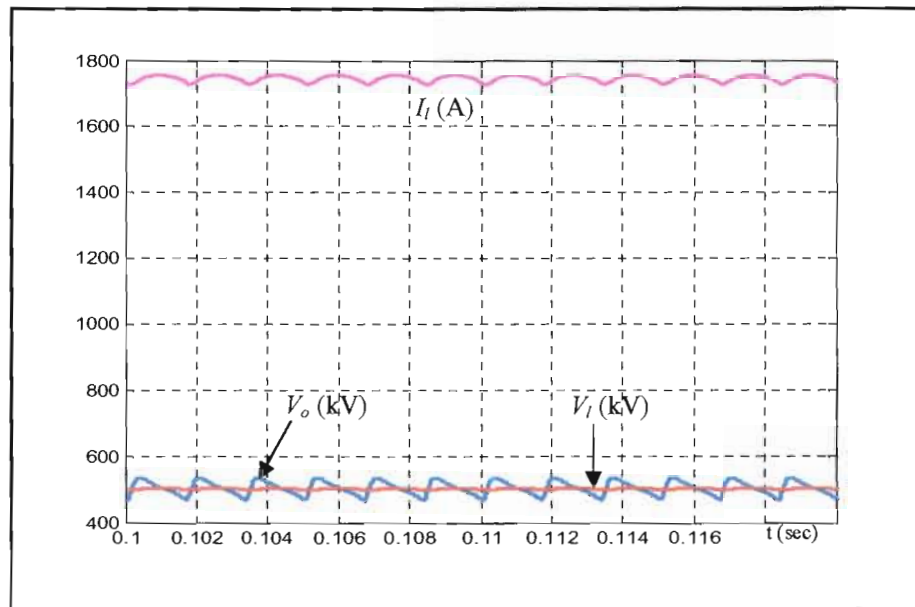
Figure 25 HVDC parameters

From this research point of view, the current ripple (I_r) presented in Figure 26 is important. It is clear, the frequency is 550 Hz and the amplitude is about 12 A. A spectral analysis (Figure 27) shows the same conclusions as before: the fundamental frequency is 550 Hz and the amplitude of the fundamental is around 13 A.
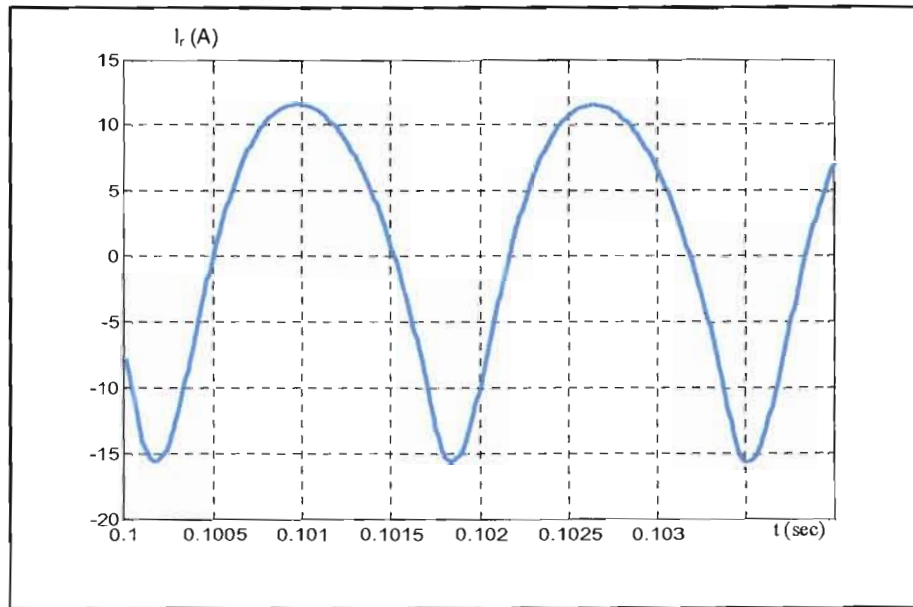
Figure 26 dc line current ripple
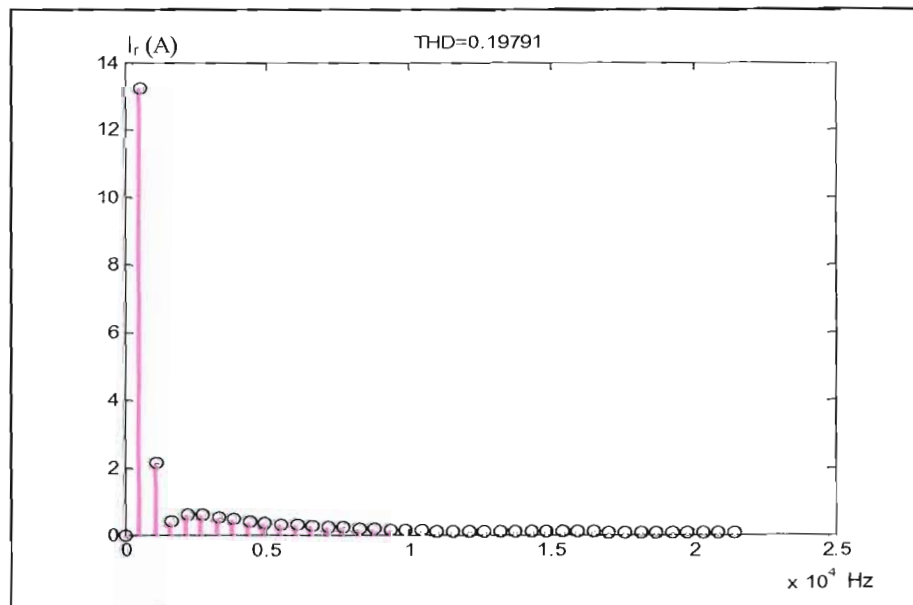
Figure 27 Current ripple: frequency spectrum

With the above observations, the imperfect HVDC lines can be treated the same as HVAC lines and the inductive methods could be applied.

5.3.2   Rogowski coil power application for dc line

Having concluded that the HVDC line can be equivalent to a single-phase line carrying approximate 13 A amplitude of the 550 Hz fundamental current, the Rogowski coil power application could be used. The basic model is illustrated in Figure 28.

Figure 28 Rogowski coil for HVDC – basic model illustration

In order to find the range of power that could be extracted, the voltage induced in Rogowski coil should be evaluated; for this, equation (4.17) should be used. If the upper side of the Rogowski coil is at the same level as the main conductor, which

50

means that $d = b/2$ and then, according to physical parameters of the line (Raynham & Goosen 1979) and some regulations used in South Africa, $D = 4$ m, $a = 250$ m (shortest distance between two towers) and $b = 9$ m (which complies with clearance above ground). The induced emf per turn is:

$$\mathcal{E} = \omega \cdot I \cdot a \cdot 10^{-7} \ln \frac{D^2 + b^2}{D^2} \tag{5.3}$$

$$\mathcal{E} = 2 \cdot \pi \cdot 550 \cdot 14 \cdot 250 \cdot 10^{-7} \ln \frac{4^2 + 9^2}{4^2} = 2,18 \ \text{V} \cdot \text{turn}^{-1} \tag{5.4}$$

$$\mathcal{E}_{rms} = 1,54 \ \text{V} \cdot \text{turn}^{-1} \tag{5.5}$$

Figure 29 illustrates the induced voltage obtained using the same simulation model as in paragraph 4.2.1.3.
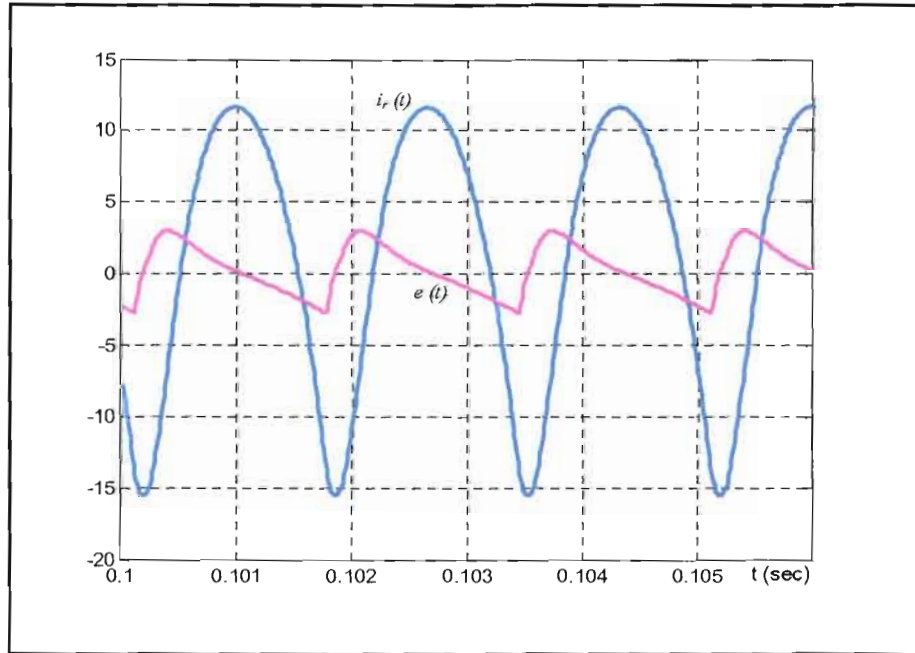
Figure 29 Induced voltage for HVDC application

As can be observed in Figure 29, the induced emf e (t) does not validate (5.4). But if the spectrum of e (t) is analyzed (Figure 30), then it is possible to conclude that the fundamental validates (5.4).
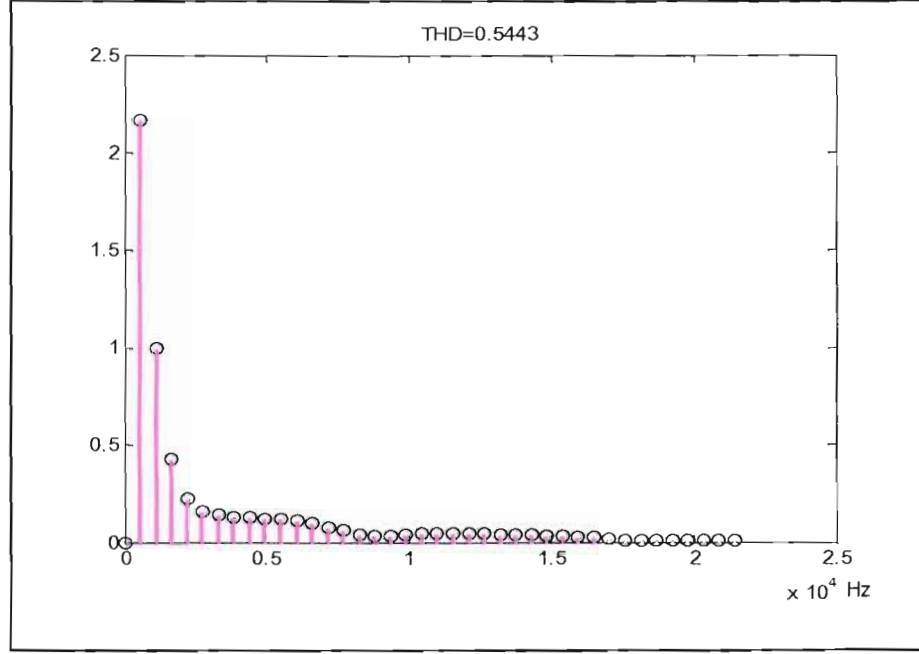
Figure 30 RCPA for HVDC Induce emf – Fourier spectrum

If (5.5) is compared with (4.37), the result is that for the same size of the Rogowski coil, an emf 20 times smaller is obtained for the HVDC application. This requires in compensation 20 times more turns. The increased number of turns can increase the voltage but at the same time the internal impedance of the Rogowski coil will increase. Let us consider the parameters of one turn presented above and a copper wire of 1,5 mm², then the internal resistance will be:

$$R_{in} = \frac{2 \cdot (a+b) \cdot \rho}{\pi \cdot r_o^2} \quad \Omega \cdot \text{turn}^{-1} \tag{5.6}$$

$$R_{in} = \frac{2 \cdot (250+9) \cdot 1,72 \cdot 10^{-8}}{1,5 \cdot 10^{-6}} = 5,94 \ \Omega \cdot \text{turn}^{-1} \tag{5.7}$$

The self-inductance will be:

$$L_{in} = 4 \cdot 10^{-7} \cdot \left[a \ln \frac{2ab}{r_o \left(a + \sqrt{a^2 + b^2} \right)} + 2\sqrt{a^2 + b^2} + b \ln \frac{2ab}{r_o \left(b + \sqrt{a^2 + b^2} \right)} - \frac{7}{4}(a+b) \right] H \quad (5.8)$$

Using the same geometrical parameters, the self-inductance is:

$$L_{in} = 1 \text{ mH} \cdot \text{turn}^{-1} \quad (5.9)$$

If the coil has 200 turns an output voltage of 308 V_{rms} is obtained. However, this will increase the internal impedance to:

$$R_{in} = 1188 \ \Omega \quad (5.10)$$

and

$$L_{in} = 40 \text{ H} \quad (5.11)$$

This impedance drastically reduces the power capability. Therefore, the self-inductance of the Rogowski coil must be capacitatively compensated. Due to the fact that the predominant frequency considered is 550 Hz, then the capacitance needed for compensation should be:

$$C = \frac{1}{L_{in} \left(2 \cdot \pi \cdot f \right)^2} \ F \quad (5.12)$$

$$C = \frac{1}{40 \left(2 \cdot \pi \cdot 550 \right)^2} = 2{,}1 \cdot 10^{-9} \ F \quad (5.13)$$

In these conditions, a power of approximately 40 W is obtained when the load is around 1,2 kΩ. This is small power, therefore special attention should be considered in the design in order to increase the power capability of this solution.

5.3.3 CT-based methods for dc line

Another method that could be involved for extracting energy from HVDC is the use of a current transformer. Based on Faraday's Law, the ripple of the main current can induce a voltage into the current transformer.

Some remarks should be presented here:

- If this solution is requested, then it must be considered an air-core solution because the huge dc current will saturate the magnetic core.
- If the power capability of the Rogowski coil is considered as a reference, it could be concluded that with this method even less power can be extracted.

5.4 Resonant methods

5.4.1 Low frequency resonant method

Reconsider now the capacitive coupling between the main conductor and the auxiliary one (Figure 23). Here, the ripple of the line voltage (V_r) is considered as an AC supply. If an inductor (L_r) and transformer (Tr) are connected in series with the coupling capacitor (C_c) and if this circuit is tuned for the fundamental frequency of the ripple (550 Hz), the transfer between the energy stored in C_c and L_r is maximum and a certain amount of power could be delivered to a load. Figure 31 illustrates the principle of the low frequency resonant method.
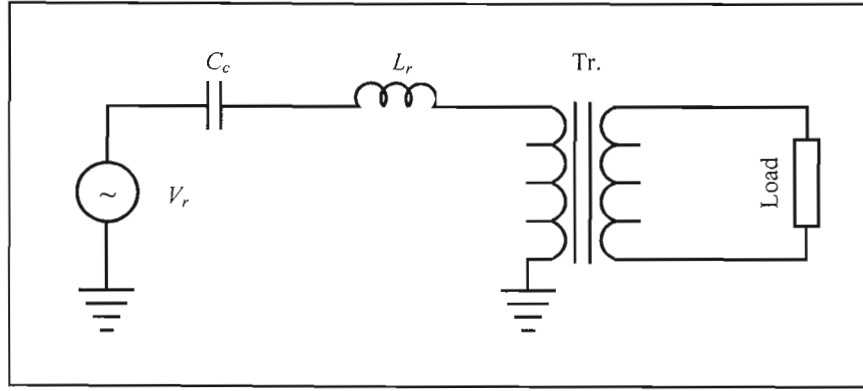
Figure 31 Low frequency resonant method – basic model

Using (3.3) and assuming an auxiliary conductor of $r_1 = 10$ mm, the equivalent radius of the main conductor of $r_2 = 114$ mm (Appendix B: B.4) and $D = 4$ m as the distance between main conductor and auxiliary, then:

$$C_c = \frac{2 \cdot \pi}{4 \cdot \pi \cdot 9 \cdot 10^9 \ln \dfrac{D^2}{r_1 \cdot r_2}} = 5,82 \text{ pF·m}^{-1} \qquad (5.14)$$

For 1 km long auxiliary wire, the coupling capacitance is $C_c = 5,82$ nF. Then the value of the inductance that reaches the resonance is:

$$L_r = \frac{1}{C_c (2\pi f)^2} = \frac{1}{5.82 \cdot 10^{-9} (2 \cdot \pi \cdot 550)^2} = 14,39 \text{ H} \qquad (5.15)$$

This is relatively high value. But L_r could be decreased if the size of the auxiliary wire is modified.

Based on the model from Figure 31, a Matlab model was created and the results of the simulation are presented in Figure 32. The voltage ripple (V_r) was considered as power supply, V_p is the input of the transformer and V_s is the secondary that feeds a load of 100 Ω with an amplitude of 268 V; this results in a power of 360 W.
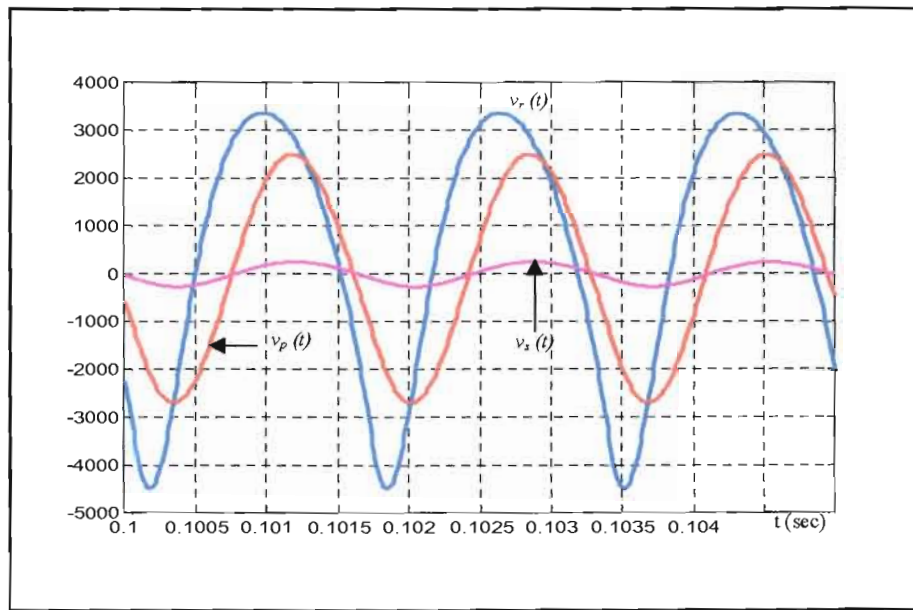
Figure 32 Low frequency resonant method – Simulation results

5.4.2 High frequency resonant method

The main challenge lies in perfect dc parameters of transmission line; the new developments (Villablanca et al. 2001) in HVDC show a great possibility of improving the reducing of the ripple. Then the attention should be directed to methods that do not exploit the ripple. The high frequency resonant method is linked with the static modulation of a ceramic/semiconductor device. As stated before (paragraph 5.2.2), this method is still in the infant stage due to the novelty thereof in the technological field and it opens a new field of research.

5.5 Comments about HVDC energy tapping methods

The HVDC transmission line is the best solution to transport electric energy for long and very long distances:

- The voltage drop across the line is much smaller than for HVAC.
- The losses due to corona are much smaller.

56

- The amount of conductive material is smaller.
- It can be very easy reticulated with other dc systems.

Along these very long transmission lines there are many remote rural areas without electricity. Hence, tapping methods of reasonable energy are needed.

As presented before in this chapter, there are methods such as Rogowski coil, CT, as well as low frequency resonant method that exploit the imperfections (ripple) of the dc parameters. These methods that are still under research can provide power of between a few tens of watts and a few kilowatts.

A very challenging method is the high frequency resonant method based on static modulation. At this stage, it is inappropriate to state the power capability of this method.

As a common property of all these methods: they are not in direct contact with the main line, which complies with the initial definition of "non-conventional methods".

6. ROGOWSKI COIL POWER APPLICATION - SOLUTION DESIGN

6.1 Block diagram

The block diagram of the RCPA is shown in Figure 33. It contains:

A - The pick-up coil

B - Isolation transformer

C - Voltage regulator, filter and control system

D - Protection system

E - Load
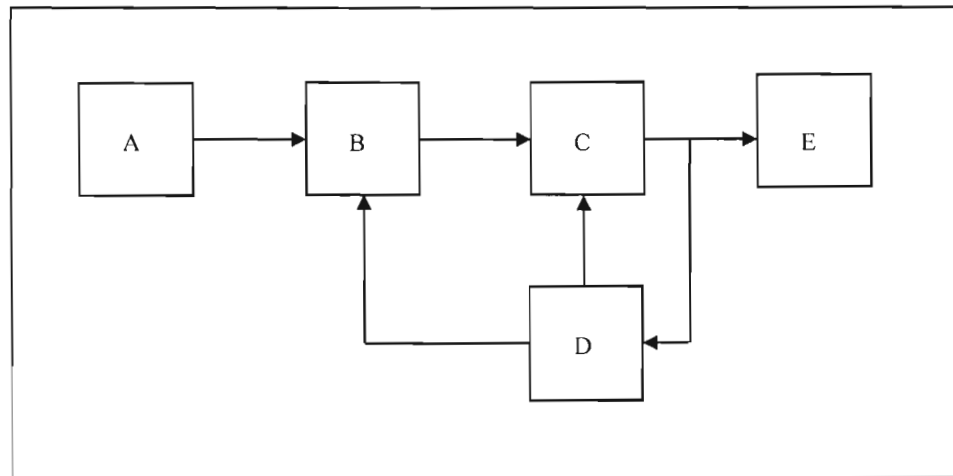
Figure 33 RCPA – Block Diagram

6.2 Basic assumptions

The basic assumptions regarding the design concern the transmission line. It is considered:

- A three-phase 440 kV flat horizontal; the design for a flat vertical line will be the same with minor modifications.

- A convenient voltage system:

$$v_1(t) = V \sin\left(\omega t - 120^0\right) \tag{6.1}$$

$$v_2(t) = V \sin\left(\omega t\right) \tag{6.2}$$

$$v_3(t) = V \sin\left(\omega t + 120^0\right) \tag{6.3}$$

with $V = V_L \sqrt{2/3} = 360$ kV

- A convenient current system:

$$i_1(t) = I \sin\left(\omega t - 120^0\right) \tag{6.4}$$

$$i_2(t) = I \sin\left(\omega t\right) \tag{6.5}$$

$$i_3(t) = I \sin\left(\omega t + 120^0\right) \tag{6.6}$$

with $I \approx 1500$ A

- A bundle of four conductors per line with $d_L = 40$ cm spacing and radius of each conductor of $r_L = 1$ cm
- A distance between lines of $D_L = 8,5$ m
- A height above the ground of $H_L = 20$ m
- A suspension tower as in Annexure C
- A distance between towers of $D_T = 250$ m
- In first approximation, RCPA is parallel with the lines

6.3   Pickup coil design

The basic phenomenon of electromagnetic force induced into a pickup was presented in Chapter 4, paragraph 4.2.2. The emf induced for a horizontal position with the coil centred in respect of the middle power line is:

$$e(t) = \sqrt{3} \cdot \mathcal{E} \sin(\omega t) \tag{6.7}$$

The emf amplitude is:

$$\mathcal{E} = k \ln \frac{\left(D_L + b/2\right)^2 + D^2}{\left(D_L - b/2\right)^2 + D^2} \tag{6.8}$$

with:

$$k = \omega \cdot I \cdot N_t \cdot a \cdot 10^{-7} \tag{6.9}$$

where:

$\omega = 2 \cdot \pi \cdot f = 314,15 \text{ rad} \cdot \text{sec}^{-1}$

a = the length of the coil

$a = D_T = 250$ m (first assumption)

b = the width of the coil

N_t = the number of turns

$b < 2D_L$

D = the distance between the power line plane and pickup coil plane

Then:

$$k = 2 \cdot \pi \cdot 50 \cdot 1500 \cdot 1 \cdot 250 \cdot 10^{-7} = 11.78 \tag{6.10}$$

A few questions raised by Walker (2004) should be answered before the actual design, such as:

- Is this the only position for the pickup coil?
- What is the influence of the very strong electric field?
- What other parameters could influence the output power?

6.3.1 Optimal positioning

In order to answer the first question put above, a study of optimal positioning was performed. In Figure 34 the positions of the pickup coil considered for this study are presented.

The ratio between emf for horizontal and vertical ($\mathcal{E}_h/\mathcal{E}_v$) was evaluated for different positions of the coil:

- A – the coil under the lines 1 or 3 (I_1 or I_3)
- B – the coil under the line 2 (I_2)

In vertical position, the coil was considered direct under the line and for horizontal position the axis of the coil is positioned directly under the line.
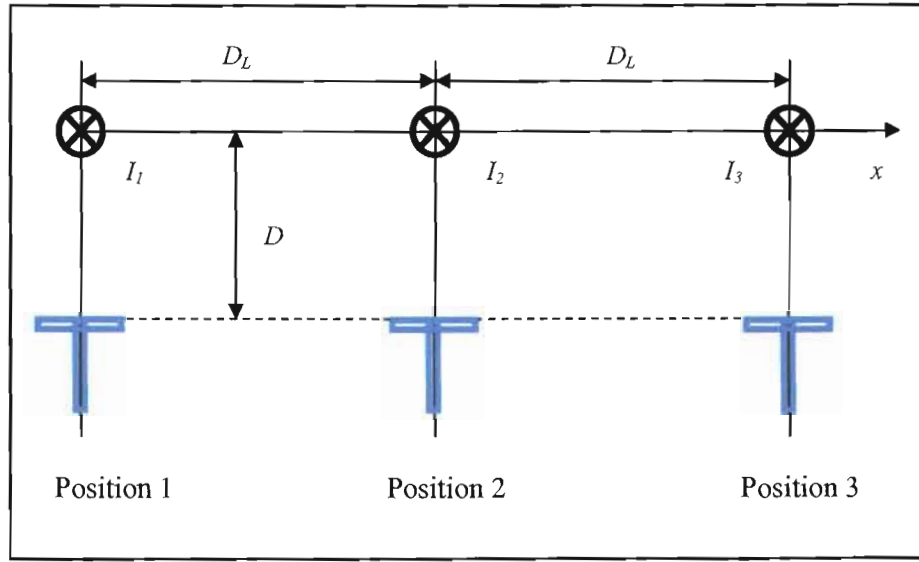
Figure 34 Pickup coil, optimal positioning study

6.3.1.1 The coil under lines 1 or 3

Due to the symmetry the ratio $\mathcal{E}_h/\mathcal{E}_v$ has the same value for either situation: coil under line 1 or line 3. Let us now consider the coil under line1.

$$e_h(t) = e_{h1}(t) + e_{h2}(t) + e_{h3}(t)$$

(6.11)

Using the same derivation as for (4.32):

$$e_{h1}(t) = 0 \tag{6.12}$$

Then:

$$e_{h2}(t) = -k \cdot \ln \frac{\left(D_L + b/2\right)^2 + D^2}{\left(D_L - b/2\right)^2 + D^2} \cos\left(\omega t\right) \tag{6.13}$$

$$e_{h3}(t) = -k \cdot \ln \frac{\left(2D_L + b/2\right)^2 + D^2}{\left(2D_L - b/2\right)^2 + D^2} \cos\left(\omega t + 120^0\right) \tag{6.14}$$

$$e_v(t) = e_{v1}(t) + e_{v2}(t) + e_{v3}(t) \tag{6.15}$$

$$e_{v1}(t) = -2 \cdot k \cdot \ln \frac{D + b/2}{D - b/2} \cos\left(\omega t - 120^0\right) \tag{6.16}$$

$$e_{v2}(t) = -k \cdot \ln \frac{D_L^2 + \left(D + b/2\right)^2}{D_L^2 + \left(D - b/2\right)^2} \cos\left(\omega t\right) \tag{6.17}$$

$$e_{v3}(t) = -k \cdot \ln \frac{\left(2D_L\right)^2 + \left(D + b/2\right)^2}{\left(2D_L\right)^2 + \left(D - b/2\right)^2} \cos\left(\omega t - 120^0\right) \tag{6.18}$$

The analysis of (6.11) to (6.18) results in an impossible straightforward analytical solution for the ratio $\mathcal{E}_h/\mathcal{E}_v$.

Let us assume that: $b = 8$ m, $D = 4$ m and $N_t = 1$. Then for the horizontal positioning:

$$e_{h2}(t) = -314,5 \cdot 1500 \cdot 1 \cdot 250 \cdot 10^{-7} \ln \frac{\left(8,5 + 4\right)^2 + 4^2}{\left(8,5 - 4\right)^2 + 4^2} \cos \omega t = -18,36 \cos \omega t \tag{6.19}$$

$$e_{h3}(t) = -11,78 \cdot \ln \frac{(17+4)^2 + 4^2}{(17-4)^2 + 4^2} \cos\left(\omega t + 120^0\right) = -10,65 \cos\left(\omega t + 120^0\right) \qquad (6.20)$$

$$e_h(t) = 0 - 18,36 \cos \omega t - 10,65 \cos\left(\omega t + 120^0\right) = 15,97 \sin\left(\omega t - 54,74^0\right) \qquad (6.21)$$

Thus:

$$\mathcal{E}_h = 15,97 \ \text{V} \cdot \text{turn}^{-1} \qquad (6.22)$$

For vertical situation:

$$e_{v1}(t) = -23,56 \cdot \ln \frac{4+8}{4} \cos\left(\omega t - 120^0\right) = -25,88 \cos\left(\omega t - 120^0\right) \qquad (6.23)$$

$$e_{v2}(t) = -11,78 \cdot \ln \frac{8,5^2 + (4+4)^2}{8,5^2 + (4-4)^2} \cos\left(\omega t\right) = -7,47 \cos \omega t \qquad (6.24)$$

$$e_{v3}(t) = -11,78 \cdot \ln \frac{(2 \cdot 8,5)^2 + (4+4)^2}{(2 \cdot 8,5)^2 + (4-4)^2} \cos\left(\omega t + 120^0\right) = -2,36 \cos\left(\omega t + 120^0\right) \qquad (6.25)$$

$$e_v(t) = -25,88 \cos\left(\omega t - 120^0\right) - 7,47 \cos \omega t - 2,36 \cos\left(\omega t + 120^0\right)$$

$$e_v(t) = 21,42 \sin\left(\omega t - 71.9^0\right) \qquad (6.26)$$

Thus:

$$\mathcal{E}_v = 21,42 \ \text{V} \cdot \text{turn}^{-1} \qquad (6.27)$$

Now:

$$\mathcal{E}_h/\mathcal{E}_v = 0,745 \tag{6.28}$$

6.3.1.2 The coil under line 2

For the horizontal positioning, the emf induced ($\mathcal{E}_h$) was presented in Chapter 4, paragraph 4.2.2.1 and is:

$$\mathcal{E}_h = \sqrt{3} \cdot k \ln \frac{\left(D_L + b/2\right)^2 + D^2}{\left(D_L - b/2\right)^2 + D^2} \tag{6.29}$$

where k is the same as in (6.9).

Thus:

$$\mathcal{E}_h = 11,78 \cdot \sqrt{3} \cdot \ln \frac{\left(8,5+4\right)^2 + 4^2}{\left(8,5-4\right)^2 + 4^2} = 31,8 \ \text{V} \cdot \text{turn}^{-1} \tag{6.30}$$

For the vertical positioning:

$$e_v(t) = e_{v1}(t) + e_{v2}(t) + e_{v3}(t) \tag{6.31}$$

$$e_{v1}(t) = -k \ln \frac{D_L^2 + (D+b/2)^2}{D_L^2 + (D-b/2)^2} \cos\left(\omega t - 120^0\right) \tag{6.32}$$

$$e_{v2}(t) = -2 \cdot k \cdot \ln \frac{D+b/2}{D-b/2} \cos \omega t \tag{6.33}$$

$$e_{v3}(t) = -k \ln \frac{D_L^2 + (D + b/2)^2}{D_L^2 + (D - b/2)^2} \cos\left(\omega t + 120^0\right) \tag{6.34}$$

$$e_{v1} + e_{v3} = k \ln \frac{D_L^2 + (D + b/2)^2}{D_L^2 + (D - b/2)^2} \cos\omega t \tag{6.35}$$

$$e_v(t) = -k \left[2\ln \frac{D + b/2}{D - b/2} - \ln \frac{D_L^2 + (D + b/2)^2}{D_L^2 + (D - b/2)^2} \right] \cos\omega t \tag{6.36}$$

$$e_v(t) = -k \ln \left[\frac{(D + b/2)^2}{(D - b/2)^2} \cdot \frac{D_L^2 + (D - b/2)^2}{D_L^2 + (D + b)^2} \right] \cos(\omega t) \tag{6.37}$$

$$e_v(t) = 11,78 \ln \left[\frac{8,5^2 + (4 + 8)^2}{8,5^2 + 4^2} \cdot \frac{4^2}{(4 + 8)^2} \right] \cos\omega t = 15,32 \cos\omega t \tag{6.38}$$

Thus:

$$\mathcal{E}_v = 15,32 \text{ V} \cdot \text{turn}^{-1} \tag{6.39}$$

Now:

$$\mathcal{E}_h / \mathcal{E}_v = 2,07 \tag{6.40}$$

Analysing (6.28) and (6.40) gives the results that the optimal position of the coil is under the centre line and horizontal. This agrees along with the simulation results obtained by Holtzhausen and Coetzee (2004); they found that the vertical component of magnetic field is maximum in the area under the central line.

6.3.1.3 Other criteria for positioning the pickup coil

Apart from power transfer criteria, the mechanical aspects should be also addressed. The conclusion from the previous paragraph was that the pickup coil should be centred in relation with the power lines and as close as possible to the plane of the lines. In Figure 35 three levels, 3,5 m apart on vertical, for installing the pickup coil are presented.
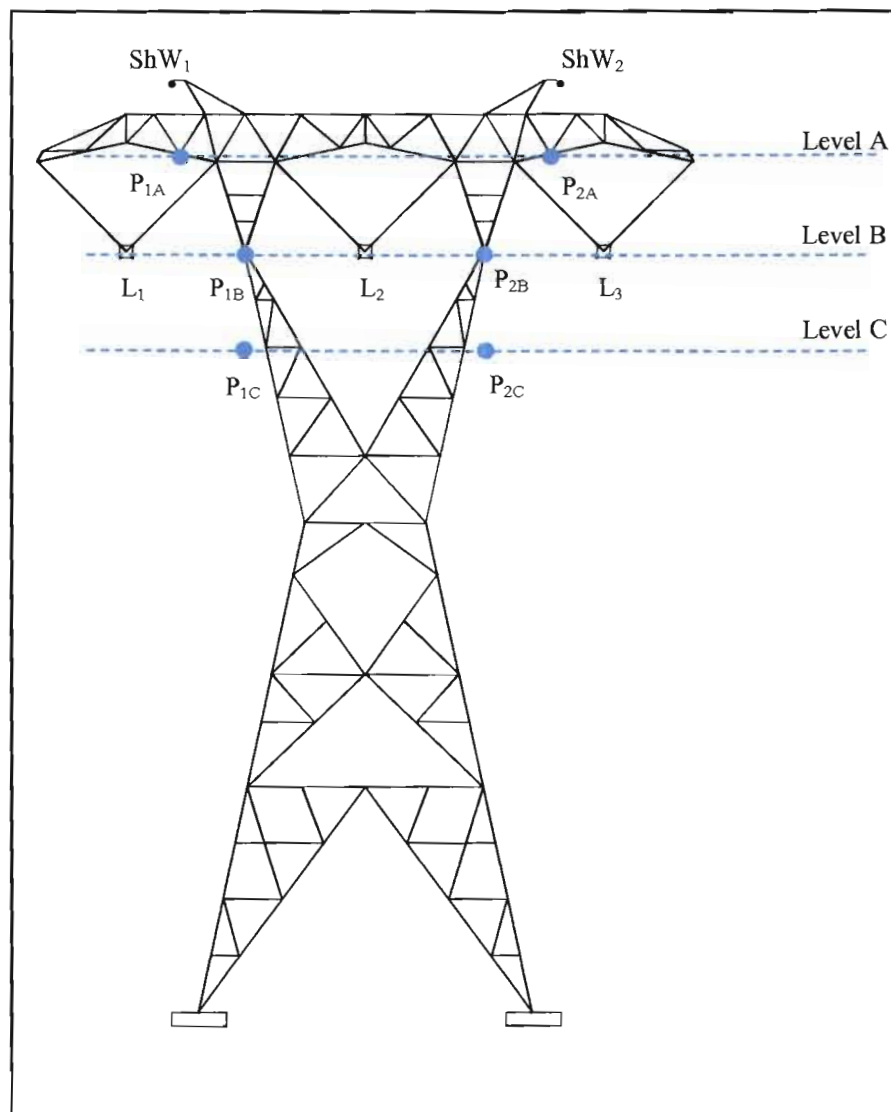
Figure 35 Three possible vertical levels of pickup coil

Level A

When the pickup coil is fixed on the tower at this level, consideration must be given to few aspects such as:

- the coil can have a big width ($b = 13,5$ m) therefore, according to (6.29), the emf will be

$$\mathcal{E} = 11,78 \cdot \sqrt{3} \cdot \ln \frac{(8,5+6,75)^2 + 3,5^2}{(8,5-6,75)^2 + 3,5^2} = 56,55 \text{ V} \cdot \text{turn}^{-1} \qquad (6.41)$$

- being on a very high level, the coil is very susceptible of being struck by lightning
- being above the power lines and in the case of mechanical breakdown, there is a strong possibility that the falling wire of the pickup coil will touch one of the lines and trigger the protection system.

Level B

If hypothetically, the pickup coil is mounted at this level, then;

- the emf induced into the pick up coil, calculated as above for $b = 9$ m, will be:

$$\mathcal{E} = 11,78 \cdot \sqrt{3} \cdot \ln \frac{(8,5+4,5)^2 + 0}{(8,5-4,5)^2 + 0} = 48,09 \text{ V} \cdot \text{turn}^{-1} \qquad (6.42)$$

- the electrostatic influence of the power lines upon the coil is maximal
- in the case of mechanical breakdown of the coil there is still a small possibility the wire thereof will touch the main lines.

Level C

If the pickup coil is mounted at this level, then:

- the emf induced is a little bit smaller than in the two previous cases, and taking $b = 9$ m:

$$\mathcal{E} = 11,78 \cdot \sqrt{3} \cdot \ln \frac{(8,5+4,5)^2 + 3,5^2}{(8,5-4,5)^2 + 3,5^2} = 37,92 \text{ V} \cdot \text{turn}^{-1} \tag{6.43}$$

- the electrostatic influence decreases
- in case of mechanical breakdown of the coil the possibility that the wire will touch the main lines is reduced to almost zero.

Analyzing the above three situations, the first recommendation is that the pickup coil be installed on level C and in this way the dimensions of the coil could defined as: a = 250 m and b = 9 m.

6.3.2 Electrostatic influence

The electrostatic influence of the power line upon the pickup coil is due to the capacitive system that exists. A cross-section area of the system: power lines and pickup coil is presented in Figure 36 as a system of seven conductors.

As was shown in paragraph 3.1.2, the potential in one point of the system follows (3.6):

$$V_i = \frac{1}{2 \cdot \pi \cdot \varepsilon_0} \sum_{j=1}^{N_c} q_j \ln \frac{D_{ij}}{H_{ij}} \tag{6.44}$$

where:

D_{ij} = the distance between conductors i and j

H_{ij} = the distance between conductor i and the image of conductor j

Even if the system has only seven conductors, it is still very difficult to find an analytical solution. A set of simulations using the Quick Field package program has been performed. This package solves an electrostatic problem. The actual evolution of the system is dynamic, therefore the simulation has been performed for a set of points of the power frequency period; a step $\Delta \omega t = 5^\circ$ has been chosen and over a

68

period of 360° a set of 73 simulations have been performed for each conductor of the pickup coil situated on two levels (B and C) as presented in Figure 35.

The initial simulation, with a bundle configuration for the main conductors ended in overloading the computer due to the huge number of nodes of the mesh. Next a successful attempt of simulation was done after the bundle had been replaced with equivalent conductors having geometrical mean radius (GMR) radius (Annexure B: B.4).
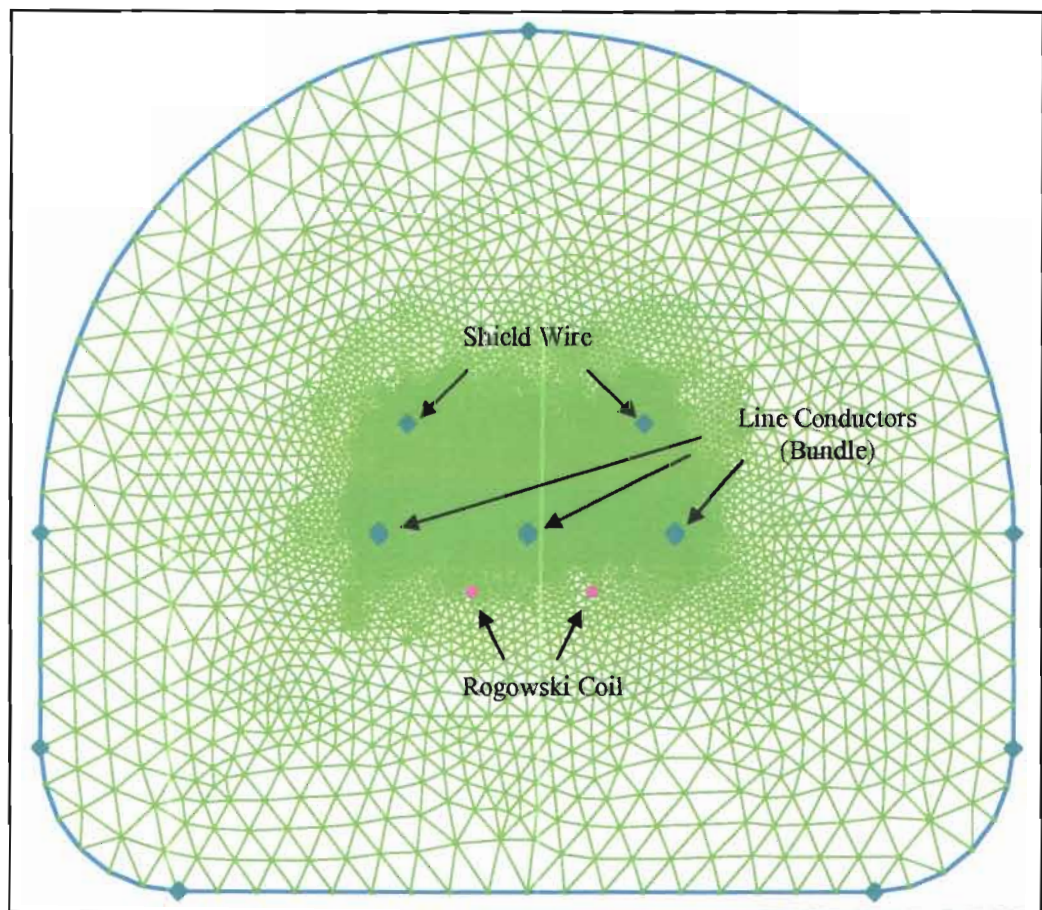
Figure 36 Cross-section of power lines and RCPA, with mesh

The equipotential line distributions around the power lines for a few significant moments: 0°, 30°, 60° and 90° are illustrated in Figures 37, 38, 39 and 40.
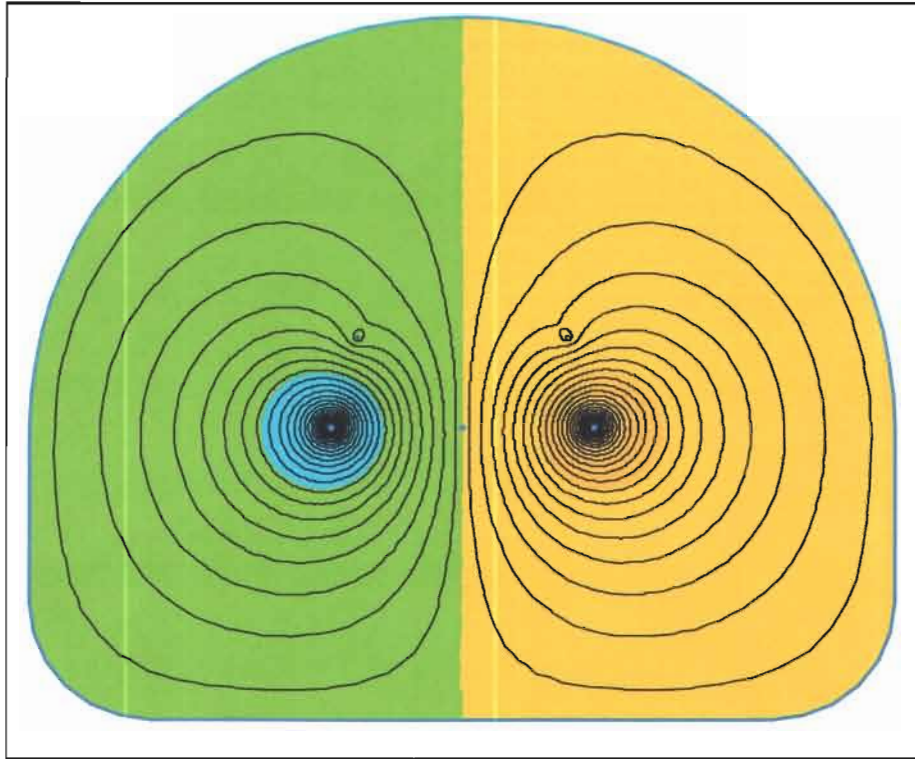
Figure 37 Equipotential distribution for $\omega t = 0^\circ$
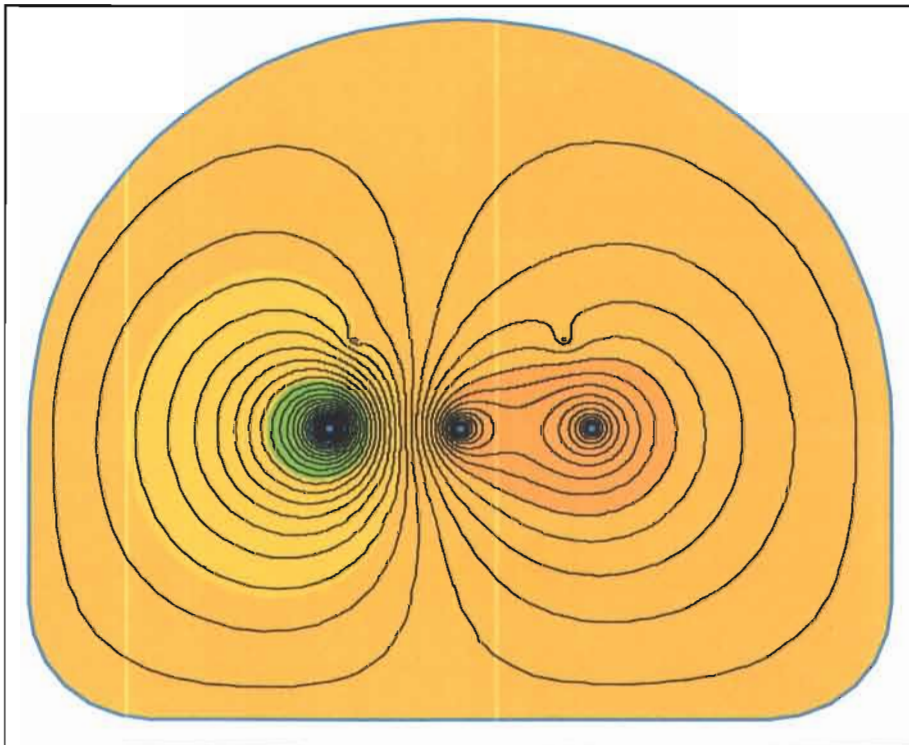
Figure 38 Equipotential distribution for $\omega t = 30^\circ$
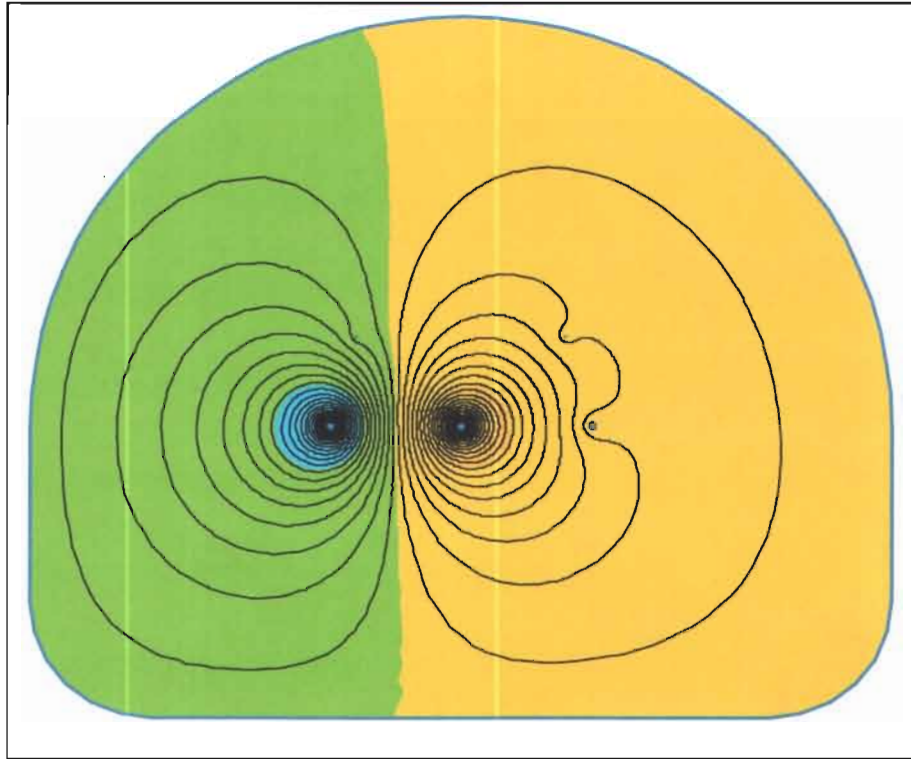
Figure 39 Equipotential distribution for $\omega t = 60°$
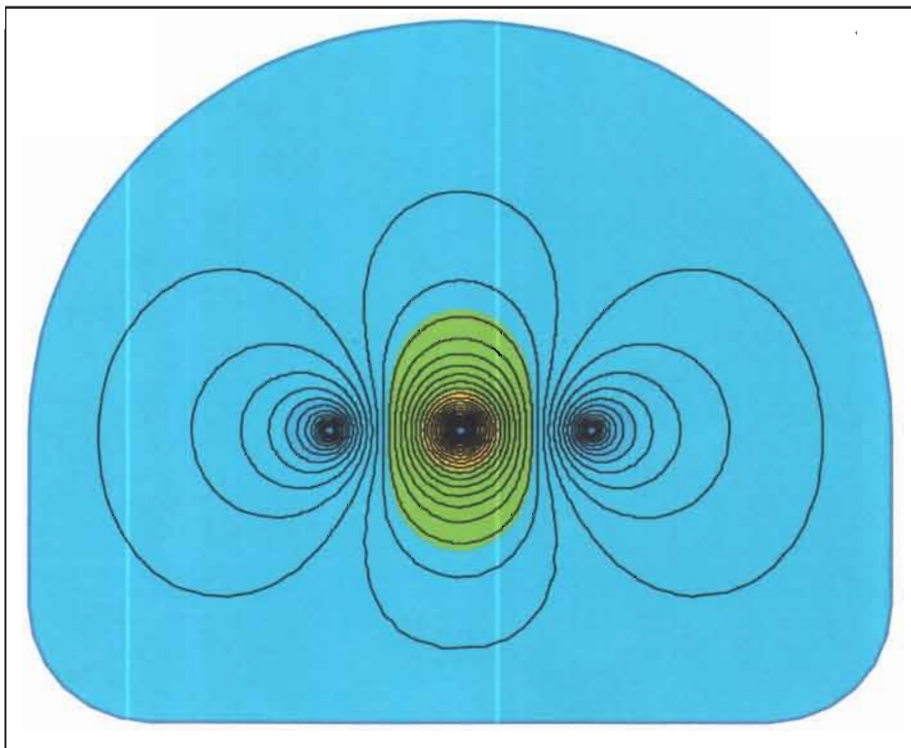
Figure 40 Equipotential distribution for $\omega t = 90°$

The main conclusion of the simulations is that the rms value of the potential on the conductors situated on level B is approximately 50 kV and on level C is approximately 39,8 kV. The profile of the potential on the conductors of the pickup coil situated on level B ($V_{P_{1B}}$ and $V_{P_{2B}}$) is presented in Figure 41 and that for the coil situated on the level C ($V_{P_{1C}}$ and $V_{P_{2C}}$) is presented in Figure 42. The complete set of results is presented in Annexure D.
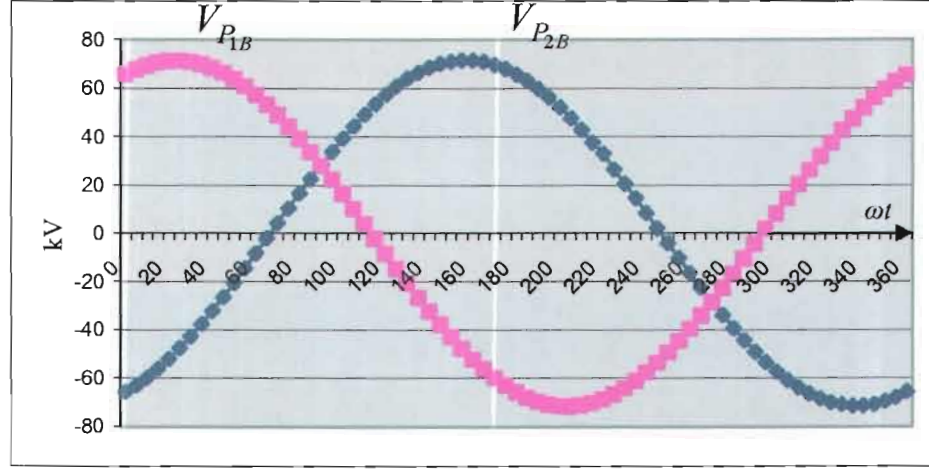
Figure 41 Potential profile for the coil situated on 'level B'
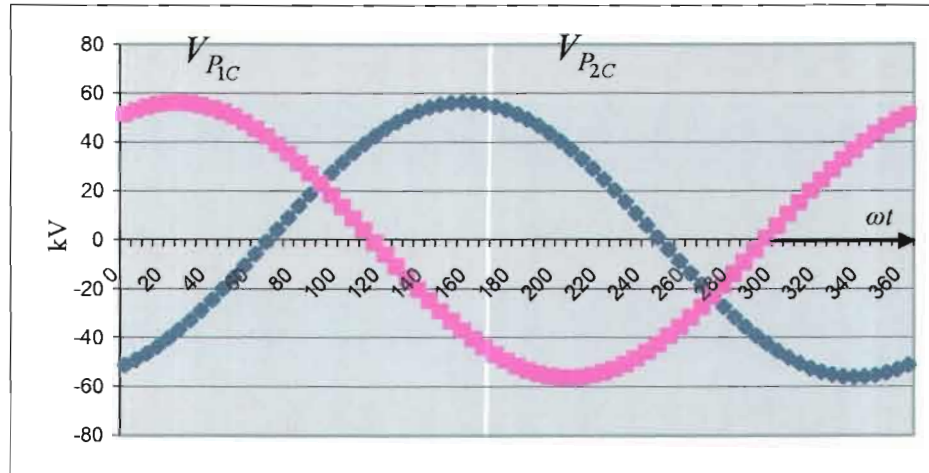
Figure 42 Potential profile for the coil situated on 'level C'

The graphs in Figures 41 and 42 show that potentials on the left and right sides of the pickup coil have the same amplitude but not the same phase. Therefore, current

circulation due to electrostatic influence should be considered. The equivalent model for one turn that takes into consideration this influence is presented in Figure 43, where R_1, R_2, L_1 and L_2 are distributed internal resistance and inductance proportional with sides; i (t) is the current circulation due to electrostatic influence. The main phenomenon of emf induction is not presented yet.
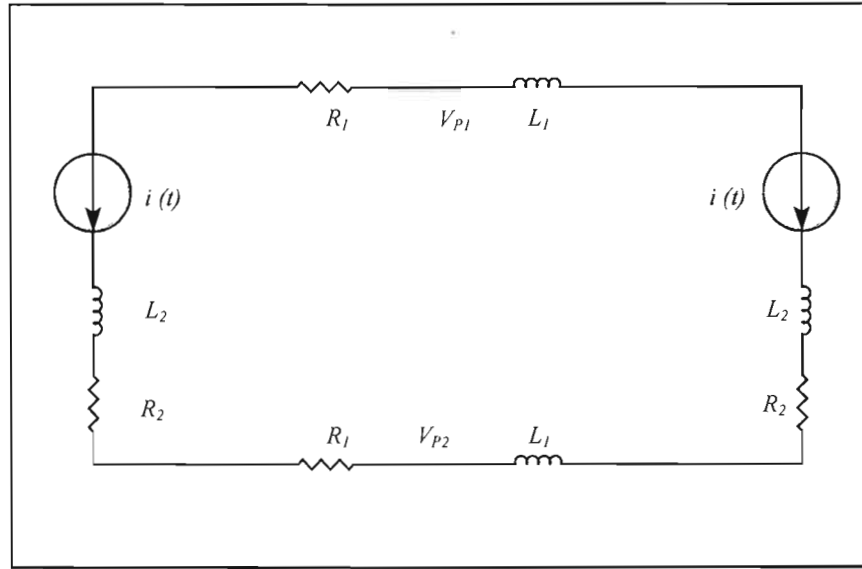
Figure 43 Equivalent model with electric field influence

The current that appears in the transversal side of the pickup coil is created due to the potential difference $V_{P1} - V_{P2}$. Apparently this should be very high, but the potential sources have capacitive internal impedance that is limiting the current to approximately 10,9 mA (Appendix E: E.10) that is much smaller than the nominal current. On the other hand, when the overall current flow through the loop is considered, the effect of these currents is cancelled naturally.

The analysis of the electric field influence arouses the following conclusions:

A - There is not a single point with null potential; neither are there two points with similar characteristics of the induced potential (amplitude and phase) where the pickup coil would have a preferential position for installation.

73

B - On the sides of the pickup coil parallel to the power line a significant potential is induced.

C - On the transversal side there is a variation of potential and therefore a current flow.

D - The isolation transformer should be connected on one of the parallel sides with the power line, preferably in the middle.

E - Not a single point of the pickup coil should be connected to ground. If done like this, a big imbalance in the potential distribution will occur (Walker 2004) and the current flow due to potential induced will not be naturally cancelled.

6.3.3   Proposed solution for Rogowski coil

According to the conclusions of the previous findings the solution proposed for the pickup coil is presented in Figure 44.
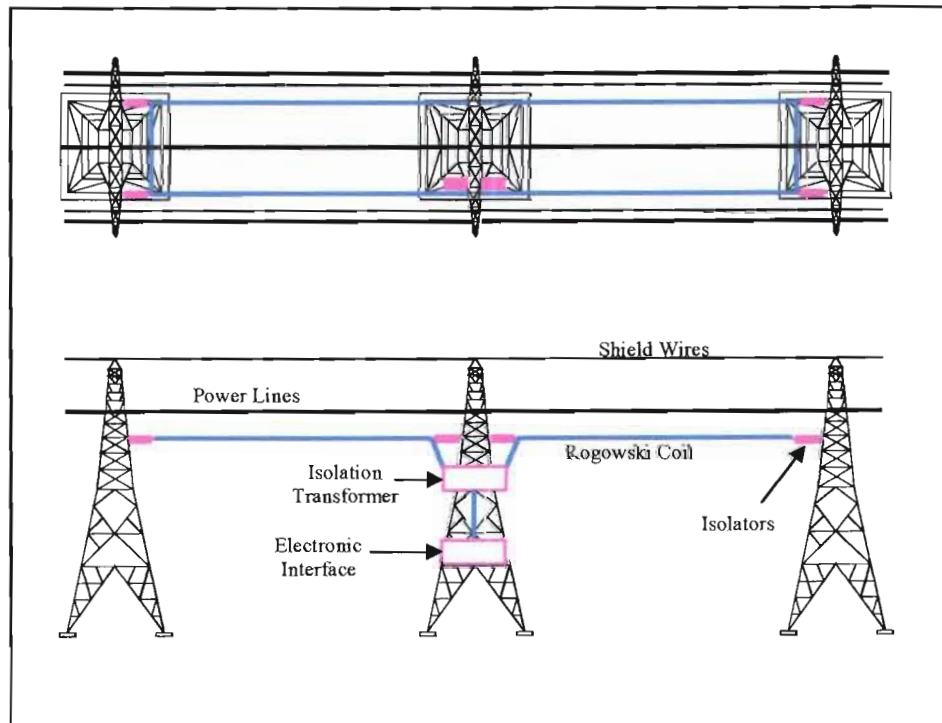
Figure 44 Proposed physical solution for Rogowski coil

In this proposed solution:

- The coil is installed on level C (see Figure 35) at $D = 3,5$ m below the plane of the power line conductors.

- Using two brackets, it could have a width of $b = 9$ m.

- Entire pickup coil should be suspended on classic isolators of approximately 4 m long (see finding E, paragraph 6.3.2); this will also comply with national regulation regarding the distance between any conductor carrying high voltage and grounded metal parts.

- The coil should be installed between three consecutive towers, the middle one having the isolation transformer on one side and a joint box on the other side (according to finding D paragraph 6.3.2). The joint box is necessary due to the long length of coil.

- According to the above points, the length of the pickup coil should be:

  $a = 2 \cdot D_T - 2 \cdot 4$ m

  $a = 492$ m   (6.45)

- For the wiring of the coil, a PVC Cabtyre of 9 cores ($N_t = 9$) of 1,5 mm^2 each is proposed. **Note: for this application another type of insulation material such as silicon UV resistant should be used!**

- The cable should have a steel suspension wire that will be equipped with an isolator to avoid a short circuit loop.

6.3.4   Equivalent model

The equivalent parallel compensated model presented in Figure 45 contains the emf - the source of energy, internal resistance (R_{in}), internal inductance (L_{in}), internal / parasite capacitance (C_p), a compensating capacitor (C_c), isolation transformer (initially considered as ideal and with unity turn-ratio) and load (R_L).

The compensating capacitor is introduced in order to come as close as possible to the requirements of maximum ac power transfer: the maximum power transfer in an ac circuit takes place when the load impedance is equal to the conjugated form of the internal impedance.
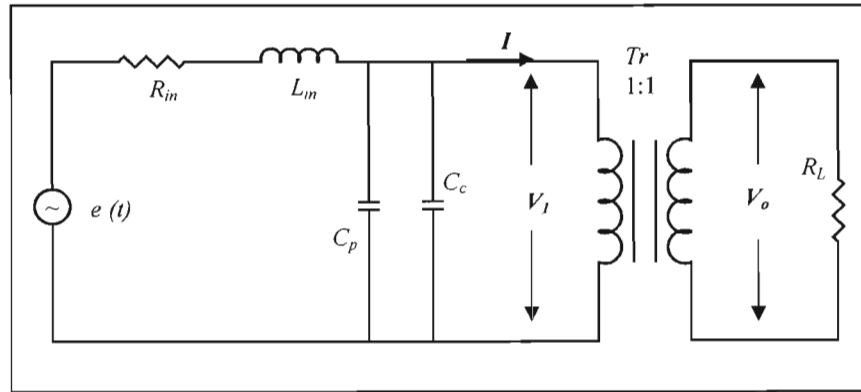
Figure 45 RCPA Equivalent parallel compensated model

A series compensated model is presented in Figure 46.
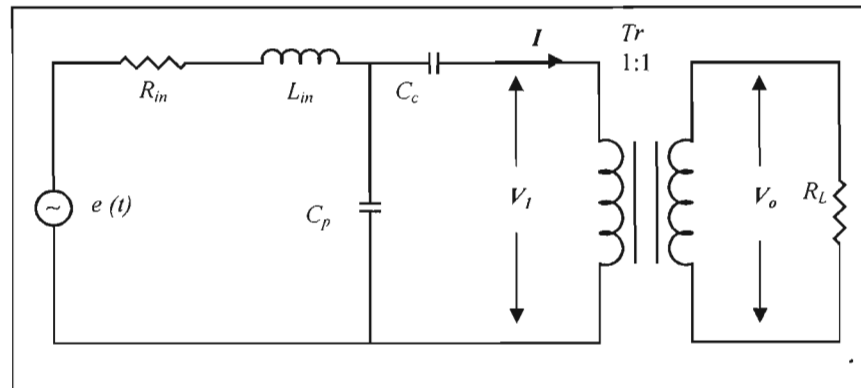
Figure 46 RCPA Equivalent series compensated model

6.3.4.1 Emf

Let us first find the emf induced into the Rogowski coil having the geometrical parameters defined previously in paragraph 6.3.3: $a = 492$ m, $b = 9$ m and $D = 3,5$ m and the number of turns $N_t = 9$. The amplitude of emf induced according to (6.7) - (6.9) is:

$$\mathcal{E} = \sqrt{3} \cdot \omega \cdot I \cdot a \cdot N_t \cdot 10^{-7} \cdot \ln \frac{\left(D_L + b/2\right)^2 + D^2}{\left(D_L - b/2\right)^2 + D^2}$$

$$\mathcal{E} = \sqrt{3} \cdot 2 \cdot \pi \cdot 50 \cdot 1500 \cdot 492 \cdot 9 \cdot 10^{-7} \cdot \ln \frac{\left(8,5 + 4,5\right)^2 + 3,5^2}{\left(8,5 - 4,5\right)^2 + 3,5^2}$$

$$\mathcal{E} = 671,76 \text{ V, or: } \mathcal{E}_{rms} = 475 \text{ V} \tag{6.46}$$

6.3.4.2 Internal resistance

The internal resistance is given by the geometrical parameters of the coil and the material for the conductors, in our case copper with $\rho = 1,72 \cdot 10^{-8}$ $\Omega \cdot$m.

$$R_{in} = \frac{\rho \cdot 2 \cdot \left(a + b\right) \cdot N_t}{\pi \cdot r_o^2} \tag{6.47}$$

$$R_{in} = \frac{1,72 \cdot 10^{-8} \cdot 2 \cdot \left(492 + 9\right) \cdot 9}{1,5 \cdot 10^{-6}}$$

$$R_{in} = 103,4 \ \Omega \tag{6.48}$$

6.3.4.3 Internal inductance

For this size, the Rogowski coil can be considered as a rectangular coil with round wires. The inductance of such a coil and for low frequency is given by Babani (1945:114):

$$L_{in} = 4 \cdot 10^{-7} N_t^2 \left[a \ln \frac{2ab}{r_o \left(a + \sqrt{a^2 + b^2}\right)} + 2\sqrt{a^2 + b^2} + b \ln \frac{2ab}{r_o \left(b + \sqrt{a^2 + b^2}\right)} - \frac{7}{4}\left(a + b\right) \right] \tag{6.49}$$

$$L_{in} = 157,3 \text{ mH} \qquad (6.50)$$

6.3.4.4 Internal capacitance

Internal capacitance between two adjacent turns can be evaluated as in (3.3):

$$C_p = \frac{2 \cdot \pi \cdot \varepsilon_0 \cdot l}{\ln\left(\dfrac{D^2}{r_1 \cdot r_2}\right)} \quad \text{F} \qquad (6.51)$$

With: $r_1 = r_2 = r_o = 0,7 \text{ mm}$

             $D = 2 \cdot r_o + 2 \text{ mm} = 3,5 \text{ mm}$

             $l = 2 \cdot (a+b) = 1002 \text{ m}$

Then:

$$C_p = 17,3 \text{ nF} \qquad (6.52)$$

6.3.4.5 Compensation capacitance

The compensation capacitance (C_c) is calculated from the resonance condition:

$$C_c + C_p = \frac{1}{\omega^2 L_{in}} \qquad (6.53)$$

Substituting (6.49) and (6.51) in (6.53), the value of the compensating capacitance is:

$$C_c + C_p = 64,42 \text{ μF}$$

and: $C_c = 64,4 \text{ μF} \qquad (6.54)$

6.3.5   Estimated power

Let us consider, in the first approximation, that the isolation transformer is ideal and has a turn ratio of one. In this way the load resistance is seen unchanged in the primary with V_1 the voltage across it. If $\mathcal{E}$, V_1 and I (see Figures 45 and 46) are complex phasors, then the active power dissipated on R_L is:

$$P = \mathcal{R}e\,[V_1 \bullet I^*] \tag{6.55}$$

An extended derivation of the active power for parallel and series compensation is presented in Annexure F and the results are:

- For parallel compensated model, the maximum power is 329 W and takes places for $R_L = 55\ \Omega$ (Annexure F: F.12).

- For series compensated model, the maximum power is 545,5 W and takes place for $R_L = 103,4\ \Omega$ (Appendix F: F.21).

The maximum power can be increased by:

- Using a bigger cross-section area of the wire e.g. 2,5 mm^2

- Increasing the number of turns e.g. $N_t = 21$ by using a PVC Cabtyre of seven cores each of 2,5 mm^2 (see Figure 47). The note about isolation material of the cable is still valid.
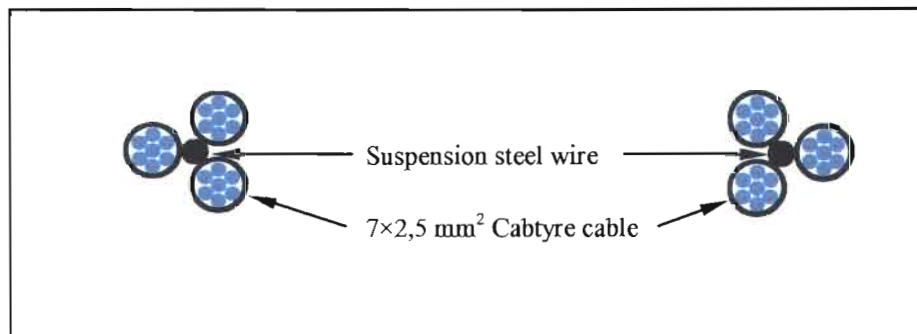
Figure 47 Cross-section of pickup coil

The new parameters in this situation are:

From (6.7) to (6.9): $\mathcal{E}_{rms} = 1108$ V   (6.56)

From (6.47): $R_{in} = 144,8 \ \Omega$ (6.57)

From (6.49): $L_{in} = 0,834$ H   (6.58)

From (6.531): $C_c = 12,1 \ \mu$F   (6.59)

For these new parameters, the maximum power (see Appendix F) is:

- For the parallel compensated model, the maximum power is 1,98 kW and takes place for $R_L = 550 \ \Omega$ (Annexure F: F.13).

- For the series compensated model, the maximum power is 2,12 kW and takes place for $R_L = 144,8 \ \Omega$ (Annexure F: F.21).

6.3.6   Simulation model

Before implementing the above model, it is necessary to validate it via simulations. The parallel compensated simulation model, presented in Figure 48, follows the equivalent model regarding the internal parameters of the pickup coil given by (6.56) - (6.59). For simulation Matlab 6 was used.
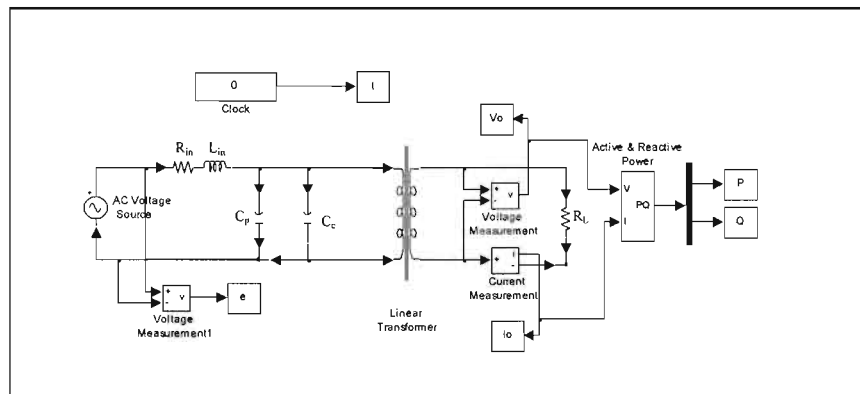
Figure 48 RCPA simulation – parallel compensated model

for $R_L = 550\ \Omega$ and series compensated in Figure 52 with $P_{max} = 2117$ W for $R_L = 145\ \Omega$.
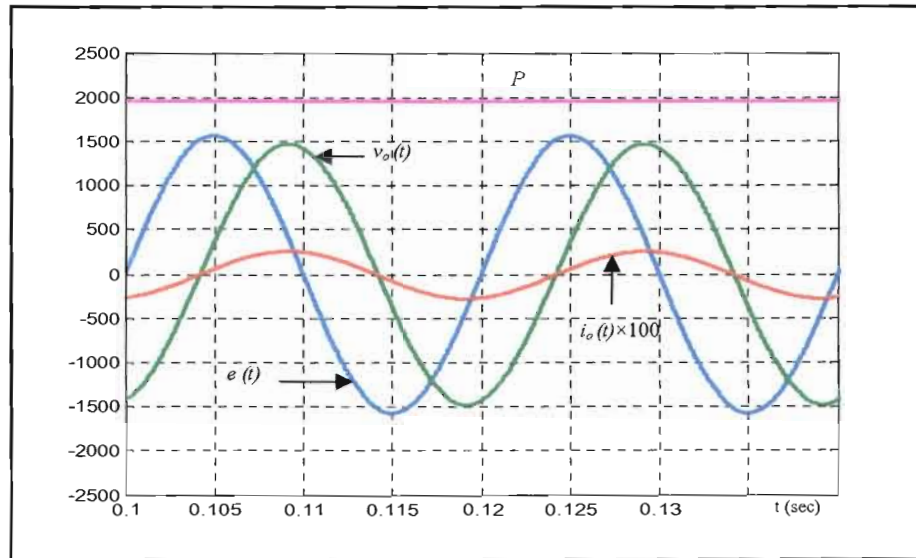
Figure 51 Simulation results – parallel compensated pickup coil
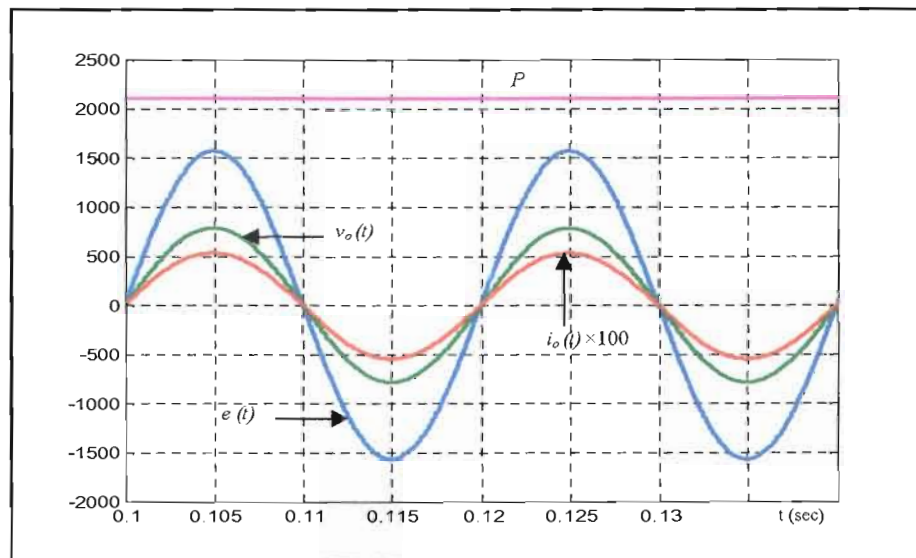
Figure 52 Simulation results – series compensated pickup coil

The results of the simulations validate the calculus.

For further investigation, the case of a pickup coil of 21 turns with 2,5 mm^2 wires and parameters (6.57) to (6.59) series compensated will be considered. This solution can deliver a power of 2,12 kW as presented above.

Another positive aspect for the series compensated solution is that all parameters are in phase and the reactive power is reduced to nothing.

6.3.7 Other parameters that affect the output power

One of the basic assumptions (paragraph 6.2) was that all the conductors were straight and parallel. However this can not be achieved due to various factors.

6.3.7.1 Mechanical tension

The weight of the conductors and the limited mechanical tension in the steel suspension create sag. The tension is limited by the strength characteristics of the steel wire but also by the strength of the insulators that suspend the pickup coil.

It is recommended, if possible, that the tension in the suspension steel wire should be such that the sag of the Rogowski coil matches the sag of power line conductors. This requires a further study of the pickup coil from the mechanical point of view, including the implications of using aluminium as conductor wire.

6.3.7.2 Temperature

The temperature is another important parameter that affects the status of the conductors. Dilatation/contraction is the direct effect of temperature upon the conductors. It should be noticed that both sets of conductors of the power line and of the pickup coil are affected in the same direction.

But a difference in temperature coefficients of the two types of conductors that create a difference in sag; this will be translated as a decrease of induced emf.

Even if the dilatation/contraction coefficients are very close, there is still a difference in the resistance temperature coefficient that will be translated as an increase/ decrease of the internal resistance of the pickup coil and accordingly in the maximum power transferred.

6.3.7.3 Wind

The wind will create a slow movement of the conductors. Because of the difference in the effective area of the two types of conductors, the pickup coil will lose the central position in relation to power line conductors and this will be translated as a decrease of induced emf.

6.3.7.4 Rain and ice

The rain and ice will modify the specific weight of both sets of conductors but in different ways. This will be translated as a difference in sag and consequently in a decrease of induced emf.

6.3.7.5 Voltage regulation

As shown in Chapter 4, paragraph 4.2.2.1 and equation (4.31) the emf induced into the Rogowski coil is directly dependent on the current flowing through the main power lines. But this current fluctuates according to load demand in the supply system and the variation could be significant, so the emf induced and the power capability of Rogowski coil would be affected.

Up to a certain extent this could be addressed by the voltage regulation system implemented for RCPA.

6.4 Isolation Transformer

The initial assumption (paragraph 6.3.4) that an isolation transformer is ideal and with unity turn-ratio was done to simplify the evaluation of power transferred to the load.

The transformer's requirements for this application are:

- The turn-ratio should be 1:2 in order to reduce the input voltage of approximately 1100 V_{rms} to a range that is much easier to be handled by the semiconductor interface (static switch).
- The rated power should be over-designed so that the magnetic core window accommodates extra-insulation; this has to isolate the primary of around 40 kV potential from the secondary that is one leg ground connected.
- The diameter of wires used for primary and secondary should be also over-rated in order to decrease the copper losses.
- The iron core lamination should also be carefully chosen to decrease the iron losses.

Meeting all the above requirements should result in a greater reliability.

6.4.1 Rated power

The estimated maximum active power (paragraph 6.3.5) that can be delivered by the Rogowski coil is 2,12 kW. This power was determined as fundamental. But, as presented in paragraph 4.2.1.2, the emf induced in the Rogowski coil is very much affected by the distortions in the main power line current and the Total Harmonic Distortion (THD) could be in the range of 10 to 20 percent; let us take the conservative figure of 20 percent.

When apparent power is estimated, a 0.8 power factor (PF) for the load it should be also considered.

The apparent power then will be:

$$S = P\sqrt{1 + \left(1 - PF^2\right) + THD^2} \quad \text{VA} \tag{6.60}$$

$$S = 2,12 \cdot \sqrt{1 + \left(1 - 0,8^2\right) + 0,2^2} = 2,97 \quad \text{kVA} \tag{6.61}$$

For further calculations, the apparent power will be:

$$S = 3 \text{ kVA} \tag{6.62}$$

6.4.2 Cross-section area

Knowing the rated power of 3 kVA the transformer should handle as well as the input and output voltages, the design to establish the cross-section area(of the transformer) can be initiated. The area-product A_p (Umanand & Bhat 1992: 18 and McLymann 1978: 106) is given by:

$$A_p = A_c \cdot A_w = \frac{S(1 + 1/\eta)}{4 \cdot K_f \cdot B_m \cdot J \cdot K_w \cdot f} \quad \text{m}^4 \tag{6.63}$$

Where:
- A_c = core iron area in m^2
- A_w = window area in m^2
- S = rated power in VA
- η = efficiency of the transformer of approximately 0,95
- K_f= form factor is 1,11 for sine wave

- B_m = allowed maximum flux density with values between 1,1 and 1,4 Tesla
- J = current density in A·m^{-2} with values of 3 to 5 ×10^6 A·m^{-2}
- K_w = window utilization factor with values of 0,3 to 0,4
- f = operating frequency, in this situation, is 50 Hz

Let us consider a magnetic circuit with a square core area and geometric form as presented in Figure 53.
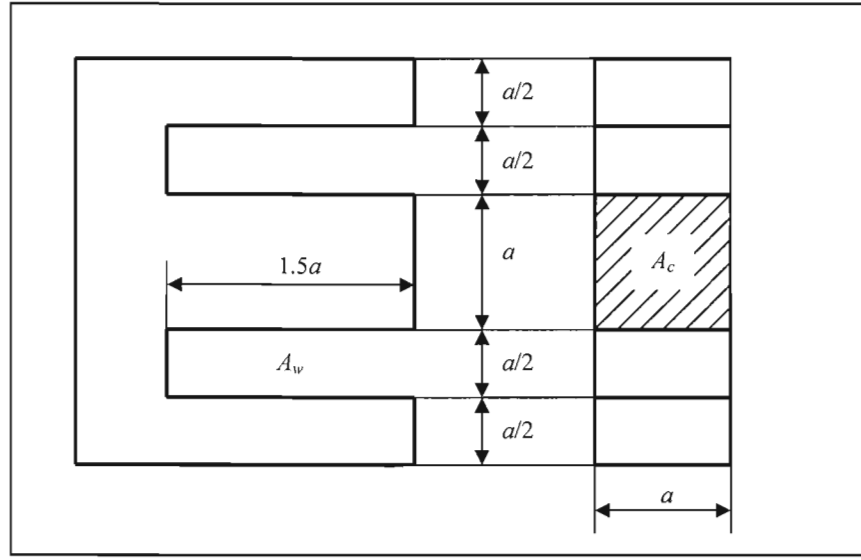
Figure 53 Transformer lamination - geometric form

As in Figure 53:

$$A_c = a^2 \tag{6.64}$$

$$A_w = 1,5 \cdot a \cdot 0,5 \cdot a = 0,75 \cdot a^2 \tag{6.65}$$

Then:

$$0,75 \cdot a^4 = \frac{3 \cdot 10^3 \left(1 + 0,95^{-1}\right)}{4 \cdot 1,11 \cdot 1,1 \cdot 3 \cdot 10^6 \cdot 0,3 \cdot 50}$$

$$a = \sqrt[4]{\frac{3 \cdot 10^3 \left(1 + 0,95^{-1}\right)}{4 \cdot 1,11 \cdot 1,1 \cdot 3 \cdot 10^6 \cdot 0,3 \cdot 50 \cdot 0,75}} = 0,078 \ \mathrm{m} \tag{6.66}$$

$$A_c = 61 \cdot 10^{-4} \ \mathrm{m}^2 \tag{6.67}$$

6.4.3   Number of turns

Knowing the core area A_c and the voltage, the number of turns in primary and secondary can be determined. The equation that bound these parameters (Marshall et al. 1996: 454, Umanand & Bhat 1992: 15 and McLymann 1978: 125) is:

$$V = 4,44 \cdot N \cdot f \cdot B_m \cdot A_c \tag{6.68}$$

where:

$$V = \begin{cases} V_1 = 1108 \ \mathrm{V}; \ \text{primary voltage} \\ \\ V_2 = 550 \ \mathrm{V}; \ \text{secondary voltage} \end{cases}$$

N = the number of turns in primary (N_1) or secondary (N_2)

6.4.3.1   The number of turns in primary:

$$N_1 = \frac{V_1}{4,44 \cdot f \cdot B_m \cdot A_c} = \frac{1108}{4,44 \cdot 50 \cdot 1,1 \cdot 61 \cdot 10^{-4}} \simeq 744 \ \text{turns} \tag{6.69}$$

6.4.3.2   The number of turns in secondary:

$$N_2 = \frac{V_2}{4,44 \cdot f \cdot B_m \cdot A_c} = \frac{550}{4,44 \cdot 50 \cdot 1,1 \cdot 61 \cdot 10^{-4}} \simeq 369 \ \text{turns} \tag{6.70}$$

Another three identical windings are added in the secondary in order to provide an auxiliary supply for electronics and for the driver of the static switch. The auxiliary (V_a) voltage provided by each winding should be 15 V_{rms}. Then:

$$N_3 = N_4 = N_5 = \frac{V_a}{4,44 \cdot f \cdot B_m \cdot A_c} = \frac{15}{4,44 \cdot 50 \cdot 1,1 \cdot 61 \cdot 10^{-4}} \simeq 10 \text{ turns} \qquad (6.71)$$

6.4.4 Wire size

The diameter of the wire (d) is determined from:

$$\frac{\pi \cdot d^2}{4} = \frac{I}{J} = \frac{S}{J \cdot V}$$

6.4.4.1 Primary wire size

$$d_1 = \frac{4 \cdot S}{\pi \cdot J \cdot V_1} = \frac{4 \cdot 3000}{\pi \cdot 3 \cdot 10^6 \cdot 1108} \simeq 1,2 \text{ mm} \qquad (6.72)$$

6.4.4.2 Secondary wire size

$$d_2 = \frac{4 \cdot S}{\pi \cdot J \cdot V_1} = \frac{4 \cdot 3000}{\pi \cdot 3 \cdot 10^6 \cdot 550} \simeq 2,4 \text{ mm} \qquad (6.73)$$

For auxiliary windings a wire of 0.5 mm diameter is recommended.

6.4.5 Internal resistance

The internal resistance, primary and secondary, depend on the geometrical parameters such as wire diameter (d_1 and d_2) and medium length turn (MLT), wire

material: in our case copper with $\rho = 1,72 \cdot 10^{-8}$ $\Omega \cdot$m, number of turns (N_1 and N_2) and is given by:

$$R = \frac{4 \cdot \rho \cdot N \cdot MLT}{\pi \cdot d^2} \quad \Omega \tag{6.74}$$

where medium length turn (McLymann, 1978: 119) is:

$MLT = 0,448$ m

6.4.5.1 Primary internal resistance

$$R_1 = \frac{4 \cdot \rho \cdot N_1 \cdot MLT}{\pi \cdot d_1^2} = \frac{4 \cdot 1,72 \cdot 10^{-8} \cdot 744 \cdot 0,448}{\pi \cdot 1,2^2 \cdot 10^{-6}} = 5,07 \ \Omega \tag{6.75}$$

6.4.5.2 Secondary internal resistance

$$R_2 = \frac{4 \cdot \rho \cdot N_2 \cdot MLT}{\pi \cdot d_2^2} = \frac{4 \cdot 1,72 \cdot 10^{-8} \cdot 369 \cdot 0,448}{\pi \cdot 2,4^2 \cdot 10^{-6}} = 0,628 \ \Omega \tag{6.76}$$

6.4.6 Copper losses

The copper losses can be written as:

$$P_{cu} = R_1 \cdot I_1^2 + R_2 \cdot I_2^2 \quad W \tag{6.77}$$

$$I_1 = \frac{S}{V_1} = \frac{3000}{1108} = 2,71 \ A$$

$$I_2 = \frac{S}{V_2} = \frac{3000}{550} = 5,45 \text{ A}$$

$$P_{cu} = 5,07 \cdot 2,71^2 + 0,628 \cdot 5,45^2 \text{ W}$$

$$P_{cu} = 56 \text{ W} \tag{6.78}$$

6.5   Static switch

The static switch is used to regulate the output voltage that can vary owing to the main line current and load modifications. The basic configuration is presented in Figure 54.
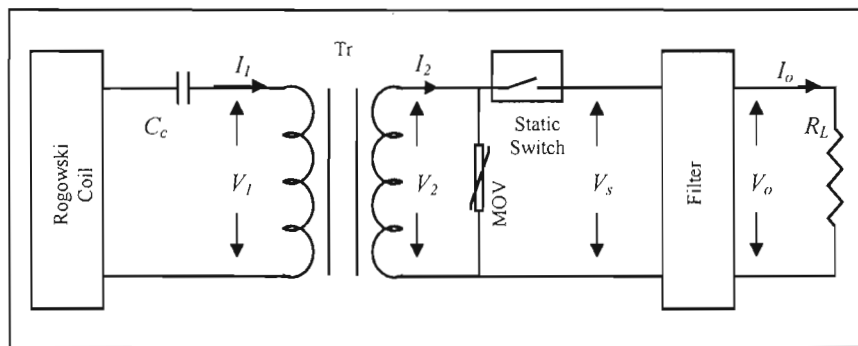
Figure 54 ac regulation – basic model

6.5.1   Switch requirements

The switch used in this application should comply with the following requirements:

- It should be able to operate with both voltage polarities: positive and negative, in other words to be a bipolar switch.

- In the ON situation, it should be able to handle twice the maximum current estimated for the load, e.g. 11 A.

- In the OFF situation it should be able to sustain the maximum voltage of around 1000 V across it.

- It should be able to operate at frequencies between 1 kHz and 10 kHz depending on the control method.

6.5.2   Switch topology

The topology considered to comply with the above requirements is presented in Figure 55 (Rashid 1988: 465). The use of only one switch and consequently one driving circuit is the main advantage of this topology. As controlled switching element, an IGBT was considered to be much more suitable for this application.
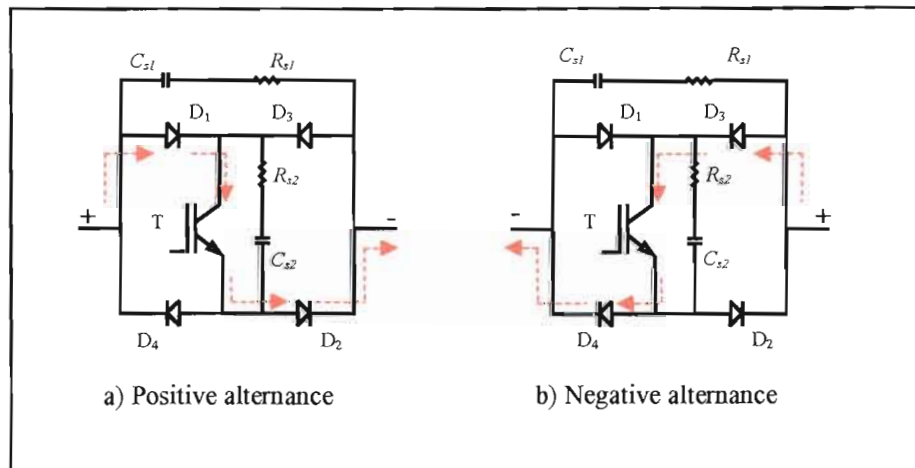
Figure 55 ac static switch topology

The snubbers C_{s1}, R_{s1} and C_{s2}, R_{s2} are needed to minimize the stress in the semiconductor devices (diodes or transistor) due to switching operation.

6.5.2.1 Operation

When the switch (T) is ON during the positive alternance, the current flow takes place through D_1, T and D_2 and during the negative alternance the current flow takes place through D_3, T and D_4.

When the switch is OFF, irrespective of the alternance, the cross-over voltage is sustained by the breakdown voltage of one diode in reverse polarity.

6.5.2.2 Choice of semiconductor devices

The choice of the semiconductor devices is done using the main parameters: voltage and current.

From the current point of view, all devices have to sustain the same type of current. If ideally all the 2,12 kW power is transferred to the secondary of the transformer, then the peak value of the current ($\hat{I}_2$) should be:

$$\hat{I}_2 = \sqrt{2}\frac{S}{V_2} = 7,72 \text{ A} \tag{6.79}$$

Then, taking a safety coefficient of 4, the average sustainable current through semiconductor devices should be 20 A.

From the voltage point of view, one diode in reverse polarity has to sustain the entire voltage when the transistor is OFF. Therefore, the maximum voltage in reverse polarity is $550 \times \sqrt{2} = 778$ V. Taking a safety coefficient of 1,5, the maximum breakdown voltage for the diode should be 1200 V.

The polarity of the voltage across the diode does not change with the switching frequency, but with main frequency of 50 Hz and therefore a standard recovery diode

In this application, the switch has to handle inductive loads and therefore a snubber circuit (R_{s2} and C_{s2}) across the transistor is used. The optimum effect (Mohan et al. 1989: 523) is achieved when:

$$C_{s2} = \frac{\hat{I}_2 \cdot t_f}{2 \cdot V_d} \text{ F}$$

(6.82)

where:

$\hat{I}_2$ = peak current through the switch

t_f = the falling switching time of the transistor

V_d = operating voltage, in this case 778 V

$$C_{s2} = \frac{7,72 \cdot 140 \cdot 10^{-9}}{2 \cdot 778} = 0,68 \cdot 10^{-9} \text{ F}$$

(6.83)

The snubber resistor, R_{s2}, is recommended (Mohan, 1989: 620) to be:

$$R_2 = \frac{V_d}{0,2 \cdot \hat{I}_2} = \frac{778}{0,2 \cdot 7,72} \approx 510 \ \Omega$$

(6.84)

6.5.4   Switch losses

6.5.4.1 Losses in diodes

The losses in diodes (P_d) are mainly due to forward conduction. When the diode is in the forward polarisation, the current has a sinusoidal-chopped shape. The sinusoid has the main frequency (f_o). For covering the worst case, the switching frequency (f_s) should be considered 10 kHz with an average duty-cycle (δ) of 50 percent. Then:

95

$$P_d = f_o \cdot \left[\int_0^{T_o} V_F \cdot \left(f_s \cdot \int_0^{T_s} \hat{I}_2 \cdot \sin \omega_o t \cdot \delta \cdot dt \right) \cdot dt \right] \text{ W} \qquad (6.85)$$

Because $\delta \cdot T_s << T_o$, the term $\sin \omega_o t$ can be considered constant for the inner integral and:

$$P_d = f_o \cdot \left(\int_0^{T_o/2} V_F \cdot \delta \cdot \hat{I}_2 \cdot \sin \omega_o t \cdot dt \right) \text{ W}$$

$$P_d = \frac{\delta}{\pi} \cdot V_F \cdot \hat{I}_2 \text{ W} \qquad (6.86)$$

Substituting the parameters of (6.84) with appropriate values, the power loss is:

$$P_d = \frac{0,5}{\pi} \cdot 0,9 \cdot 7,72 = 1,1 \text{ W} \qquad (6.87)$$

6.5.4.2 Losses in transistor

The losses in transistor cannot be evaluated entirely analytically due to the switching ON and OFF. A general accepted way to determine the power loss is to use the catalogue data of energy loss during switching ON and OFF; the conduction loss can be determined analytically and is recommended to be done in the worst conditions with voltage and current at maximum values.

$$P_t = f_s \cdot \left(E_{ON} + E_{cond} + E_{OFF} \right) \text{ W} \qquad (6.88)$$

where:

E_{ON} = turn ON switching energy loss = 0,95 mJ (Annexure H)

E_{OFF} = turn OFF switching energy loss = 1,15 mJ (Annexure H)

E_{cond} = energy loss in the transistor during ON period

f_s = switching frequency

$$E_{cond} = \delta \cdot T_s \cdot V_{ce-sat} \cdot \hat{I}_2 = 0,5 \cdot 10^{-4} \cdot 3,1 \cdot 7,72 = 1,2 \cdot 10^{-3} \text{ J} \tag{6.89}$$

$$P_t = 10^4 \cdot (0,95 + 1,2 + 1,15) \cdot 10^{-3} = 33 \text{ W} \tag{6.90}$$

It has to be noticed that the result is higher than actual power loss.

6.5.5 Heat-sink

The heat-sink has to transfer the thermal energy dissipated on the semiconductor device to the air, maintaining the junction temperature to acceptable levels below the maximum temperature given by the manufacturer.

The generally accepted relation between power dissipated on a semiconductor device, junction temperature, ambient temperature, intrinsic thermal parameters of the device and heat-sink thermal resistance (Lander 1993:26, Krein 1998:476, Rashid 1988:593) is:

$$T_j = P_D \cdot \left(R_{th-jc} + R_{th-cs} + R_{th-sa} \right) + T_a \tag{6.91}$$

$$R_{th-sa} = \frac{T_j - T_a}{P_D} - \left(R_{th-jc} + R_{th-cs} \right) \text{ }^\circ\text{C/W} \tag{6.92}$$

where:

T_j = junction temperature

T_a = ambient temperature

P_D = power dissipated on the semiconductor device

R_{th-jc} = thermal resistance junction to case

R_{th-cs} = thermal resistance case to sink

R_{th-sa} = thermal resistance sink to air

6.5.5.1 Diodes heat-sink

The imposed parameters are junction temperature of 105 °C and ambient temperature of 40 °C. If all four diodes are mounted on the same heat-sink, then the total power dissipated will be 4,4 W.

$$R_{th-sa} = \frac{105-40}{4,4} - (1,3+0,5) = 12,9 \ °C/W \qquad (6.93)$$

6.5.5.2 Transistor heat-sink

$$R_{th-sa} = \frac{105-40}{33} - (1,2+0,24) = 0,53 \ °C/W \qquad (6.94)$$

6.6 Filter

Figure 56 shows the switched voltage (v_s) when the switch is used with fixed frequency and variable duty-cycle (1 kHz and 50 percent for this illustration).
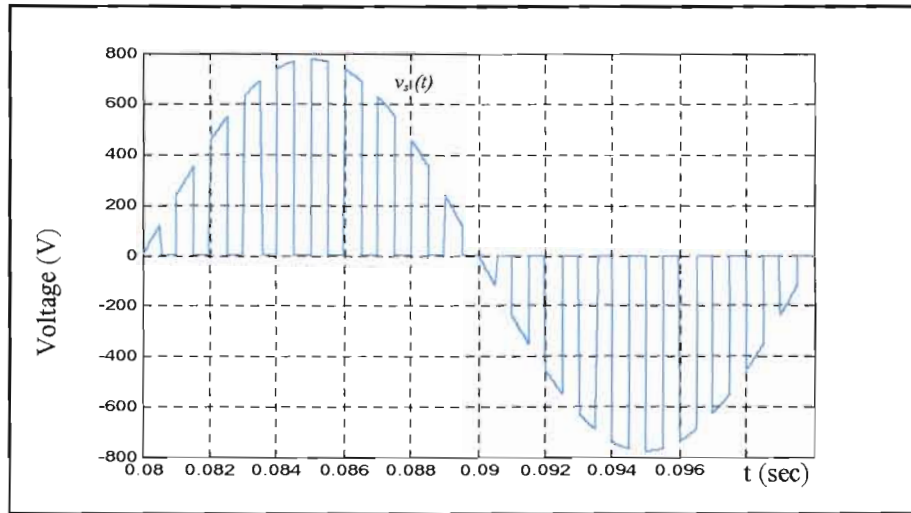
Figure 56 Switched voltage (V_s)

When written in Fourier series, the switched voltage generates a lot of harmonics:

$$v_s(t) = \delta \cdot \hat{V}_2 \cdot \sin \omega_o t + \frac{\hat{V}_2}{\pi} \times \sum_{1}^{\infty} \left\{ \frac{\sin n\delta\pi}{n} \times [\sin(\omega_o + n\omega_s)t + \sin(\omega_o - n\omega_s)t] \right\} \qquad (6.95)$$

98

The purpose of the filter is to retain only the fundamental. From (6.95) it is very clear now that the output voltage, after the filtering, will depend on the duty-cycle (δ).

An LC filter is considered for this application. The main characteristics of this filter should be:

- To cut harmonics as a low pass filter, the cut-off frequency should be lower than switching frequency but higher than operating frequency of 50 Hz.
- The cut-off frequency should not coincide with any of the main frequency harmonics, e.g. 630 Hz.
- The voltage drop across the filter should be as small as possible.

Then:

$$L_f \cdot C_f = \left(2\pi f_f\right)^{-2} \tag{6.96}$$

where:

L_f = filter inductance

C_f = filter capacitance

f_f = cut-off frequency

$$L_f \cdot C_f = \left(2 \cdot \pi \cdot 630\right)^{-2} \cong 64 \cdot 10^{-9} \tag{6.97}$$

Thus:

$$L_f = 20 \cdot 10^{-3} \ \text{H} \tag{6.98}$$

$$C_f = 3,3 \cdot 10^{-6} \ \text{F} \tag{6.99}$$

The filtered output voltage for a 1 kHz switching frequency is presented in Figure 57. As one can notice, the ripple of the voltage is relatively high and therefore a higher switching frequency should be considered.
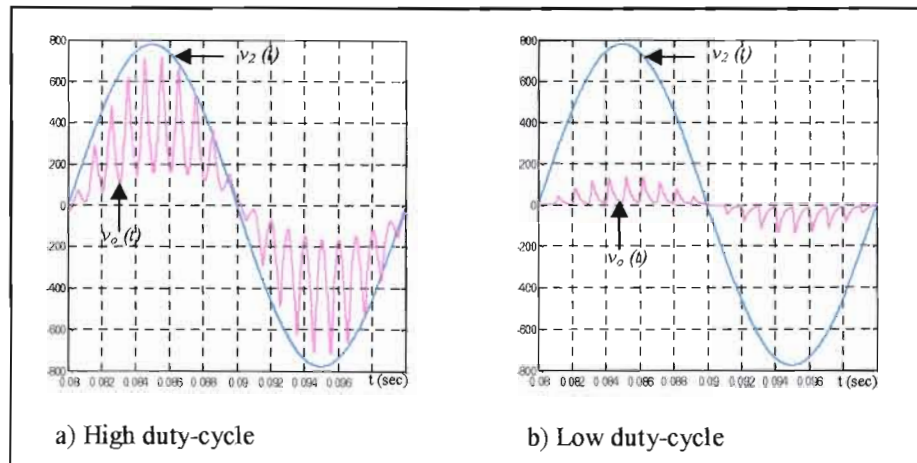
Figure 57 Filtered output voltage for 1 kHz switching frequency

The basic situation as above but with 10 kHz switching frequency is presented in Figure 58.
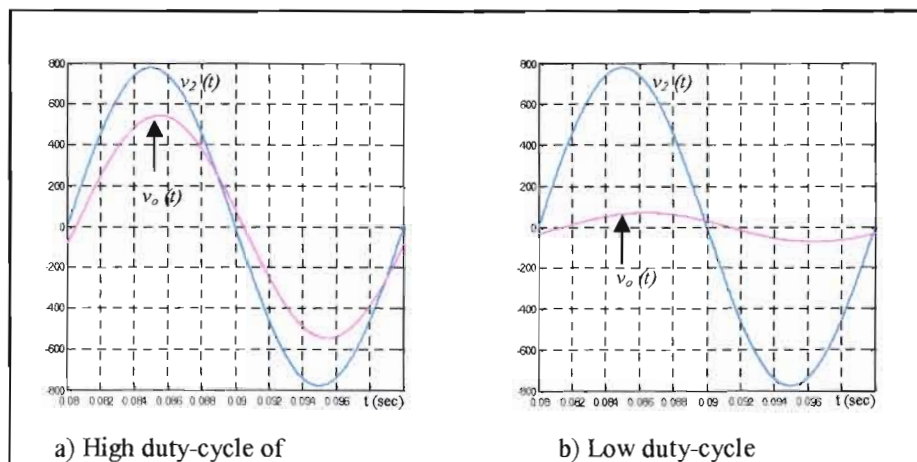
Figure 58 Filtered output voltage for 10 kHz switching frequency

It is obviously an improvement in output voltage waveform for a higher switching frequency, but there is also noticeable a phase shift; this improvement comes with an increase in the power loss into the switch. Therefore the switching frequency will be a compromise between output voltage quality, thermal regime of the switch and the type of control for the output voltage.

6.7   Control system

The control system that includes the switch and low-pass filter has the aim of controlling/regulating the output voltage. The basic diagram of the control system is presented in Figure 59.
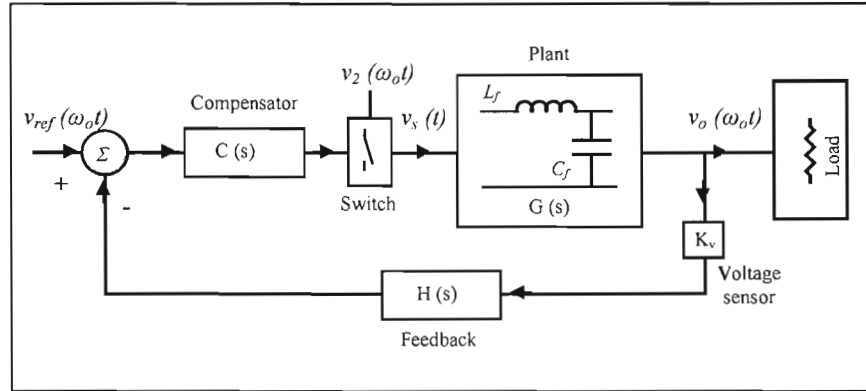
Figure 59 RCPA – control system

Two control methods have been considered for this application:

•   **Fixed frequency with variable duty-cycle.** As presented in paragraph 6.6, Figures 57 and 58, this method provides very good results for higher switching frequency. But together with good quality of output voltage come a high thermal stress on the semiconductor device acting as switch.

From the point of view of electromagnetic interference, this method presents the disadvantage that a large part of switching energy is concentrated in one spectral line that is the switching frequency (f_s). And the higher the switching frequency is the stronger is the unwanted electromagnetic field created due to switching.

A low switching frequency implies another design of the filter in order to improve the quality of output voltage. But also implies a review of the switch itself that will further complicate the driving circuitry. The switch proposed in paragraph 6.5 with topology in Figure 55 does not have a very good direct dependence between output

voltage and duty-cycle because in OFF situation the energy stored in the filter cannot discharge to track the fundamental closely. This will reduce the range of regulation and the linearity of the control could be compromised; this could be an important drawback when compensating for the harmonics that are present in the voltage delivered by the Rogowski coil.

- **Hysteresis algorithm.** In this method, the output voltage is compared with the reference: if the output voltage is higher than reference, then the switch is OFF and when the output voltage is lower than reference, then the switch is ON. But this results in a very high switching frequency.

From the electromagnetic point of view, this method is better than the fixed frequency because the switching energy is spread over a range of frequencies; the switching frequency depends on the level of the output voltage.

This method can be improved if the highest switching frequency is limited and controlled.

For this study, the hysteresis control with limited switching frequency was chosen. In order to achieve the limitation of the switching frequency, a second order low-pass filter will be used in the feedback path. As compensator a simple lag solution was considered.

6.7.1   Transfer function

The analysis of the control system should start by determining the transfer function of each component and then the closed loop transfer function. By means of simulation, using Matlab, some critical parameters will be determined in such a way that the stability and linearity of the system will not be compromised.

6.7.1.1 Plant transfer function

For this application, the output filter represents the plant. The transfer function (G) for a real LC filter can be written as:

$$G(s) = \frac{1 + s \cdot r_c \cdot C_f}{s^2 \cdot L_f \cdot C_f + s \cdot (r_c + r_f) \cdot C_f + 1} \tag{6.100}$$

Where: r_f = internal resistance of filter inductor (0,01 Ω)

L_f = inductance of filter inductor (20 mH)

r_c = series equivalent internal resistance of filter capacitor (0,01 Ω)

C_f = capacitance of filter capacitor (3,3 μF)

s = Laplace operator

The values of L_f, C_f have been chosen so that the cut-off frequency is not a multiple of 50 Hz on one hand and, on the other hand, the fundamental is passing unaffected in magnitude and phase. From the Bode diagram, shown in Figure 60, one can see that the fundamental 50 Hz (or ω_o = 314,15 rad·sec^{-1}) is unaffected in magnitude and phase, only the higher frequencies (switching and harmonics) are attenuated.
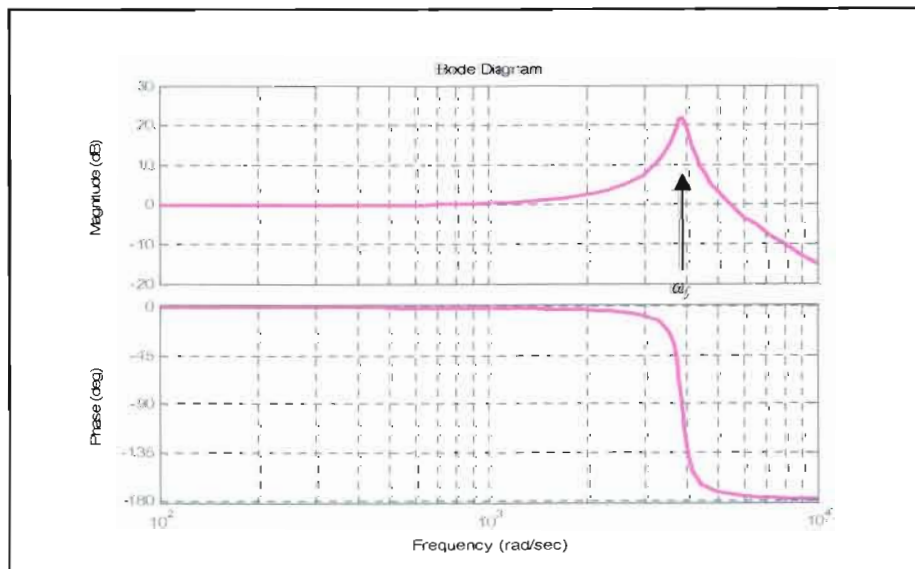
Figure 60 LC filter – Bode diagram

The values of the filter components will be refined as a result of simulations.

6.7.1.2 Feedback transfer function

As presented above, a second order low-pass filter achieves the limitation of the switching frequency when using the hysteresis method. One other requirement for this filter is not to affect the fundamental, therefore a Sallen-Key topology with Butterworth response and unity gain was considered (see Figure 61).
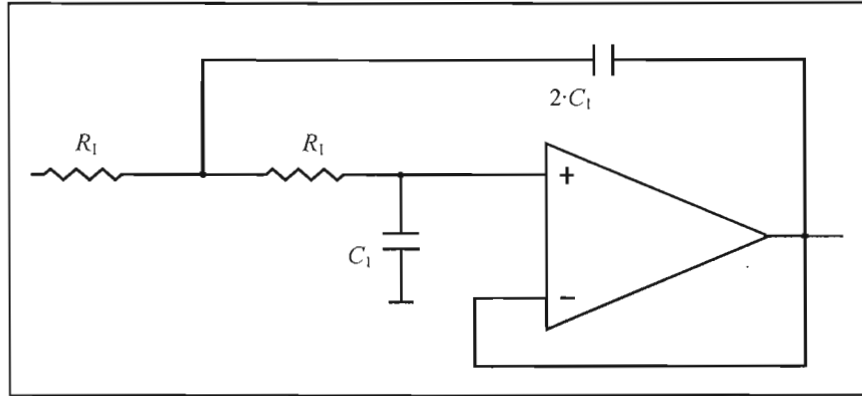
Figure 61 Second order Butterworth filter

This type of filter was considered for the flat magnitude in the band and very low phase-shift introduced for the fundamental. The transfer function of this filter is:

$$H(s) = \frac{\omega_2^2}{s^2 + 2 \cdot \xi \cdot \omega_2 \cdot s + \omega_2^2}$$

(6.101)

Where: $\omega_2 = 2 \cdot \pi \cdot f_2 = (R_1 \cdot C_1)^{-1}$ cut-off pulsating frequency

ξ = damping factor (0,707 for Butterworth response)

s = Laplace operator

If f_2 is 10 kHz, then:

$R_1 = 10 \text{ k}\Omega$ (6.102)

$C_1 = 1,6 \text{ nF}$ (6.103)

The Bode diagram of the proposed filter with a cut-off frequency (f_2) of 10 kHz is shown in Figure 62.
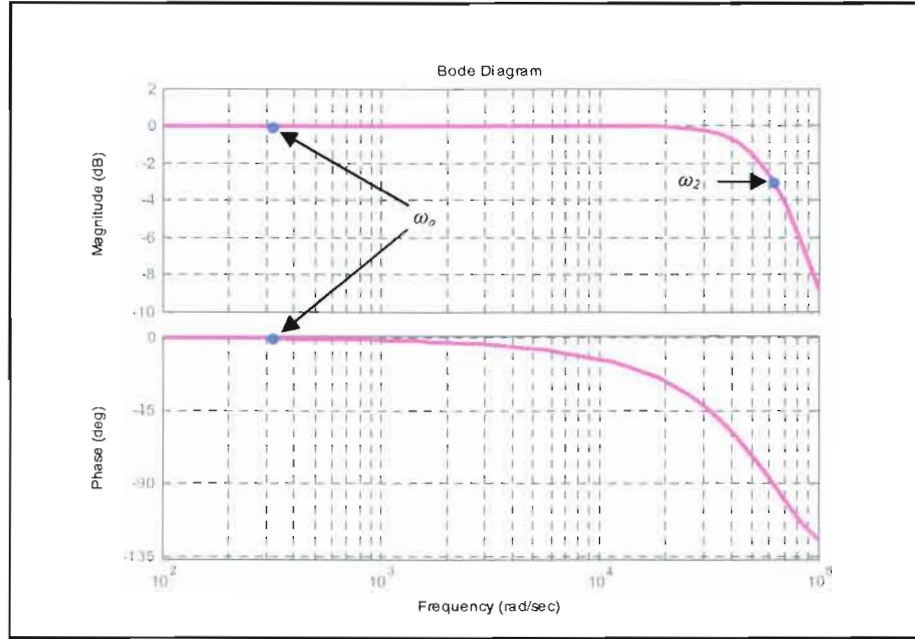
Figure 62 Second order Butterworth filter: bode diagram

6.7.1.3 Compensator transfer function

The compensator/regulator chosen for this application is a simple "lag" equivalent with a PI regulator. The topology of this compensator is presented in Figure 63.

The transfer function of this lag compensator can be written as:

$$C(s) = -\frac{v_{out}(s)}{v_{in}(s)} \tag{6.104}$$

$$C(s) = -\frac{R_3 \,//\,(1/sC_3)}{R_2 \,//\,(1/sC_2)} = -\frac{C_2}{C_3} \cdot \frac{s + (R_2 \cdot C_2)^{-1}}{s + (R_3 \cdot C_3)^{-1}} \tag{6.105}$$
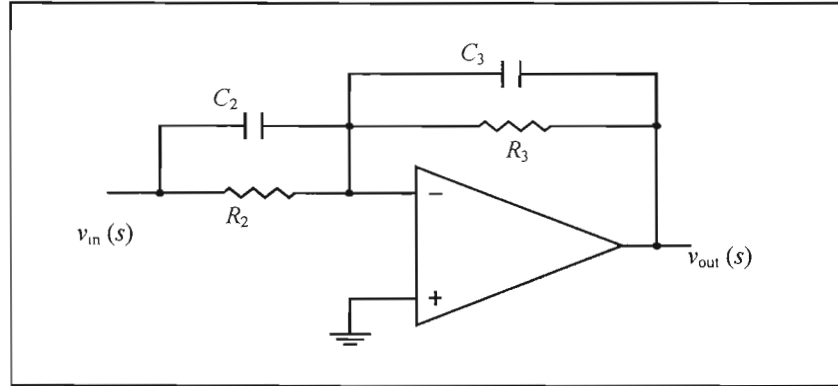
Figure 63 Lag compensator: topology

$$C\ (s) = -K_c \frac{s + \omega_3}{s + \omega_4}$$ (6.106)

where: $K_c = C_2 \cdot C_3^{-1}$ = compensator's gain

$\omega_3 = (R_2 \cdot C_2)^{-1}$ = "zero" pulsating frequency

$\omega_4 = (R_3 \cdot C_3)^{-1}$ = "pole" pulsating frequency

An ideal lag compensator has the pole on the origin (Nise 2000: 505). In practice, the pole is near the origin. The place of the pole (close to origin) improves the static error. The static error constant (K_{vo}) for a system (Nise 2000: 505) is:

$$K_{vo} = K_c \frac{(z_1 \cdot z_2 \cdots) \cdot z_c}{(p_1 \cdot p_2 \cdots) \cdot p_c}$$ (6.107)

Where: K_c = compensator gain

$z_1, z_2, \ldots$ = zeros of the uncompensated system

$p_1, p_2, \ldots$ = poles of the uncompensated system

z_c = compensator's zero

p_c = compensator's pole

As shown in (6.107), the static error constant is improved with the ratio z_c/p_c. Theoretically, if the zero is placed far away: $\omega_4 \ll \omega_3$, then the improvement in

static error is very high. But this will affect the transient response. From this point of view, the zero should be relatively close to the pole (Nise 2000: 506).

The initial set of parameters used was: $K_c = 1$, $\omega_4 = 2 \cdot \pi \cdot 10$ rad·sec^{-1} and $\omega_3 = 2 \cdot \pi \cdot 250$ rad·sec^{-1}. The Bode diagram of this compensator is presented in Figure 64.
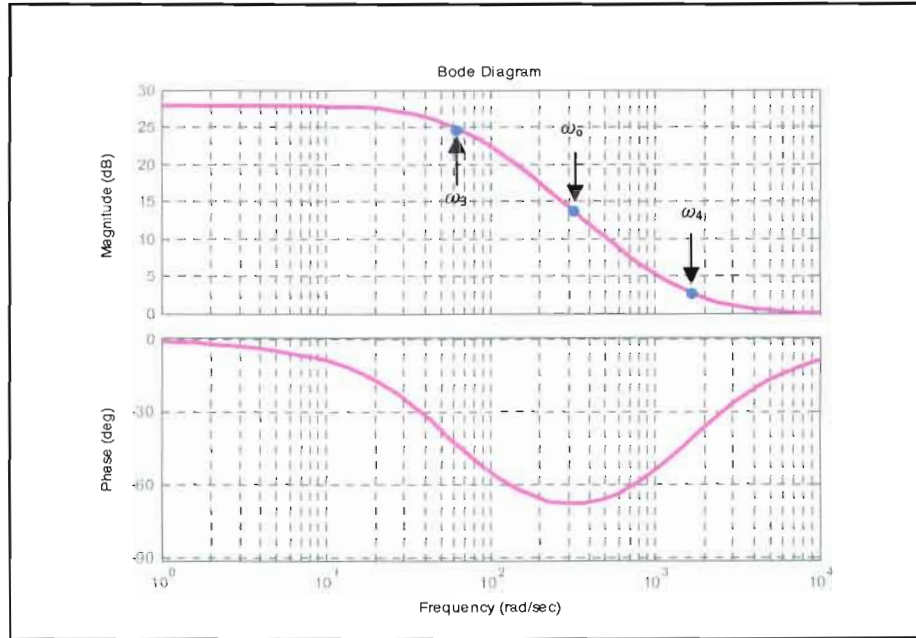
Figure 64 Lag compensator: Bode diagram

6.7.1.4 Control system configuration
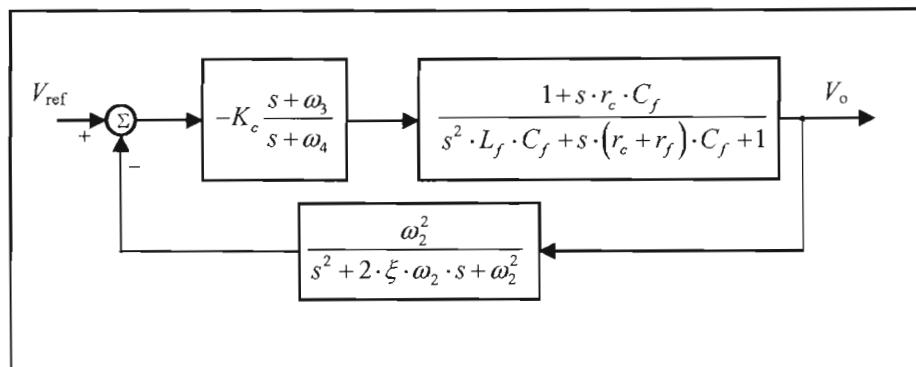
Figure 65 RCPA: control system configuration

107

6.7.1.5 Simulation model: control system

The simulation model of the closed loop system is presented in Figure 66.
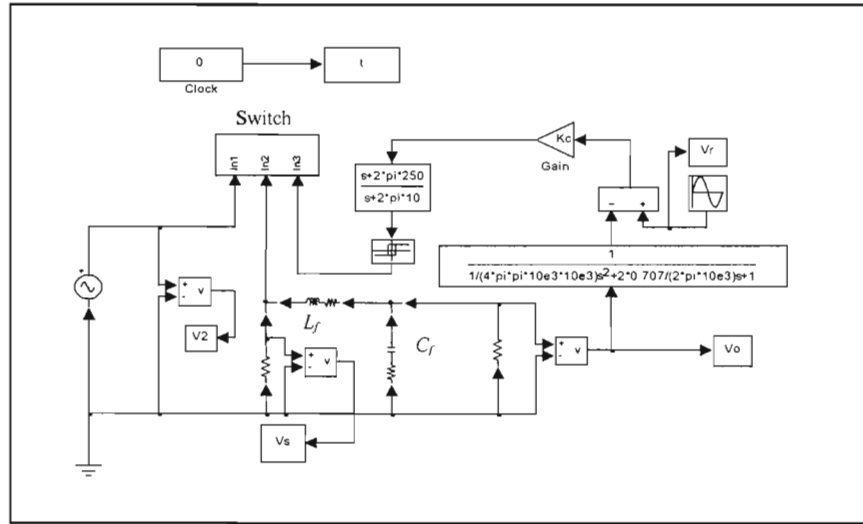
Figure 66 Control system: simulation model

• **The first set of simulations** has been done with the comparator only and without the second order low-pass filter and compensator. Thereafter the low-pass filter has been introduced in order to show the decrease in the switching frequency. The results are presented in Figure 67. From this figure the disadvantages of the simple hysteresis method are noticeable: high static error and high switching frequency – in this situation of approximately 15 kHz (Figure 67a). When the second order low-pass filter was introduced (Figure 67b), the switching frequency became smaller and was approximately 6,5 kHz with a little bit higher ripple and lower static error.

During this set of simulations, the elements of the filter (L_f and C_f) have been refined as follows:

$$L_f = 2 \text{ mH} \tag{6.108}$$

$$C_f = 10 \text{ } \mu F \tag{6.109}$$

108
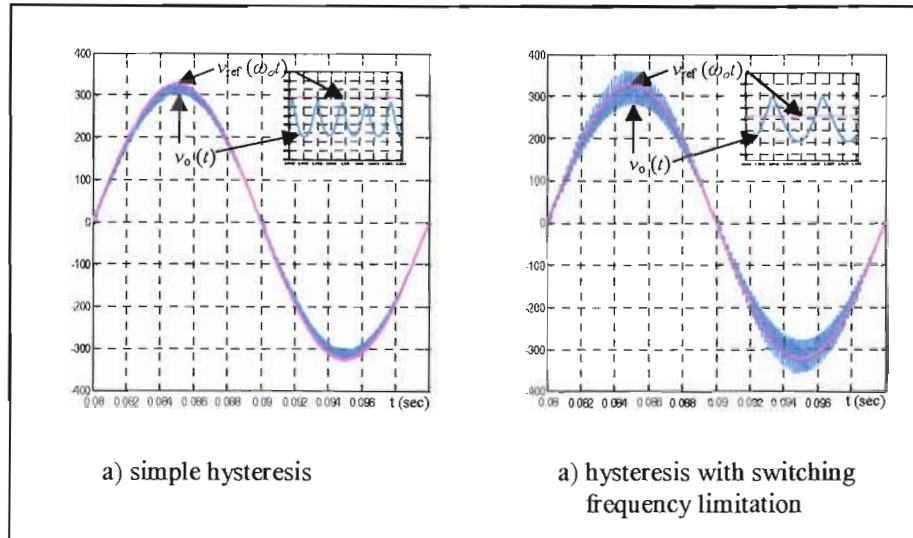
Figure 67 Influence of switching frequency limitation

- **A second set of simulations** has been done to show that spectral lines are spread over a range of frequencies as shown in Figure 68; spectral analysis has been done on a wider than normal (industrial) range of frequencies.
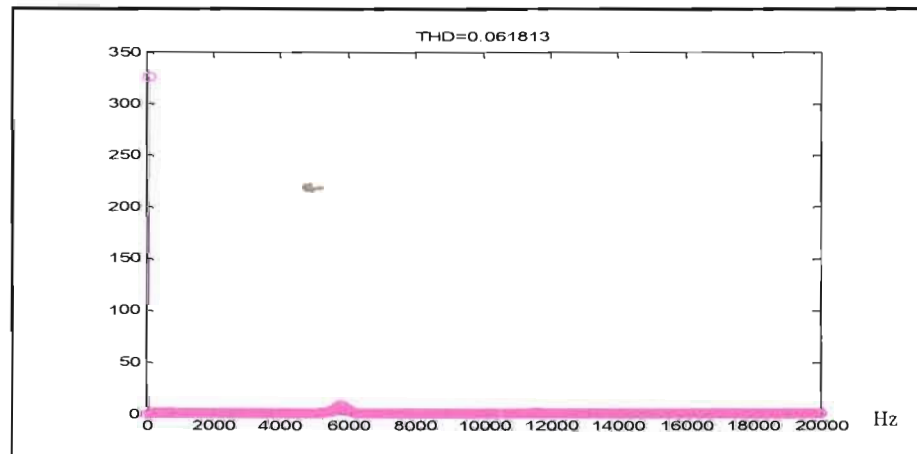
Figure 68 Output voltage: spectral analysis

- **A third set of simulations** has been done to show the improvement brought about by the compensator (Figure 69).
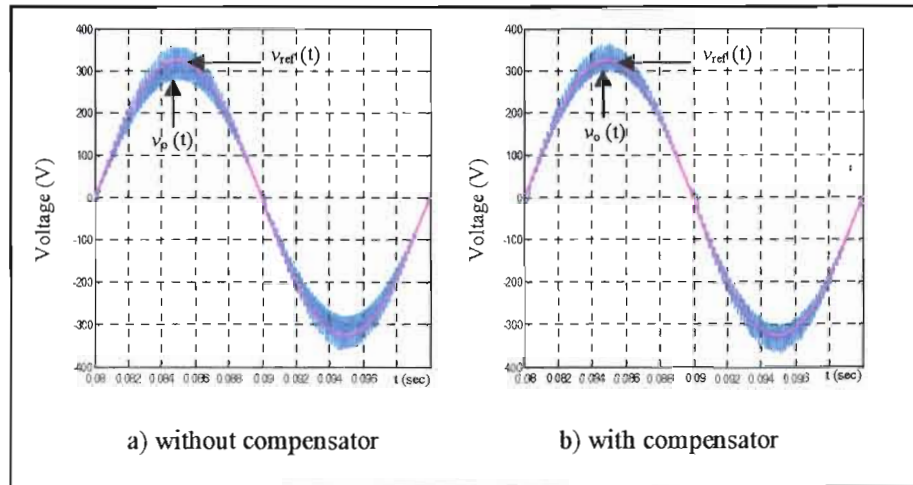
Figure 69 Influence of the lag compensator

For a better illustration, the spectral analysis has been done to find the amplitude of the fundamental. From Figure 70 and associated simulations, it is possible to show a better following of the reference (amplitude of 326 V) in case of compensator presence.
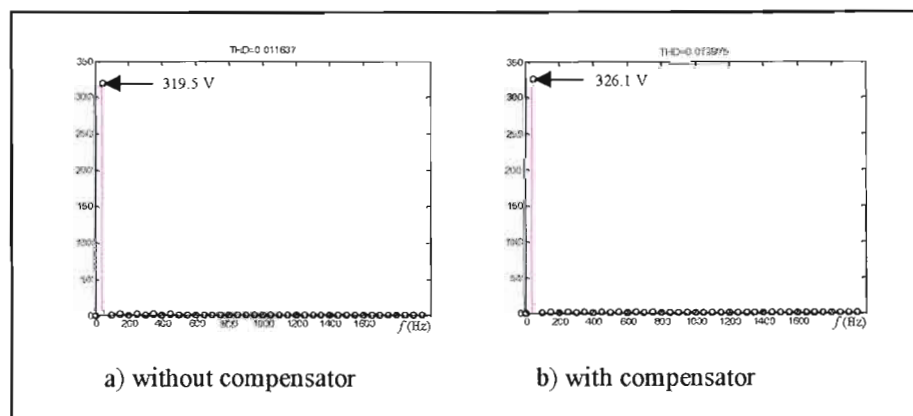
Figure 70 Output voltage: static error of the fundamental

6.7.2   Stability tests

The next step was to perform the stability test for the final refinement of the elements of the system. Using "control system toolbox" of Matlab, the stability tests have been done.

110

6.7.2.1 Bode stability evaluation
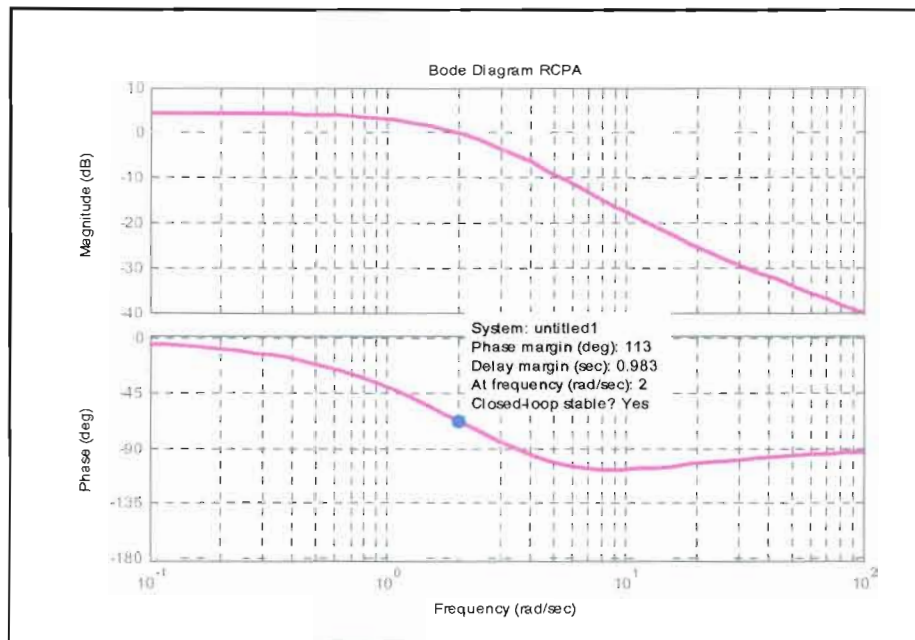
Figure 71 RCPA: Bode stability evaluation

6.7.2.2 Nyquist stability evaluation
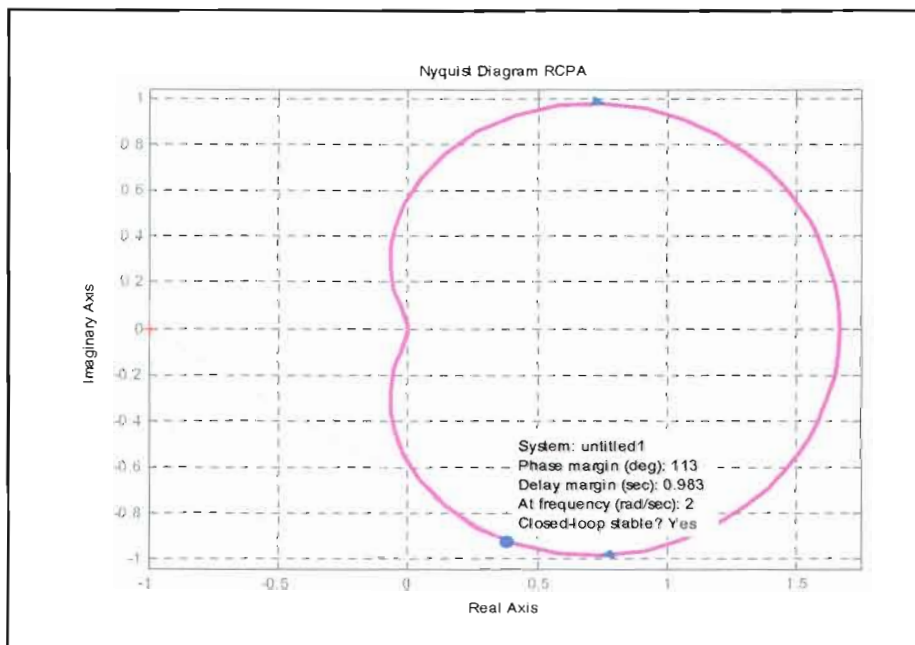
Figure 72 Nyquist stability evaluation

6.7.2.3 Nichols stability evaluation
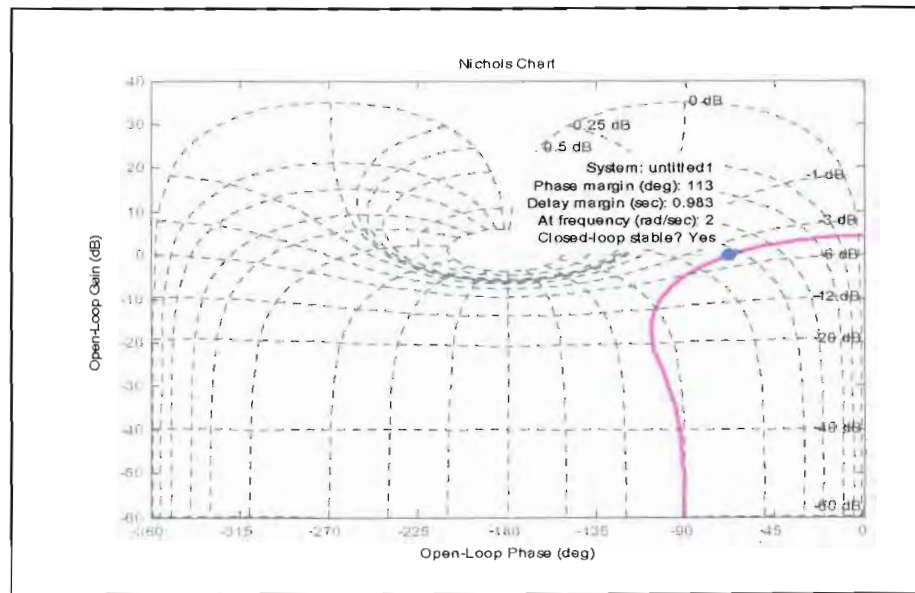
Figure 73 Nichols stability evaluation

All stability tests performed show a stable system.

6.7.3   Load step test

In this test, the load current was increased three times. As can be seen in Figure 74, the voltage follows the reference in phase, while only the ripple increases.
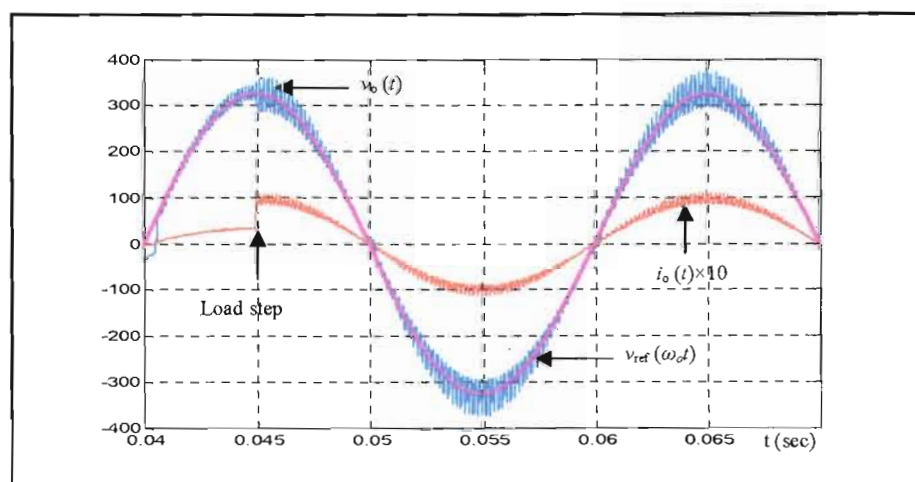
Figure 74 Load step test

6.8   Reference source

An important part of the control system is the sinusoidal reference source. As presented in paragraph 6.7, the control system regulates the output voltage by forcing it to follow a sinusoidal reference. In this way the amplitude and shape is controlled. Therefore the performance of the reference is as equally important as the rest of the control system.

The reference source (Figure 75) has to:

- follow the main frequency in phase with it
- have a stable amplitude

All these requirements can be achieved using a PLL in order to follow the main frequency and a microprocessor to synthesize the sinusoidal shape. The refinements of the components' values have been done in cooperation with Janse van Rensburg (programming the synthesizer); the details will be presented in Annexure I.
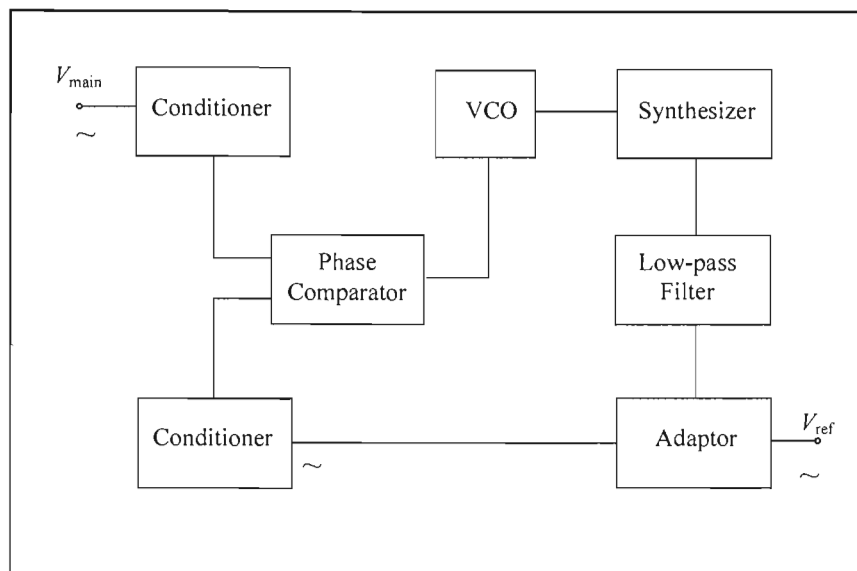
Figure 75 Reference source: block diagram

6.9 Protection system

The aim of the protection system is to ensure a safe operation of the RCPA and to increase the reliability of it. The components of the protection system such as Metal Oxide Variable resistors (MOV) and relays are passive but there are also active components in order to trigger isolation relays in case of abnormal conditions.

6.9.1 Over-voltage protection

In the main transmission lines current surges that will be translated into voltage spikes induced in RCPA can occur. In order to protect the isolation transformer, a MOV should be installed on the primary. The rated voltage of this protection device could be 50 percent higher than the estimated emf induced in pickup coil.

6.9.2 Short circuit protection

The load can be short circuited due to various reasons. In order to protect the switch and the other components of the system, a current sensor should be installed on the output for monitoring. If a current higher than that corresponding to the maximum estimated is detected, then a relay will be triggered, the output of the transformer will be disconnected and a warning light should be ON.

6.10 Auxiliary power supply

In order to ensure functionality of the entire system an auxiliary power supply is required. The energy for it is taken from the isolation transformer by adding another two auxiliary secondary centre-tap connected as in Figure 76. This auxiliary power supply has to provide the bipolar supply (V_+ and V_-) for the operational amplifiers. The entire electronics draws below 0,5 A.

This auxiliary secondary is also the source of the input signal for the reference source (v_{main}).
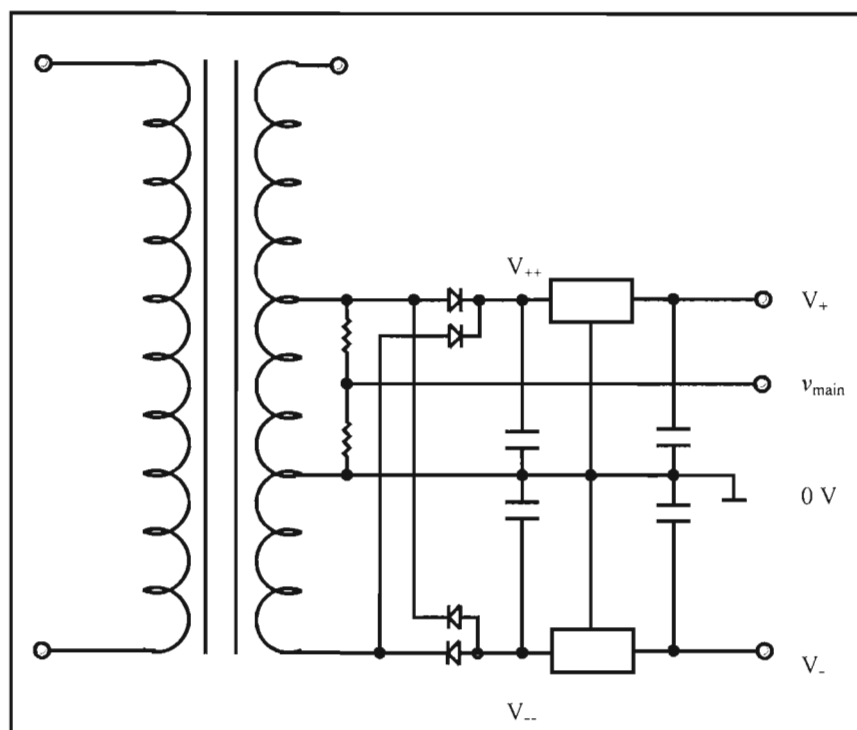
Figure 76 Auxiliary power supply

The details of this power supply will be presented in Annexure I.

7. EXPERIMENTS ON ROGOWSKI COIL POWER APPLICATION MODEL

Due to the nature of the Rogowski Coil Power Application, the validations of the theoretical modeling have been done on reduced scale models. For these experiments two pickup coils have been built.

7.1 Experimental set-up

The characteristics of the experimental pickup coils are presented in Table 1.

Table 1 Characteristics of experimental coils

	a (m)	b (m)	r_o (mm)	N_t (turns)	R_{in} (Ω)	L_{in} (mH)	Support
Coil 1	2,01	0,46	0,375	100	18,9	42,5	wood
Coil 2	2,01	0,855	0,375	200	43,2	177,9	wood

The measurements have been taken using:

- Tape measure with 1 mm accuracy
- RLC meter with 0,1 µH and 0,1 Ω accuracy

The experiments for single-phase have been done using coil 1 and those for three-phase with coil 2. For measurements, the following instruments have been used:

- Multi-meter TBM 811 (Toptronic) as voltmeter with 0,1 mV accuracy to measure output voltage.
- Digital clamp-meter 3280-10 (Hioki) with 0,1 A accuracy to measure output voltage.

116

- THS 720P (Tektronix) portable oscilloscope with FFT facility to determine the Total Harmonic Distortions (THD).
- Power resistors as load.

The basic measuring diagram is shown in Figure 77.
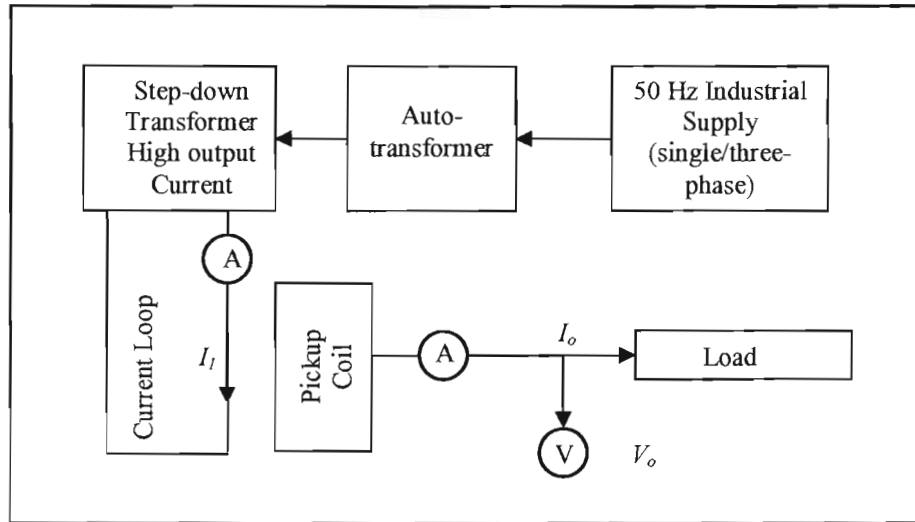
Figure 77 Basic measuring diagram

7.2   Experimental validation of single-phase model
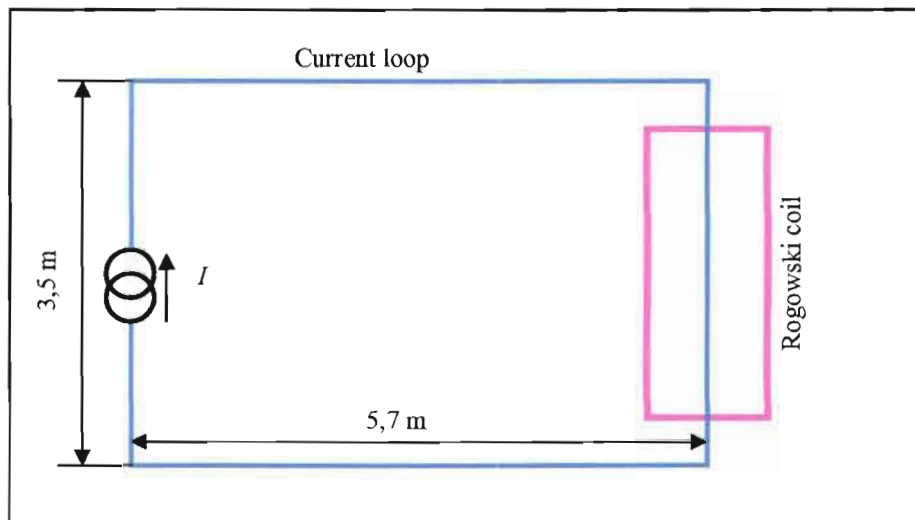
Figure 78 Single-phase setup

7.2.1 Emf: current dependency

The first set of experiments were meant to check that the induced voltage into the Rogowski coil is directly dependent on current I. The position of the coil 1 was vertical with $D = 0$ m and $d = 0,245$ m. The current was varied from 0 to 50 A_{rms}.

As presented in Figure 2, the current loop does not have very large dimensions in relation to the experimental coil. Therefore equation (4.17) giving the induced emf into the pickup coil must be corrected in relation to the induced emf of the current loop side parallel to the main line.

$$\mathcal{E} = 2 \cdot 2 \cdot \pi \cdot 50 \cdot I \cdot 100 \cdot 10^{-7} \left[\ln \frac{(0,23+0,245)^2}{(0,23-0,245)^2} - \ln \frac{5,7^2+(0,23+0,245)^2}{5.7^2+(0,23-0,245)^2} \right]$$

Thus:

$$\mathcal{E}_{est} = 0,04338 \text{ x } I_{rms} \text{ (V)} \tag{7.1}$$

Table 2 Emf: current dependency

I (A)	5	10	15	20	25	30	35	40	45	50
$\mathcal{E}_{mes}$ (V)	0,198	0,396	0,586	0,774	0,975	1,160	1,365	1,558	1,757	1,968
$\mathcal{E}_{est}$ (V)	0,217	0,434	0,651	0,868	1,084	1,301	1,518	1,735	1,952	2,169
$\Delta\mathcal{E}$ (V)	-0,019	-0,038	-0,065	-0,094	-0,109	-0,141	-0,153	-0,177	-0,195	-0,201

Observation: The errors are a bit high. Some reasons to explain these errors can be considered:

- The distortions of the induced emf. As will be further presented, the THD of the induced emf is 12,5 percent with a dominant fifth harmonic that usually is in opposite phase related to the fundamental. If this influence could be quantified, then the errors might be reduced significantly.

- Other currents flowing in the floor of the laboratory related to the main current through the loop, such as the supply current of the auto-transformer.
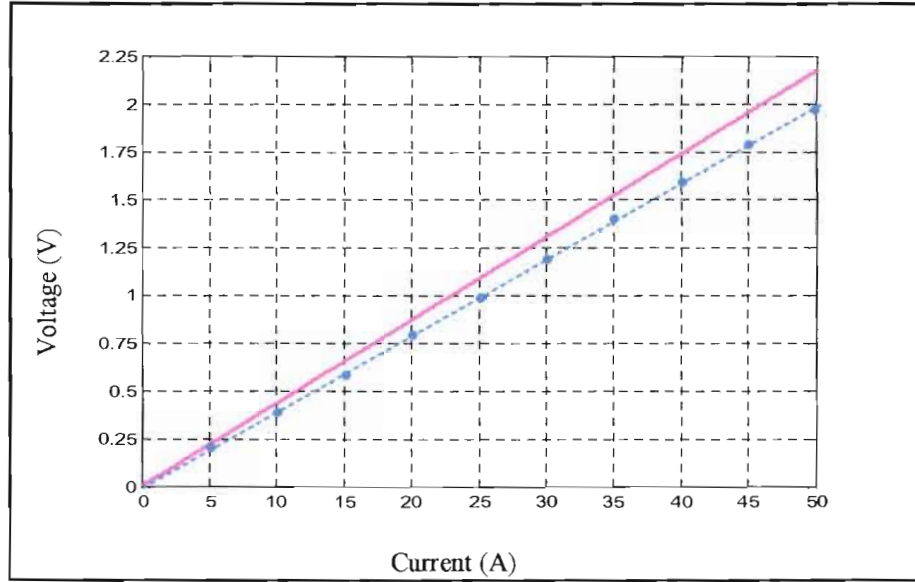
Figure 79 Emf: current dependency

7.2.2 Emf: dependency on D

The second set of measurements with coil 1 has been done to check the variation of the induced emf into Rogowski coil with D. The position of the coil was vertical with $I_{rms} = 50$ A and $d = 0,245$ m. D is the distance between the conductor and the plane of the coil. Using equation (4.17) corrected in the same manner as above, the emf can be written as:

$$\mathcal{E}_{est.} = 50 \cdot 2 \cdot 2 \cdot \pi \cdot 50 \cdot 100 \cdot 10^{-7} \cdot \left[\ln \frac{D^2 + 0,475^2}{D^2 + 0,015^2} - \ln \frac{\left(5,7+D\right)^2 + 0,475^2}{\left(5,7+D\right)^2 + 0,015^2} \right]$$

$$\mathcal{E}_{est.} = 0,314 \cdot \left[\ln \frac{D^2 + 0,475^2}{D^2 + 0,015^2} - \ln \frac{\left(5,7+D\right)^2 + 0,475^2}{\left(5,7+D\right)^2 + 0,015^2} \right] \text{ (V)} \qquad (7.2)$$

119

The coil was moved left and right of the main line with 5 cm steps. The results are presented in Table 3 and Figure 80.

Table 3 Emf: dependency on D

D (cm)	-30	-25	-20	-15	-10	-5	0	5	10	15	20	25	30
E_{mes} (V)	0,287	0,364	0,472	0,615	0,830	1,175	1,968	1,248	0,863	0,620	0,466	0,352	0,270
E_{est} (V)	0,391	0,477	0,591	0,749	0,984	1,389	2,169	1,389	0,984	0,749	0,591	0,477	0,391
ΔE (V)	-0,104	-0,113	-0,119	-0,134	-0,154	-0,214	-0,201	-0,141	-0,121	-0,129	-0,125	-0,125	-0,121
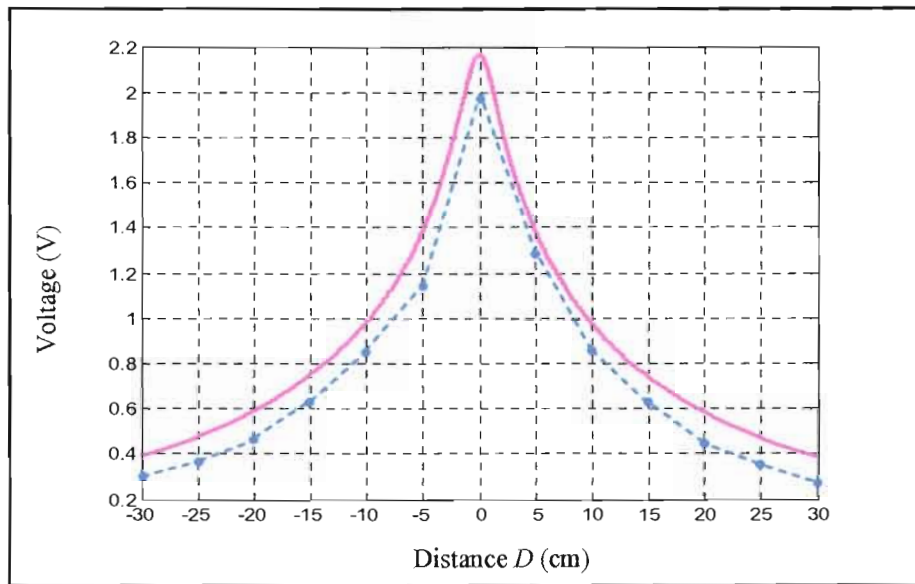
Figure 80 Emf: dependency on D

The same observations as stated in 7.2.1 are valid to explain the errors that occurred.

7.2.3 Emf: dependency on d

Another set of measurements with coil 1 has been done to check the variation with d of the induced emf into the Rogowski coil, where d is the distance between the main line and centre line of the coil (see Figure 15). The position of the coil was horizontal with $I = 50$ A$_{rms}$ and $D = 0,015$ m. The coil was moved left and right of the main line with 5 cm steps. The results are presented in Table 4 and Figure 81.

In this new situation, for the estimation of the emf induced, apart from the above mentioned corrections, the influence of the other sides of the current loop should be taken in consideration.

$d < 0$ (left)

$$\mathcal{E}_{est.} = 0,314 \cdot \left[\ln \frac{0,015^2 + (0,23 - d)^2}{0,015^2 + (0,23 + d)^2} \cdot \frac{0,015^2 + (5,93 + d)^2}{0,015^2 + (5,47 + d)^2} + (0,23 + d) \ln \frac{0,015^2 + (1 + 1,75)^2}{0,015^2 + (1 - 1,75)^2} \right] \quad (V) \qquad (7.3)$$

$d > 0$ (right)

$$\mathcal{E}_{est.} = 0,314 \cdot \left[\ln \frac{0,015^2 + (0,23 + d)^2}{0,015^2 + (0,23 - d)^2} \cdot \frac{0,015^2 + (5,47 + d)^2}{0,015^2 + (5,93 + d)^2} + (0,23 - d) \ln \frac{0,015^2 + (1 + 1,75)^2}{0,015^2 + (1 - 1,75)^2} \right] \quad (V) \qquad (7.4)$$

Table 4 Emf: dependency on d

d (cm)	0	-5	-10	-15	-20	-23	-25	-30
$\mathcal{E}_{mes}$ (V)	0,119	0,409	0,707	1,061	1,601	1,787	1,701	1,169
$\mathcal{E}_{est}$ (V)	0,144	0,442	0,768	1,175	1,631	2,392	2,097	1,499
$\Delta\mathcal{E}$ (V)	-0,025	-0,033	-0,061	-0,114	-0,030	-0,605	-0,396	-0,330

d (cm)	0	5	10	15	20	23	25	30
$\mathcal{E}_{mes}$ (V)	0,119	0,192	0,425	0,798	1,267	1,635	1,386	1,006
$\mathcal{E}_{est}$ (V)	0,144	0,400	0,684	1,050	1,664	2,200	1,905	1,306
$\Delta\mathcal{E}$ (V)	-0,025	-0,208	-0,259	-0,252	-0,397	-0,565	-0,519	-0,300
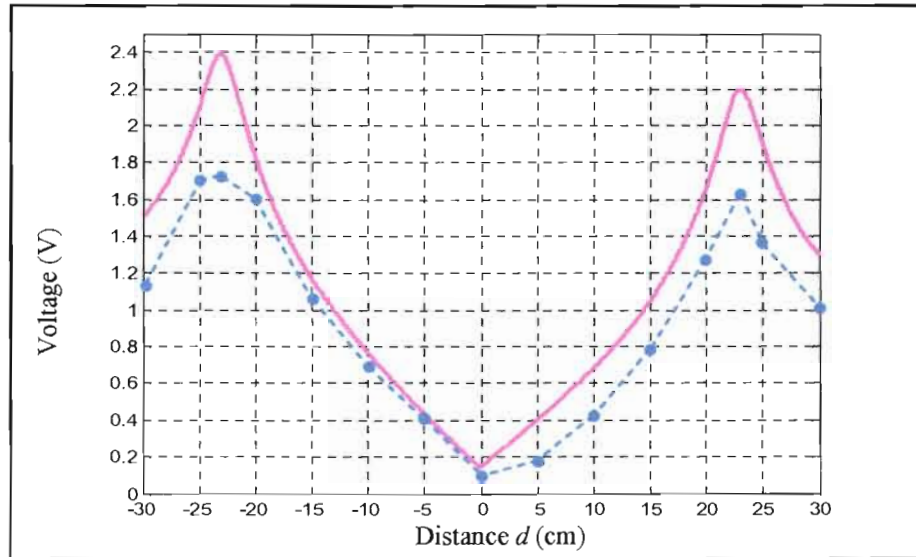
Figure 81 Emf: dependency on d

7.2.4 Emf: dependency on current's THD

Figure 82 shows the oscillograph of the output voltage versus input current of 50 A_{rms}. A more explicit dependency of the emf on the current's THD is presented in Figure 83.
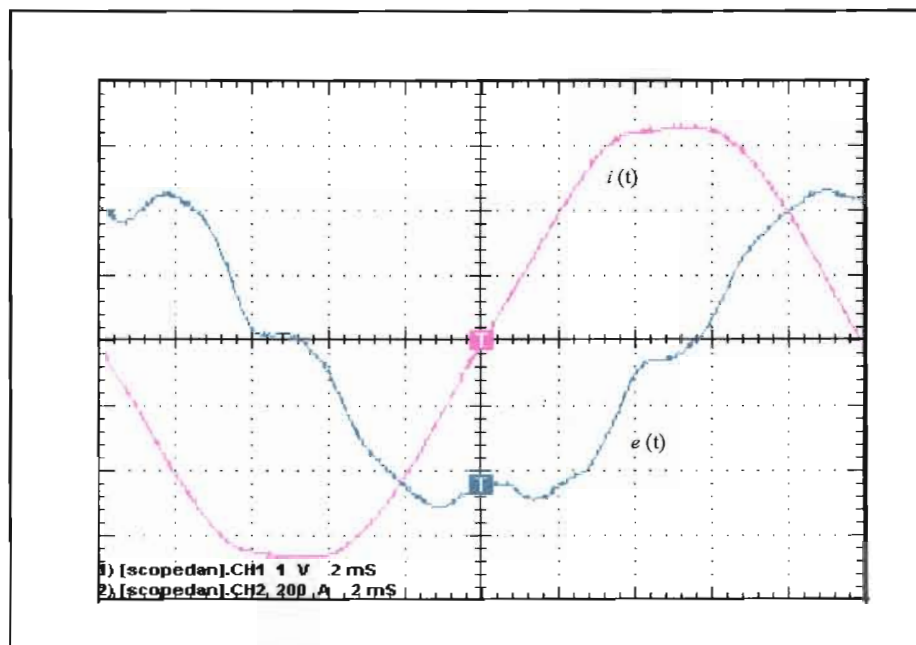
Figure 82 Oscillograph: output voltage versus input current
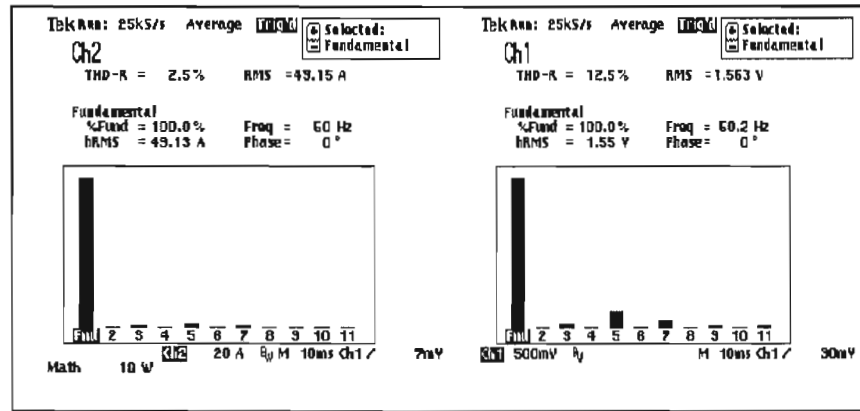
Figure 83 Input current and output voltage: Fourier analysis

From Figure 83, the THD of the output voltage is 12,5 percent while that of the input current is 2,5 percent. The ratio of these two figures is five and because the dominant harmonic is also five, the relation (4.21) is validated very accurately.

All in all the results for the single-phase model allow us to conclude a very good validation of the theoretical model.

7.3   Experimental validation of three-phase model

7.3.1   Measurements in the laboratory

In order to validate the three-phase model, a set of measurements has been done with coil 2. The coil has been successively positioned under the line 1, line 2 and line 3; for each situation the plan of the coil related to that of the lines was horizontal and vertical. The distance between lines has been set for 0,45 m and the rms value of the current was set for 50 A. The results are presented in Table 5 where D and d are determined in relation with the line under which the coil is installed. For the estimated values, the relations derived in paragraph 6.3.1 have been used. The oscillographs for central (under line 2) position are illustrated in Figures 84 and 85.

Table 5 Three-phase system measurements

	Under line 1		Under line 2		Under line 3	
	horizontal	vertical	horizontal	vertical	horizontal	vertical
D (cm)	2,5	0	2,5	0	2,5	0
d (cm)	0	45	0	45	0	45
$\mathcal{E}_{mes}$ (V)	3,692	4,112	6,465	3,975	3,568	4,242
$\mathcal{E}_{est}$ (V)	4,699	3,797	6,983	5,993	4,699	3,797
$\Delta\mathcal{E}$ (V)	-1,007	0,315	-0,518	-2,018	-1,131	0,445

Figure 84 Oscillograph: output voltage versus input current for three-phase system
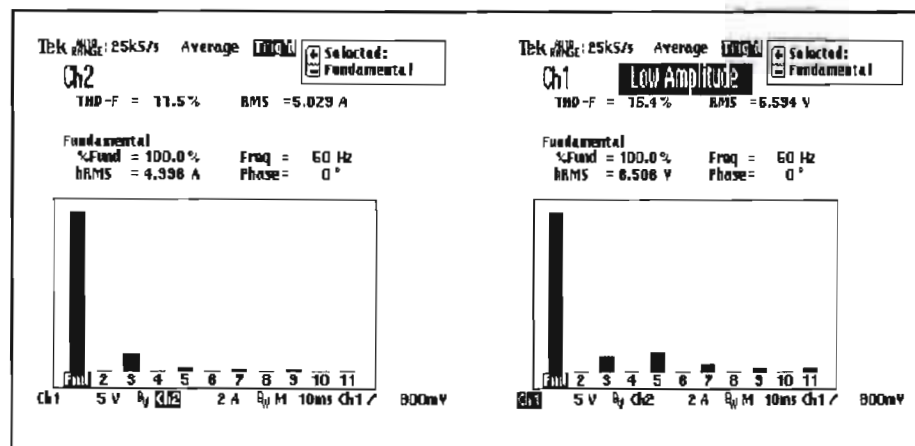
Figure 85 Fourier analysis: input current and output voltage for three-phase system

124

The differences between estimated and measured emf are big. However, there are the following understandable reasons that explain the errors such as:

- Geometry of the current loop. The sides of the current loop induce small emfs with different phases that do not compensate themselves and result in a small phase-shift between input current and output voltage.
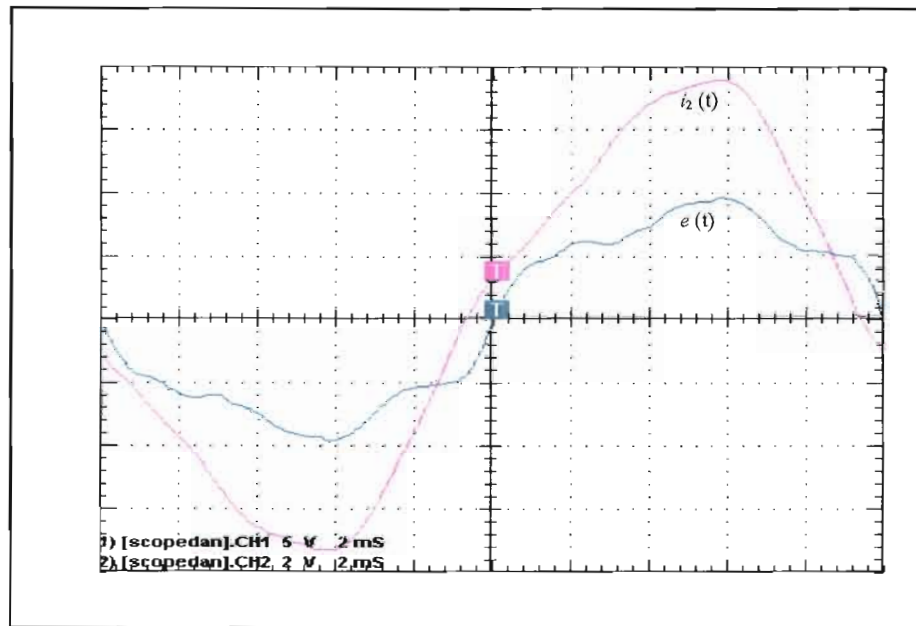- Unbalancing of the current system is one reason for the errors. This is the main reason for the phase shift between the emf and reference current. During the measurements, it has been noticed that the balancing of the currents was not constant.
- Another important reason for the errors is the distortion of the input current (see Figure 85) which cannot be easily quantified. It also should be noticed that the relation (4.21) is apparently not validated because some harmonics have the tendency to cancel naturally, e.g. the third, provided the current system is balanced.

Due to the above mentioned reasons, the measurements have been repeated on a Saturday. The improvement in results has not been significant.

7.3.2 Measurements on field under the transmission lines

Another set of measurements with coil 2 have been done in the field under a double/parallel 440 kV transmission line on outskirts of Vereeniging. The coils have been positioned 8,5 m under the level of the main lines; this distance has been telemetrically determined.

In order to eliminate the uncertainty of the line current, the ratio $\mathcal{E}_{h(rms)} / \mathcal{E}_{v(rms)}$ has been measured and estimated (Annexure J). The result of the measurement under the extreme right line produced the value for the ratio $\mathcal{E}_{h(rms)} / \mathcal{E}_{v(rms)}$ of 0,585 compared to an estimated value of 0,559. The measurements for vertical and horizontal position have not been done simultaneously and this could explain the difference.

Overall, it can be concluded that the measurements validate the theoretical model.

7.4   Voltage regulation

The experiments regarding voltage regulation targeted two aspects:

- Reference source (PLL).
- Output parameters.

7.4.1   Reference source

The reference source was designed to follow the frequency of the input signal in the range 45 Hz to 55 Hz while the amplitude remains constant. The experiments have been done with a signal generator as input source. Figure 86a presents the results for 45 Hz and 86b for 50 Hz.

a) 45 Hz   b) 50 Hz
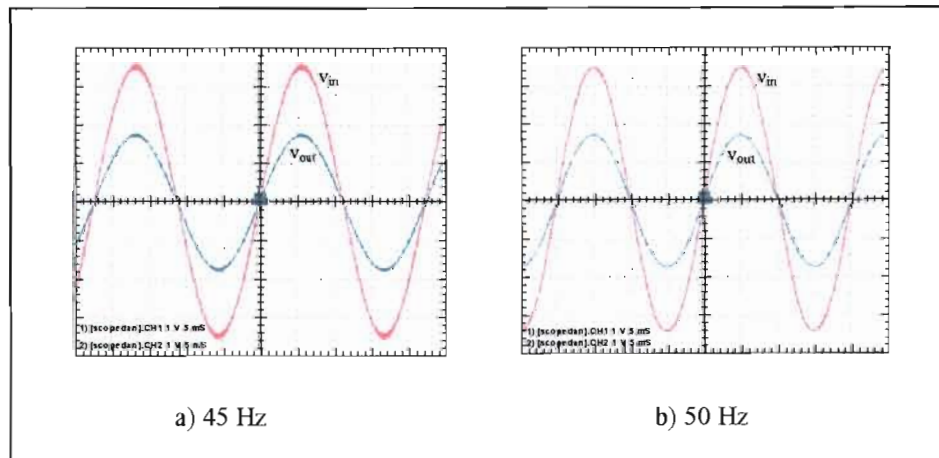
Figure 86 Reference source – frequency tracking

7.4.2   Output parameters

The experiments have been done on a reduced power transformer 100 VA. The output voltage has been set to 230 V and the load resistance 1 kΩ. The measurements have been done tracking the main frequency of 50 Hz.

Figure 87 shows the graphs for the output voltage versus reference voltage. The imposed output voltage was 230 V and the actual value measured has been 226,8 V. The output voltage has been picked up from the output divider in order to be compared with the reference voltage.
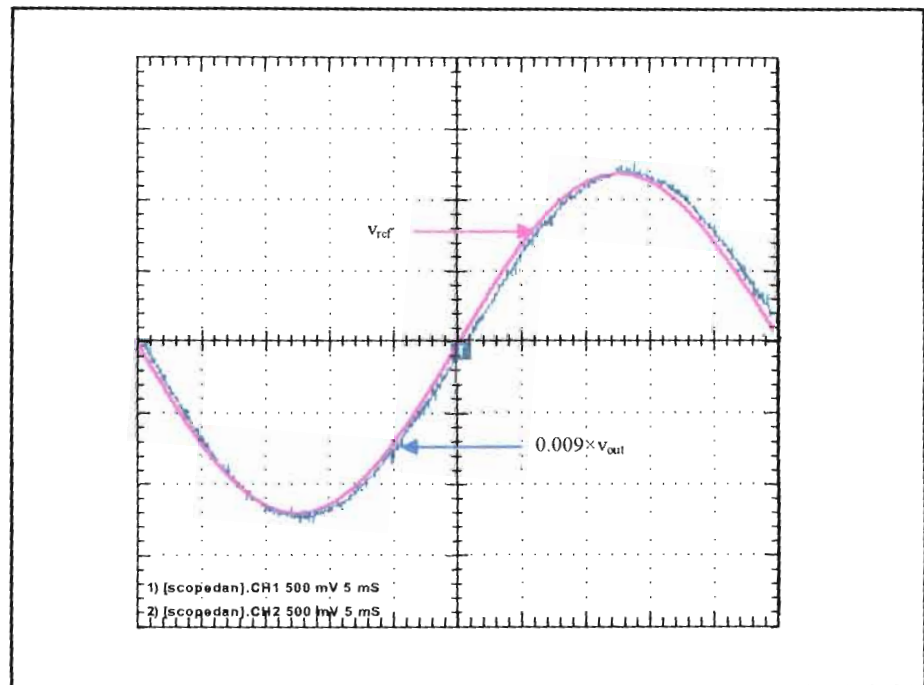
Figure 87 Output voltage versus reference voltage

A very small phase shift between output voltage and reference voltage still can be noticed.

All the above measurements show a good validation of the voltage regulation.

8. CONCLUSIONS

8.1 Conclusions about present research

At the end of this study some conclusions can be drawn:

- As defined in this study, the non-conventional methods to extract energy from high voltage transmission line present the main advantage of safety: not being in direct contact with the main lines, the risk of triggering the protection system is almost zero.

- The drawback of these methods consists in limited power that can be extracted. But for remote rural areas, a power of several kilowatts can make the difference between dark age and civilization.

- In this research a new non-conventional method for tapping energy has been developed: Rogowski Coil Power Application. The theoretical background has been presented, the power available was evaluated, the influence of various factors upon the extracted energy was analyzed and experimental validation on reduced-scale model has been achieved.

- Rogowski Coil Power Application presents a series of advantages that makes it eligible for full scale implementation:
  - ➢ It provides a reasonable power of 2 kW.
  - ➢ It is very safe for the main line.
  - ➢ It is very simple to implement.
  - ➢ The control system provides a stable and regulated standard ac output voltage.
  - ➢ The electronic circuitry is simple and reliable.

- From this study, a very challenging conclusion can be drawn: there are non-conventional methods to extract energy from HVDC. Some of these methods exploit the imperfection of the electrical parameters: the ripple of the current and voltage.

- A new method to extract energy from HVDC was identified: static capacitance modulation for power applications. Due to its novelty, a new field of research can be developed.

8.2   Recommendations for future research

This study produced a few possibilities for further research:

- Before starting the implementation of the Rogowski Coil Power Application, a deeper analysis from the mechanical point of view is recommended. With this occasion, the possibility of substituting copper wires with aluminum wires should be investigated considering both aspects mechanical as well as electrical: if the weight is lighter then the number of turns could be increased with a gain in available power.

- Another recommendation for further studies is the implementation of an energy meter that will give control for energy provider.

- Due to the novelty of static capacitance modulation for power applications, it is recommended that further research of the theoretical analysis and technological implementation be undertaken.

BIBLIOGRAPHY

ACKERMANN, D W, 1999. *The accuracy of power system current measuring devices.* Paper presented at SAUPEC 99, Durban, South Africa, pp.60-63.

AGHAEBRAHIMI, M R and MENZIES, R W, 1997. Small power tapping from HVDC transmission systems: a novel approach. *IEEE Transactions on Power Delivery,* Vol. 12, No. 4, October 1997, pp. 1698-1703

AGRAWAL, J P, 2001. *Power electronic systems: theory and design.* New Jersey: Prentice-Hall

AREDES, M, PORTELA, C and WATANABE, E H, 2001. HVDC tapping using soft-switching techniques. *Electrical Engineering Research Journal - Archiv fur Elektrotechnik,* Vol. 83, No. ½, January 2001, pp. 33-40

BABANI, B, 1945. *Radio reference handbook.* London: Bernards

BAHRMAN, M et al., 1995. Integration of small taps into (existing) HVDC links. *IEEE Transactions on Power Delivery,* Vol. 10, No. 3, July 1995, pp. 1699-1706

BERTHIAUME, R and BLAIS, R, 1980. Microwave repeater power supply tapped from the overhead ground wire on 735 kV transmission line. *IEEE Transaction on Power Apparatus and Systems,* Vol. PAS-99, No. 1, pp. 183-184

BOCHARD, B, BOLDUC, L and BEAULIEU, G, 1997. Capacitive divider substation. *IEEE Transaction on Power Delivery,* Vol. 12, No. 3, July 1997, pp. 1202-1209

BOLDUC, L, 2002. *INFO SCC,* e-mail on July 30, 2002

CHETTY, L, IJUMBA, N M and BRITTEN, A C, 2004. *Tapping small amounts of power from HVDC transmission lines using a novel voltage source inverter.* Paper presented at SAUPEC 04, Stellenbosch, South Africa

EKSTROM, A and LAMELL, P, 1991. *HVDC tapping station: power tapping from a DC transmission line to a local AC network.* Proceedings of 5th International Conference on AC and DC Power Transmission, London, England, pp. 126-131

GLOVER, J D and SARMA, M, 1994. *Power system analysis and design.* Boston: PWS Publishing

GRAINGER, J J and STEVENSON, W D Jr, 1994. *Power system analysis.* Singapore: McGraw-Hill

GURURAJ, B I and NANDAGOPAL, M R, 1970. Design parameters for earth wire tapping. *Proceedimngs IEE*, Vol. 117, No. 1, pp. 177-182

HALLEN, E, 1962. *Electromagnetic Theory.* New York: John Wiley

HAYT, W H Jr, 1989. *Engineering electromagnetics.* Singapore: McGraw-Hill

HOLTZHAUSEN, J P and COETZEE, B, 2004. *Power frequency electric and magnetic fields of power lines.* Paper presented at SAUPEC 04, Stellenbosch, South Africa

HOOLE, S R H & HOOLE, P R P, 1996. *Engineering electromagnetics.* Oxford: Oxford University Press

JANSE van RENSBURG, J F and CASE, M J, 2002. *Tapping power via a current transformer.* Paper presented at SAUPEC 02, Vanderbijlpark, South Africa

JANSE van RENSBURG, J F and NICOLAE, D V 2004. *Cooperation research*, Vanderbijlpark, South Africa

KOEN, J, HOLTZHAUSEN, J P, VOSLOO W and DINGLEY C E, 1999. *Ion cloud coupling between high voltage direct current transmission lines and adjacent conductors.* Paper presented at SAUPEC 99, Durban, South Africa

KREIN, P T, 1998. *Elements of power electronics.* Oxford: Oxford University Press

KUO, B C, 1995. *Automatic Control Systems.* Englewood Cliffs: Prentice-Hall

LANDER, C W, 1993. *Power electronics.* London: McGraw-Hill

LATEGAN, R and SWART, P H, 2002. *Using three-phase induction motor as flywheel in order to stabilize the CAPTAP system.* Paper presented at SAUPEC 02, Vanderbijlpark, South Africa

MARSHALL, S V, DuBROFF R E and SKITEK G G, 1996. *Electromagnetics concepts and applications.* New Jersey: Prentice Hall

McLYMANN, W T, 1978. *Transformer & inductor design handbook.* New York: Marcel Dekker

MOHAN, N, UNDELAND, T M and ROBBINS, W P, 1989. *Power electronics: converters, applications and design.* New York: John Wiley

NICOLAE, D V and CASE, M J, 2004. Contactless power coupling system. Submitted for publication in *SAIEE Transactions*, March 2004

NICOLAE, DV and CASE, MJ, 2004. *Contactless Power Coupling System.* Paper presented at the 9th International Conference OPTIM'04, 20-23 May, Brasov, Romania

NICOLAE, D V and CASE, M J, 2004. *Rogowski Coil Power Application*. Paper presented at the 11th International Power Electronics and Motion Control Conference, 2-4 September 2004, Riga, Latvia

NICOLAE, D V, 2004. *Non-conventional methods of extracting energy from high voltage transmission lines*. Presentation delivered at Engineering Faculty Research Day, Vaal University of Technology, 14th January, Vanderbijlepark, South Africa

NISE, N S, 2000. *Control System Engineering*. New York: John Wiley

PURCELL, E M, 1982. *Electricity and magnetism*. Bucuresti: Editura Didactica si Pedagogica

RAPHALALANI, V, IJUMBA, N M and JIMOH, A A, 2001. *Capacitive divider for feeding a distribution network from an EHV line*. Paper presented at SAUPEC 01, Cape Town

RASHID, M H, 1988. *Power electronics: circuits, devices and applications*. Englewood Cliffs: Prentice-Hall

RAYNHAM, E F and GOOSEN, P, 1979. Cabora Bassa Apollo H.V.D.C. scheme: control and protection. *SAIEE Transactions*, March 1979, pp. 46 – 62

RYDER, J D, 1957. *Engineering electronics*. Tokyo: McGraw-Hill

STUBBS, L, 1994. *Tapping power from high voltage transmission lines using insulated lighting shield-wires and series compensation*. Dissertation for Master Degree, Witwatersrand University, Johannesburg

UMANAND, L and BHAT, SR, 1992. *Design of magnetic components for switched mode power converters*. New Delhi: Wiley Eastern

VILLABLANCA, M, et al. 2001. 36-Pulse HVDC transmission for remotely sited generation. *IEEE Transaction on Power Delivery,* Vol. 16, No. 4, October 2001, pp. 462-467

WALKER, J J, 2004. Private conversation at "Engineering Faculty Research Day" at Vaal University of Technology , 14th January, Vanderbijlpark, South Africa

ANNEXURE A

VECTOR CALCULUS

Gradient (rectangular): $\nabla f = \vec{x}\dfrac{\partial f}{\partial t} + \vec{y}\dfrac{\partial f}{\partial t} + \vec{z}\dfrac{\partial f}{\partial t}$ (A.1)

Divergence (rectangular): $\nabla \cdot A = \dfrac{\partial A}{\partial x} + \dfrac{\partial A}{\partial y} + \dfrac{\partial A}{\partial z}$ (A.2)

Curl (rectangular): $\nabla \times A = \vec{x}\left(\dfrac{\partial A_z}{\partial y} - \dfrac{\partial A_y}{\partial z}\right) + \vec{y}\left(\dfrac{\partial A_x}{\partial z} - \dfrac{\partial A_x}{\partial x}\right) + \vec{z}\left(\dfrac{\partial A_y}{\partial x} - \dfrac{\partial A_x}{\partial y}\right)$ (A.3)

Laplacian (rectangular): $\nabla^2 f = \dfrac{\partial^2 f}{\partial x^2} + \dfrac{\partial^2 f}{\partial y^2} + \dfrac{\partial^2 f}{\partial z^2}$ (A.4)

Vector identities

$A \cdot B = B \cdot A$

$A \times B = -B \times A$ (A.6)

$A \cdot (B + C) = A \cdot B + A \cdot C$ (A.7)

$A \times (B + C) = A \times B + A \times C$ (A.8)

$A \cdot (B \times C) = B \cdot (C \times A) = (B \times C) \cdot A = C \cdot (A \times B)$ (A.9)

$A \times (B \times C) = (A \cdot C)B - (A \cdot B)C$ (A.10)

$\nabla (fg) = f\nabla g + g\nabla f$ (A.11)

$\nabla \cdot (fA) = f(\nabla \cdot A) + A \cdot \nabla f$ (A.12)

$\nabla \cdot (A \times B) = B \cdot (\nabla \times A) - A \cdot (\nabla \times B)$ (A.13)

$\nabla \times (fA) = \nabla f \times A + f\nabla \times A$ (A.14)

$\nabla \cdot \nabla f = \nabla^2 f$ (A.15)

$$\nabla \times (\nabla f) = 0 \tag{A.16}$$

$$\nabla \cdot (\nabla \times A) = 0 \tag{A.17}$$

$$\nabla \times (\nabla \times A) = \nabla (\nabla \cdot A) - \nabla^2 A \tag{A.18}$$

$$\nabla \times (f \nabla g) = \nabla f \times \nabla g \tag{A.19}$$

Divergence theorem: $\displaystyle \oint_S A \cdot ds = \int_v \nabla \cdot A \, dv \tag{A.20}$

Stokes's theorem: $\displaystyle \oint_l A \cdot dl = \int_v \nabla \times A \cdot ds \tag{A.21}$

ANNEXURE B

COMPOSITE CONDUCTORS

1 Stranded conductor

1.1 Geometric mean radius (GMR) from the inductance point of view for a multi-stranded conductor (Glover & Sarma 1994: 171):

"The GMR of strand conductors is provided by conductor manufacturers."   (B.1)

1.2 Geometric mean radius (GMR) from the capacitance point of view (Glover & Sarma 1994: 188):

"…, it is a normal practice when calculating line capacitance to replace a stranded conductor by a perfect cylindrical whose diameter equals the outside radius of the stranded conductor."   (B.2)

2 Bundle conductor

2.1 Geometric mean radius (GMR) for N_b conductors per bundle:

$$d_{eq} = \sqrt[N_b]{N_b \cdot d \cdot A^{(N_b-1)}}$$ (B.3)

d_{eq} = the equivalent diameter of the bundle

N_b = the number of conductors per bundle

d = the diameter of one conductor

A = the radius of the circle of the bundle

2.2 GMR for a quad S.C.A 42 x 4,14 mm Al. + 7 x 2,32 St. (Raynham & Goosen 1979)

The copper equivalent approximate cross-section area: 343 mm^2

$$d = \sqrt{\frac{4 \cdot 343}{\pi}} \cong 21 \text{ mm}$$

$N_b = 4$

Distance between conductors of the bundle is 45 cm and therefore:

$$A = \frac{45}{\sqrt{2}} = 31,8 \text{ cm}$$

$$d_{eq} = \sqrt[4]{4 \cdot 21 \cdot 318^{(4-1)}} = 228 \text{ mm}$$

$r_{eq} = 114 \text{ mm}$ \hfill (B.4)

ANNEXURE C

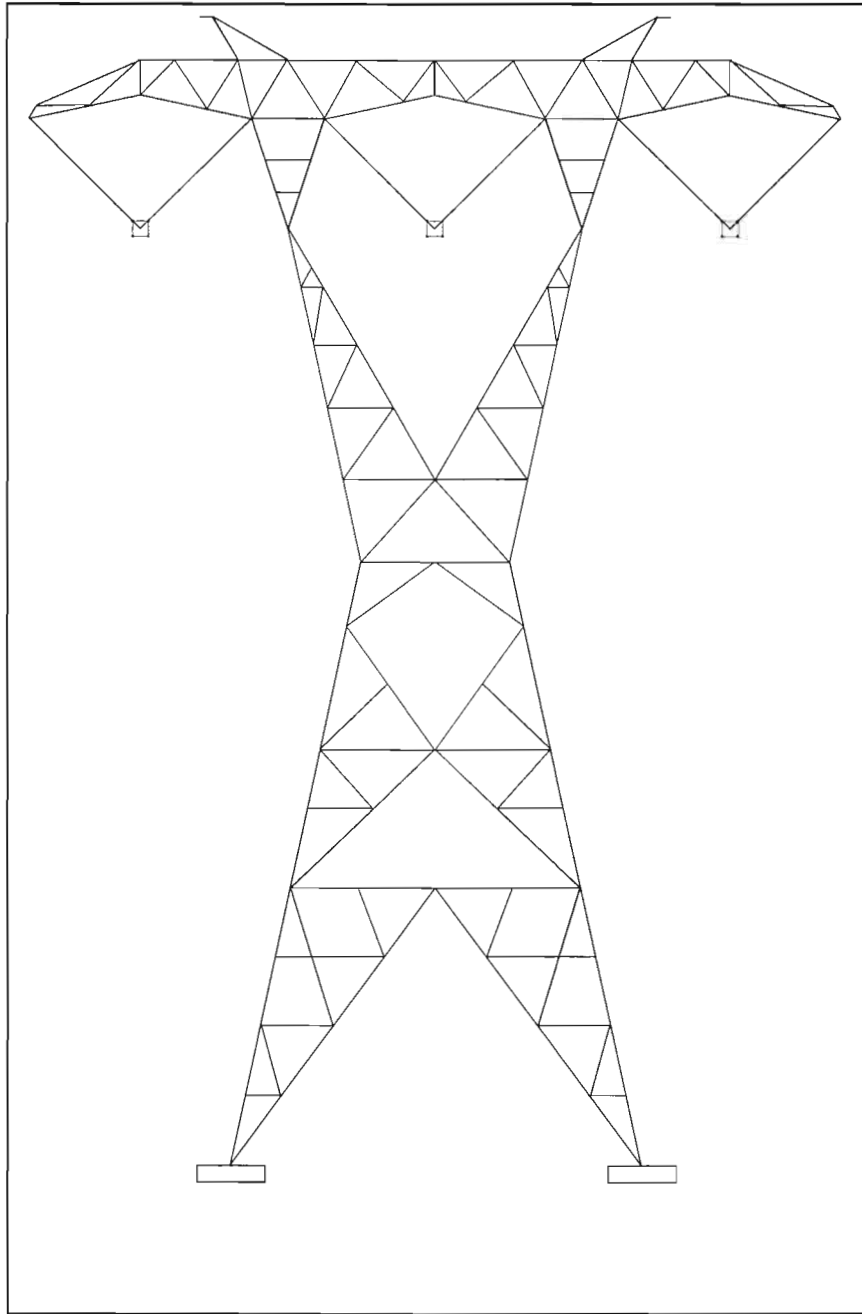## 518 H-TYPE SUSPENSION TOWER

Figure 88 518 H-Type suspension tower

ANNEXURE D

QUICK FIELD SIMULATION RESULTS
440 kV THREE-PHASE TRANSMISSION LINES
WITH BUNDLE CONDUCTORS AND SHIELD WIRES

1 Potential profile for points P_{1B} and P_{2B} on level B (see Figure 35)

Table 6 Simulation results – potential profile for P_{1B} and P_{2B}

ωt (°)	V_{L1} (kV)	V_{L2} (kV)	V_{L3} (kV)	V_{P1B} (kV)	V_{P2B} (kV)
0	-311,8	0	311,8	-65,697	65,667
5	-326,3	31,4	294,9	-62,974	67,884
10	-338,3	62,5	275,8	-59,78	69,582
15	-347,7	93,2	254,6	-56,107	70,77
20	-354,5	123,1	231,4	-52,043	71,379
25	-358,6	152,1	206,5	-47,571	71,47
30	-360	180	180	-42,733	71,021
35	-358,6	206,5	152,1	-37,562	70,02
40	-354,5	231,4	123,1	-32,116	68,493
45	-347,7	254,6	93,2	-26,41	66,468
50	-338,3	275,8	62,5	-20,533	63,898
55	-326,3	294,9	31,4	-14,49	60,862
60	-311,8	311,8	0	-8,325	57,357
65	-294,9	326,3	-31,4	-2,097	53,412
70	-275,8	338,3	-62,5	4,136	49,069
75	-254,6	347,7	-93,2	10,327	44,328
80	-231,4	354,5	-123,1	16,472	39,287
85	-206,5	358,6	-152,1	22,473	33,933
90	-180	360	-180	28,314	28,315
95	-152,1	358,6	-206,5	33,935	22,476
100	-123,1	354,5	-231,4	39,291	16,478
105	-93,2	347,7	-254,6	44,335	10,336
110	-62,5	338,3	-275,8	49,078	4,147
115	-31,4	326,3	-294,9	53,423	-2,083
120	0	311,8	-311,8	57,371	-8,309
125	31,4	294,9	-326,3	60,878	-14,472
130	62,5	275,8	-338,3	63,916	-20,513
135	93,2	254,6	-347,7	66,489	-26,388
140	123,1	231,4	-354,5	68,515	-32,093
145	152,1	206,5	-358,6	70,044	-37,537

150	180	180	-360	71,046	-42,706
155	206,5	152,1	-358,6	71,496	-47,544
160	231,4	123,1	-354,5	71,407	-52,015
165	254,6	93,2	-347,7	70,798	-56,078
170	275,8	62,5	-338,3	69,611	-59,751
175	294,9	31,4	-326,3	67,913	-62,945
180	311,8	0	-311,8	65,697	-65,667
185	326,3	-31,4	-294,9	62,974	-67,884
190	338,3	-62,5	-275,8	59,78	-69,582
195	347,7	-93,2	-254,6	56,107	-70,77
200	354,5	-123,1	-231,4	52,043	-71,379
205	358,6	-152,1	-206,5	47,571	-71,47
210	360	-180	-180	42,733	-71,021
215	358,6	-206,5	-152,1	37,562	-70,02
220	354,5	-231,4	-123,1	33,116	-68,493
225	347,7	-254,6	-93,2	26,41	-66,468
230	338,3	-275,8	-62,5	20,533	-63,898
235	326,3	-294,9	-31,4	14,49	-60,862
240	311,8	-311,8	0	8,325	-57,357
245	294,9	-326,3	31,4	2,097	-53,412
250	275,8	-338,3	62,5	-4,136	-49,069
255	254,6	-347,7	93,2	-10,327	-44,328
260	231,4	-354,5	123,1	-16,472	-39,287
265	206,5	-358,6	152,1	-22,473	-33,933
270	180	-360	180	-28,314	-28,315
275	152,1	-358,6	206,5	-33,935	-22,476
280	123,1	-354,5	231,4	-39,291	-16,478
285	93,2	-347,7	254,6	-44,335	-10,336
290	62,5	-338,3	275,8	-49,078	-4,147
295	31,4	-326,3	294,9	-53,423	2,083
300	0	-311,8	311,8	-57,371	8,309
305	-31,4	-294,9	326,3	-60,878	14,472
310	-62,5	-275,8	338,3	-63,916	20,513
315	-93,2	-254,6	347,7	-66,489	26,388
320	-123,1	-231,4	354,5	-68,515	32,093
325	-152,1	-206,5	358,6	-70,044	37,537
330	-180	-180	360	-71,046	42,706
335	-206,5	-152,1	358,6	-71,496	47,544
340	-231,4	-123.1	354,5	-71,407	52,015
345	-254,6	-93,2	347,7	-70,798	56,078
350	-275,8	-62,5	338,3	-69,611	59,751
355	-294,9	-31,4	326,3	-67,913	62,945
360	-311,8	0	311,8	-65,697	65,667

2 Potential profile for points P_{1C} and P_{2C} on level C (see Figure 35)

Table 7 Simulation results – potential profile for P_{1C} and P_{2C}

ωt ($^\circ$)	V_{L1} (kV)	V_{L2} (kV)	V_{L3} (kV)	V_{P1B} (kV)	V_{P2B} (kV)
0	-311,8	0	311,8	-51,366	51,36
5	-326,3	31,4	294,9	-49,166	53,16
10	-338,3	62,5	275,8	-46,598	54,554
15	-347,7	93,2	254,6	-43,655	55,55
20	-354,5	123,1	231,4	-40,411	56,088
25	-358,6	152,1	206,5	-36,849	56,22
30	-360	180	180	-33,002	55,929
35	-358,6	206,5	152,1	-28,899	55,202
40	-354,5	231,4	123,1	-24,585	54,06
45	-347,7	254,6	93,2	-20,069	52,528
50	-338,3	275,8	62,5	-15,428	50,56
55	-326,3	294,9	31,4	-10,66	48,266
60	-311,8	311,8	0	-5,801	45,521
65	-294,9	326,3	-31,4	-0.898	42,466
70	-275,8	338,3	-62,5	4,002	39,095
75	-254,6	347,7	-93,2	8,862	35,405
80	-231,4	354,5	-123,1	13,683	31,478
85	-206,5	358,6	-152,1	18,385	27,3
90	-180	360	-180	22,955	22,909
95	-152,1	358,6	-206,5	27,346	18,339
100	-123,1	354,5	-231,4	31,525	13,639
105	-93,2	347,7	-254,6	35,451	8,819
110	-62,5	338,3	-275,8	39,141	3,96
115	-31,4	326,3	-294,9	42,51	-0,938
120	0	311,8	-311,8	45,564	-5,838
125	31,4	294,9	-326,3	48,267	-10,694
130	62,5	275,8	-338,3	50,6	-15,459
135	93,2	254,6	-347,7	52,565	-20,097
140	123,1	231,4	-354,5	54,095	-24,61
145	152,1	206,5	-358,6	55,233	-28,921
150	180	180	-360	55,957	-33,02
155	206,5	152,1	-358,6	56,245	-36,863
160	231,4	123,1	-354,5	56,11	-40,421
165	254,6	93,2	-347,7	55,568	-43,661
170	275,8	62,5	-338,3	54,568	-46,6
175	294,9	31,4	-326,3	53,17	-49,164
180	311,8	0	-311,8	51,366	-51,36
185	326,3	-31,4	-294,9	49,166	-53,16
190	338,3	-62,5	-275,8	46,598	-54,544
195	347,7	-93,2	-254,6	43,655	-55,55

200	354,5	-123,1	-231,4	40,411	-56,088
205	358,6	-152,1	-206,5	36,849	-56,22
210	360	-180	-180	33,002	-55,929
215	358,6	-206,5	-152,1	28,899	-55,202
220	354,5	-231,4	-123,1	24,585	-54,06
225	347,7	-254,6	-93,2	20,069	-52,528
230	338,3	-275,8	-62,5	15,428	-50,56
235	326,3	-294,9	-31,4	10,66	-48,266
240	311,8	-311,8	0	5,801	-45,521
245	294,9	-326,3	31,4	0,898	-42,466
250	275,8	-338,3	62,5	-4,002	-39,095
255	254,6	-347,7	93,2	-8,862	-35,405
260	231,4	-354,5	123,1	-13,683	-31,478
265	206,5	-358,6	152,1	-18,385	-27,3
270	180	-360	180	-22,955	-22,909
275	152,1	-358,6	206,5	-27,346	-18,339
280	123,1	-354,5	231,4	-31,525	-13,639
285	93,2	-347,7	254,6	-35,451	-8,819
290	62,5	-338,3	275,8	-39,141	-3,96
295	31,4	-326,3	294,9	-42,51	0,938
300	0	-311,8	311,8	-45,564	5,838
305	-31,4	-294,9	326,3	-48,267	10,694
310	-62,5	-275,8	338,3	-50,6	15,459
315	-93,2	-254,6	347,7	-52,565	20,097
320	-123,1	-231,4	354,5	-54,095	24,61
325	-152,1	-206,5	358,6	-55,233	28,921
330	-180	-180	360	-55,957	33,02
335	-206,5	-152,1	358,6	-56,245	36,863
340	-231,4	-123,1	354,5	-56,11	40,421
345	-254,6	-93,2	347,7	-55,568	43,661
350	-275,8	-62,5	338,3	-54,568	46,6
355	-294,9	-31,4	326,3	-53,17	49,164
360	-311,8	0	311,8	-51,366	51,36

ANNEXURE E

SHORT-CIRCUIT CURRENT FOR
CAPACITIVE IMPEDANCE SOURCE

The maximum current delivered by a source takes place for a short-circuit. If one of the pickup coil conductors is grounded as in Figure 89, then the total short circuit current will be:

$$I_{sh} = I_{sh1} + I_{sh2} + I_{sh3} \tag{E.1}$$
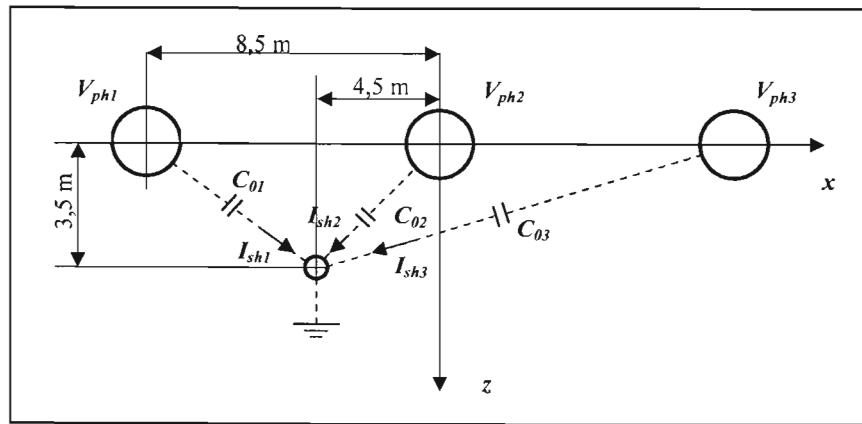
Figure 89 Capacitive impedance source

$$I_{sh} = j \cdot \omega \cdot C_{om} \cdot V_{phm} \tag{E.2}$$

with:

m = 1, 2, 3

$$V_{ph} = V_L / \sqrt{3} = 254 \text{ kV}$$

144

and:

$$C_{om} = \frac{2 \cdot \pi \cdot \varepsilon_0 \cdot a}{\ln\left(\dfrac{D_{om}^2}{r_0 \cdot r_{eq}}\right)} \quad \text{F} \tag{E.3}$$

where:

D_{om} = the distance between pickup coil conductor and main line conductor; each value is determined from the above figure.

a = the length of the pickup coil conductor (250 m)

r_0 = the radius of pickup coil conductor (0,7 mm)

r_{eq} = the equivalent radius of bundle conductors (see Appendix B.4) and is 114 mm

ε_0 = $1/(36\pi 10^9)$ F·m^{-1} = 8,842 pF·m^{-1}

$$C_{o1} = \frac{2 \cdot \pi \cdot 8,842 \cdot 10^{-12} \cdot 250}{\ln\left[\dfrac{(8,5-4,5)^2 + 3,5^2}{0,7 \cdot 10^{-3} \cdot 0,114}\right]} = 1,09 \cdot 10^{-9} \quad \text{F} \tag{E.4}$$

$$C_{o2} = \frac{2 \cdot \pi \cdot 8,842 \cdot 10^{-12} \cdot 250}{\ln\left[\dfrac{4,5^2 + 3,5^2}{0,7 \cdot 10^{-3} \cdot 0,114}\right]} = 1,08 \cdot 10^{-9} \quad \text{F} \tag{E.5}$$

$$C_{o3} = \frac{2 \cdot \pi \cdot 8,842 \cdot 10^{-12} \cdot 250}{\ln\left[\dfrac{(8,5+4,5)^2 + 3,5^2}{0,7 \cdot 10^{-3} \cdot 0,114}\right]} = 0,949 \cdot 10^{-9} \quad \text{F} \tag{E.6}$$

$$I_{sh1} = j \cdot 2 \cdot \pi \cdot 50 \cdot 1,09 \cdot 10^{-9} \cdot 254 \cdot 10^3 \underline{|-120^o} \cong 87 \cdot 10^{-3} \underline{|-30^o} \quad \text{A} \tag{E.7}$$

145

$$I_{sh2} = j \cdot 2 \cdot \pi \cdot 50 \cdot 1,08 \cdot 10^{-9} \cdot 254 \cdot 10^{3} \underline{|0^{o}} = 86,2 \cdot 10^{-3} \underline{|90^{o}} \quad \text{A} \qquad (E.8)$$

$$I_{sh3} = j \cdot 2 \cdot \pi \cdot 50 \cdot 0,949 \cdot 10^{-9} \cdot 254 \cdot 10^{3} \underline{|+120^{o}} = 75,7 \cdot 10^{-3} \underline{|210^{o}} \quad \text{A} \qquad (E.9)$$

$$I_{sh} = 87 \cdot 10^{-3} \underline{|-30^{o}} + 86,2 \cdot 10^{-3} \underline{|90^{o}} + 75,7 \cdot 10^{-3} \underline{|210^{o}}$$

$$I_{sh} = 10^{-3} \left[(75,34 - j43,5) + j86,2 + (-65,56 - j37,85) \right]$$

$$I_{sh} = 10^{-3} (9,78 + j4,85) = 10,9 \cdot 10^{-3} \underline{|26,4^{o}} \quad \text{A} \qquad (E.10)$$

ANNEXURE F

POWER TRANSFERRED TO A RESISTIVE LOAD
FROM ROGOWSKI COIL

1 Parallel compensated model

Figure 90 shows the parallel compensated equivalent diagram of the Rogowski coil with a resistive load R_L. For an ideal 1:1 isolation transformer, the load from the secondary is seen unchanged in the primary.
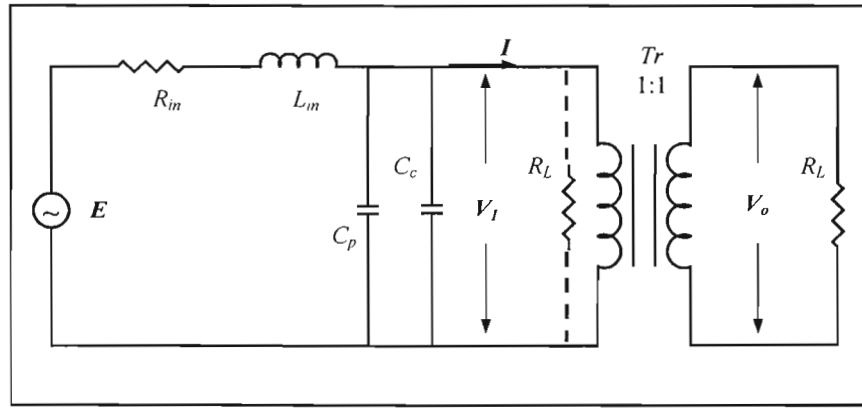
Figure 90   RCPA parallel compensated equivalent model

If E, V_I and I are complex phasors, then the active power dissipated on R_L is:

$$P = \mathcal{R}e\,[V_I \bullet I^*] \tag{F.1}$$

If the load (and transformer) is replaced with its image in the primary, which is R_L, then the impedance of the circuit is:

$$Z = R_{in} + jX_L + \frac{R_L(-jX_C)}{R_L - jX_C} \tag{F.2}$$

where:

R_{in} = internal resistance

X_L = internal inductive reactance

X_C = capacitive reactance that includes internal and compensation capacitance

R_L = load resistance

$$Z = \frac{(R_{in} + jX_L)(R_L - jX_C) - jR_LX_C}{R_L - jX_C}$$

$$Z = \frac{(R_{in}R_L + X_LX_C) - j(R_{in}X_C + R_LX_C - R_LX_L)}{R_L - jX_C} \tag{F.3}$$

$$V_1 = \frac{E}{Z} \cdot \frac{-jR_LX_C}{R_L - jX_C} \tag{F.4}$$

$$V_1 = E\frac{R_L - jX_C}{(R_{in}R_L + X_LX_C) - j(R_{in}X_C + R_LX_C - R_LX_L)} \cdot \frac{-jR_LX_C}{R_L - jX_C}$$

$$V_1 = E\frac{-jR_LX_C}{(R_{in}R_L + X_LX_C) - j(R_{in}X_C + R_LX_C - R_LX_L)}$$

$$V_1 = E\frac{-jR_LX_C[(R_{in}R_L + X_LX_C) + j(R_{in}X_C + R_LX_C - R_LX_L)]}{(R_{in}R_L + X_LX_C)^2 + (R_{in}X_C + R_LX_C - R_LX_L)^2}$$

$$V_1 = E\frac{(R_{in}R_LX_C^2 + R_L^2X_C^2 - R_L^2X_LX_C) - j(R_{in}R_L^2X_C + R_LX_LX_C^2)}{(R_{in}R_L + X_LX_C)^2 + (R_{in}X_C + R_LX_C - R_LX_L)^2}$$

$$V_1 = E \frac{R_L \left[\left(R_{in} X_C^2 + R_L X_C^2 - R_L X_L X_C \right) - j \left(R_{in} R_L X_C + X_L X_C^2 \right) \right]}{\left(R_{in} R_L + X_L X_C \right)^2 + \left(R_{in} X_C + R_L X_C - R_L X_L \right)^2} \tag{F.5}$$

$$I = V_1 / R_L \tag{F.6}$$

$$I = \frac{E}{R_L} \cdot \frac{R_L \left[\left(R_{in} X_C^2 + R_L X_C^2 - R_L X_L X_C \right) - j \left(R_{in} R_L X_C + X_L X_C^2 \right) \right]}{\left(R_{in} R_L + X_L X_C \right)^2 + \left(R_{in} X_C + R_L X_C - R_L X_L \right)^2}$$

$$I = E \cdot \frac{\left(R_{in} X_C^2 + R_L X_C^2 - R_L X_L X_C \right) - j \left(R_{in} R_L X_C + X_L X_C^2 \right)}{\left(R_{in} R_L + X_L X_C \right)^2 + \left(R_{in} X_C + R_L X_C - R_L X_L \right)^2} \tag{F.7}$$

$$I^* = E \cdot \frac{\left(R_{in} X_C^2 + R_L X_C^2 - R_L X_L X_C \right) + j \left(R_{in} R_L X_C + X_L X_C^2 \right)}{\left(R_{in} R_L + X_L X_C \right)^2 + \left(R_{in} X_C + R_L X_C - R_L X_L \right)^2} \tag{F.8}$$

$$V_1 \cdot I^* = E^2 \frac{R_L \left[\left(R_{in} X_C^2 + R_L X_C^2 - R_L X_L X_C \right)^2 + \left(R_{in} R_L X_C + X_L X_C^2 \right)^2 \right]}{\left[\left(R_{in} R_L + X_L X_C \right)^2 + \left(R_{in} X_C + R_L X_C - R_L X_L \right)^2 \right]^2} \tag{F.9}$$

The above expression is real, therefore:

$$P = E^2 \frac{R_L \left[\left(R_{in} X_C^2 + R_L X_C^2 - R_L X_L X_C \right)^2 + \left(R_{in} R_L X_C + X_L X_C^2 \right)^2 \right]}{\left[\left(R_{in} R_L + X_L X_C \right)^2 + \left(R_{in} X_C + R_L X_C - R_L X_L \right)^2 \right]^2} \tag{F.10}$$

As derived in the paragraph 6.3.5, the main parameters are:

- $E_{rms} = 475$ V
- $R_{in} = 103,4$ Ω
- $X_L = 2\pi f L_{in} = 49,4$ Ω
- $X_C = X_L = 49,4$ Ω

149

The maximum power takes place when:

$$\frac{\partial P}{\partial R_L} = 0 \qquad\qquad (\text{F.}11)$$

But expression (F.11) is complicated enough for this derivation. In order to overcome this problem, MathCAD was used to plot the power versus load graph (see Figure 91) and calculations for few values of R_L were performed (see Table 8).

Table 8 Parallel-compensated model 1: power versus load

R_L (Ω)	40	50	55	60	80
P (W)	318	328	329	328	313
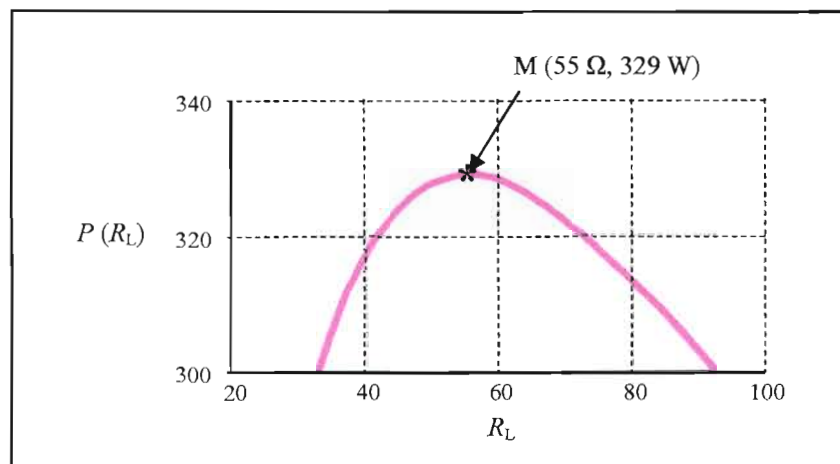
Figure 91 Parallel-compensated model 1: power versus load graph

The maximum power is transferred for $R_L = 55\ \Omega$ and the value is:

$$P = 329\ \text{W} \qquad\qquad (\text{F.}12)$$

The calculation was done again for parameters presented in paragraph 6.3.5:

- $E_{rms} = 1108$ V
- $R_{in} = 144,8 \ \Omega$
- $L_{in} = 0,834$ H
- $C_c = 12,1 \ \mu F$

Table 9 Parallel-compensated model 2: power versus load

$R_L \ (\Omega)$	200	300	400	500	550	600	700	800	900
P (W)	1535	1805	1930	1975	1979	1974	1946	1903	1852
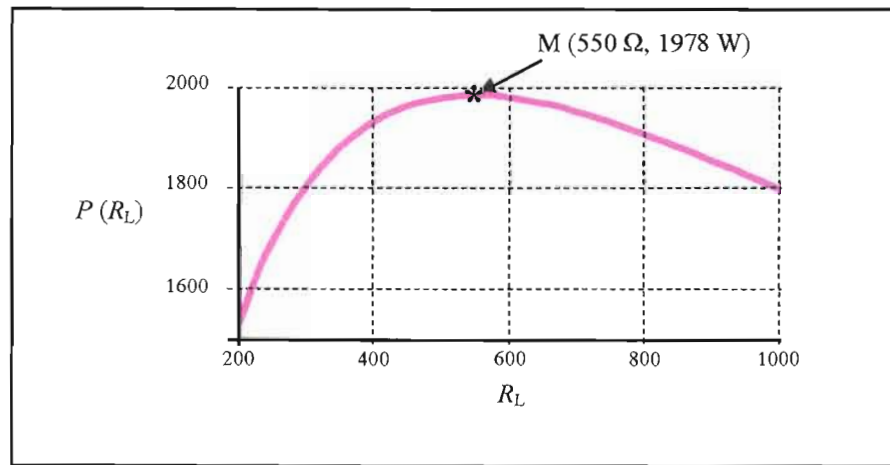
Figure 92 Parallel-compensated model 2: power versus load graph

The maximum power is transferred for $R_L = 550 \ \Omega$ and the value is:

$$P = 1979 \text{ W} \tag{F.13}$$

2 Series compensated model

Figure 90 shows the series compensated equivalent diagram of the Rogowski coil with a resistive load R_L. For an ideal 1:1 isolation transformer, the load from the secondary is seen unchanged in the primary.

151
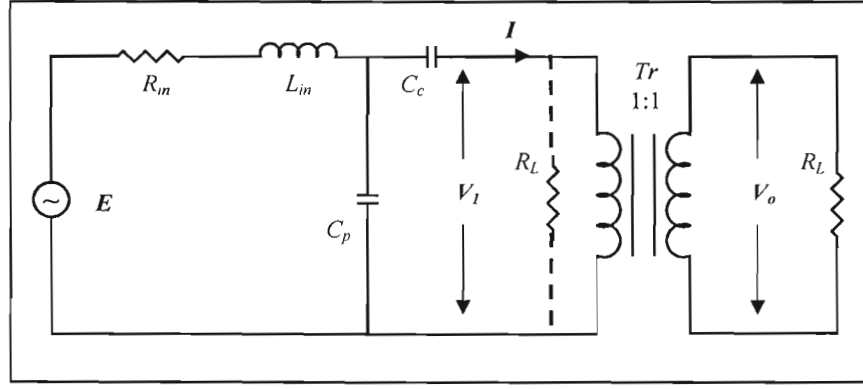
Figure 93 RCPA series compensated equivalent model

The derivation of power dissipated on RL follows the same logic as for the parallel compensated model. It should be noticed that:

$$C_c \gg C_p \tag{F.14}$$

Then:

$$X_C = 1/\omega C_c \tag{F.15}$$

Total impedance of the circuit is:

$$Z = R_{in} + jX_L - jX_C + R_L$$

But $X_L = X_C$ and:

$$Z = R_{in} + R_L \tag{F.16}$$

$$I = E/(R_{in} + R_L)$$

$$V_1 = I \cdot R_L$$

$$V_1 = E \cdot R_L/(R_{in}+R_L) \tag{F.17}$$

The expression of the current is real and then:

$$I^* = I = E/(R_{in} + R_L) \tag{F.18}$$

$$P = E^2 \cdot R_L \cdot (R_{in}+R_L)^{-2} \tag{F.19}$$

The maximum power takes place when:

$$\frac{\partial P}{\partial R_L} = 0$$

$$\frac{\partial P}{\partial R_L} = E^2 \cdot \frac{R_{in} - R_L}{R_{in} + R_L} = 0 \tag{F.20}$$

And the condition for maximum power is:

$$R_L = R_{in} \tag{F.21}$$

$$P_{max} = E^2/4R_L$$

$$P_{max} = 545{,}5 \text{ W} \tag{F.22}$$

If the wire of 2,5 mm^2 is used, then:

$$R_L = R_{in} = 144{,}8 \ \Omega$$

$$P_{max} = 2119{,}6 \text{ W} \tag{F.23}$$

International **IØR** Rectifier

SAFE**IR** Series
20ETS..

INPUT RECTIFIER DIODE

Description/Features

The 20ETS.. rectifier *SAFEIR* series has been optimized for very low forward voltage drop, with moderate leakage. The glass passivation technology used has reliable operation up to 150°C junction temperature.

Typical applications are in input rectification and these products are designed to be used with International Rectifier Switches and Output Rectifiers which are available in identical package outlines.
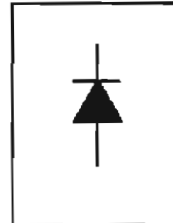
V_F	< 1V @ 10A
I_{FSM}	= 300A
V_{RRM}	800 to 1600V

Output Current in Typical Applications

	Single-phase Bridge	Three-phase Bridge	Units
Capacitive input filter $T_A = 55°C$, $T_J = 125°C$, common heatsink of 1°C/W	16.3	21	A

Major Ratings and Characteristics

Characteristics	20ETS..	Units
$I_{F(AV)}$ Sinusoidal waveform	20	A
V_{RRM}	800 to 1600	V
I_{FSM}	300	A
V_F @ 10 A, $T_J = 25°C$	1.0	V
T_J	-40 to 150	°C

Package Outline

TO-220AC
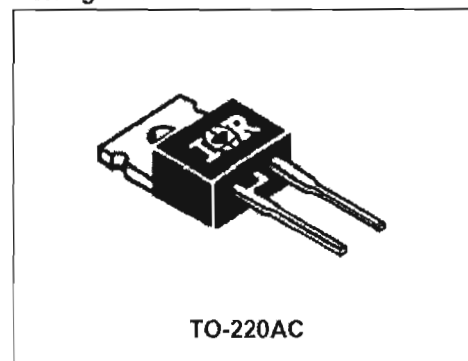
Also available in SMD-220 package (series 20ETS..S)

1

20ETS.. *SAFE*IR Series
Bulletin I2101 rev. B 07/97

International
IQR Rectifier

Voltage Ratings

Part Number	V_{RRM}, maximum peak reverse voltage V	V_{RSM}, maximum non repetitive peak reverse voltage V	I_{RRM} 150°C mA
20ETS08	800	900	1
20ETS12	1200	1300	
20ETS16	1600	1700	

Provide terminal coating for voltages above 1200V

Absolute Maximum Ratings

	Parameters	20ETS..	Units	Conditions
$I_{F(AV)}$	Max. Average Forward Current	20	A	@ T_C = 105°C, 180° conduction half sine wave
I_{FSM}	Max. Peak One Cycle Non-Repetitive	250	A	10ms Sine pulse, rated V_{RRM} applied
	Surge Current	300		10ms Sine pulse, no voltage reapplied
I^2t	Max. I^2t for fusing	316	A^2s	10ms Sine pulse, rated V_{RRM} applied
		442		10ms Sine pulse, no voltage reapplied
$I^2\sqrt{t}$	Max. $I^2\sqrt{t}$ for fusing	4420	$A^2\sqrt{s}$	t=0.1 to 10ms, no voltage reapplied

Electrical Specifications

	Parameters	20ETS..	Units	Conditions	
V_{FM}	Max. Forward Voltage Drop	1.1	V	@ 20A, T_J = 25°C	
r_t	Forward slope resistance	10.4	mΩ	T_J = 150°C	
$V_{F(TO)}$	Threshold voltage	0.85	V		
I_{RM}	Max. Reverse Leakage Current	0.1	mA	T_J = 25 °C	V_R = rated V_{RRM}
		1.0		T_J = 150 °C	

Thermal-Mechanical Specifications

	Parameters		20ETS..	Units	Conditions
T_J	Max. Junction Temperature Range		-40 to 150	°C	
T_{stg}	Max. Storage Temperature Range		-40 to 150	°C	
R_{thJC}	Max. Thermal Resistance Junction to Case		1.3	°C/W	DC operation
R_{thJA}	Max. Thermal Resistance Junction to Ambient		62	°C/W	
R_{thCS}	Typ. Thermal Resistance Case to Heatsink		0.5	°C/W	Mounting surface, smooth and greased
wt	Approximate Weight		2 (0.07)	g (oz.)	
T	Mounting Torque	Min.	6 (5)	Kg-cm (lbf-in)	
		Max.	12 (10)		
	Case Style		TO-220AC		

2

International
IOR Rectifier

20ETS.. SAFE*IR* Series
Bulletin I2101 rev. B 07/97
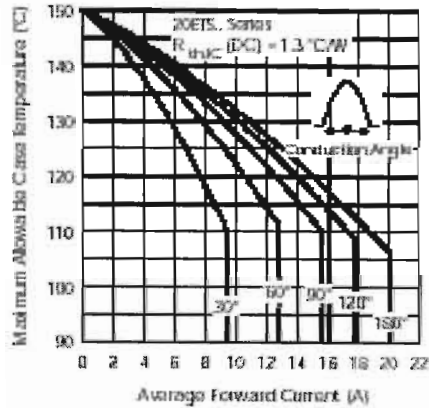
Fig. 1-Current Rating Characteristics
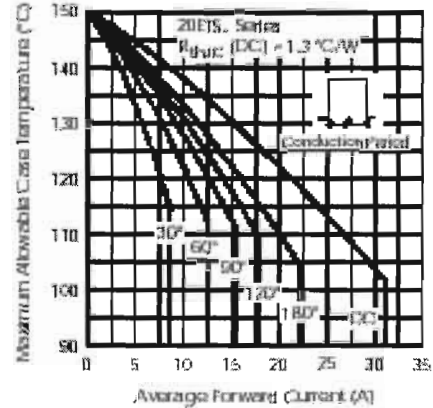
Fig. 2-Current Rating Characteristics
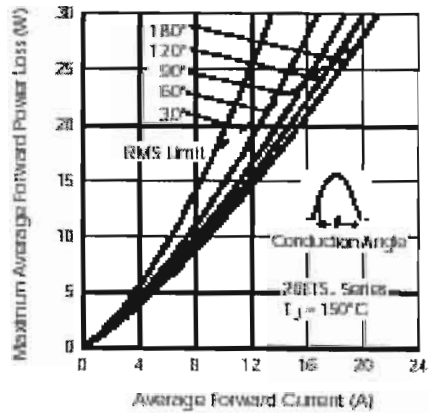
Fig. 3-Forward Power Loss Characteristics
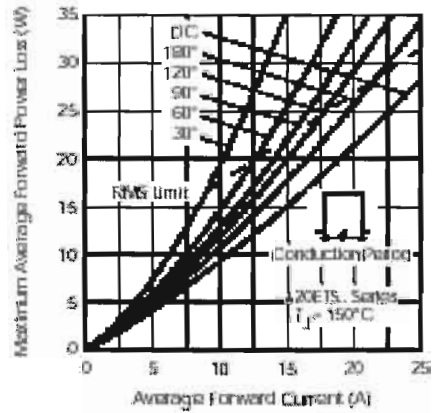
Fig. 4-Forward Power Loss Characteristics
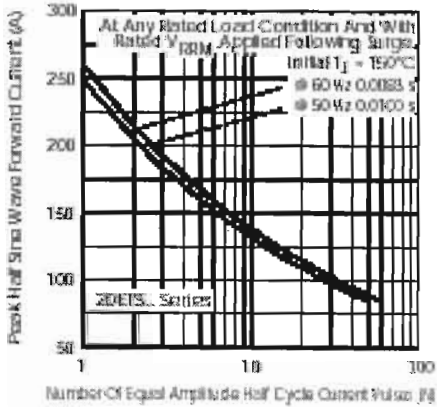
Fig. 5-Maximum Non-Repetitive Surge Current
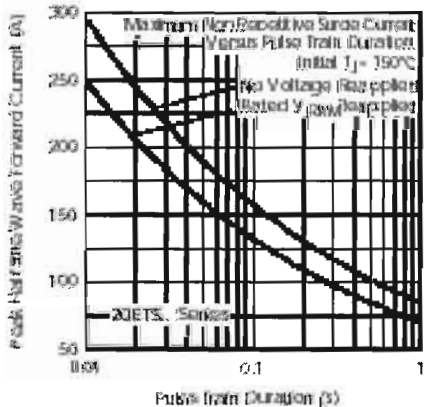
Fig. 6-Maximum Non-Repetitive Surge Current
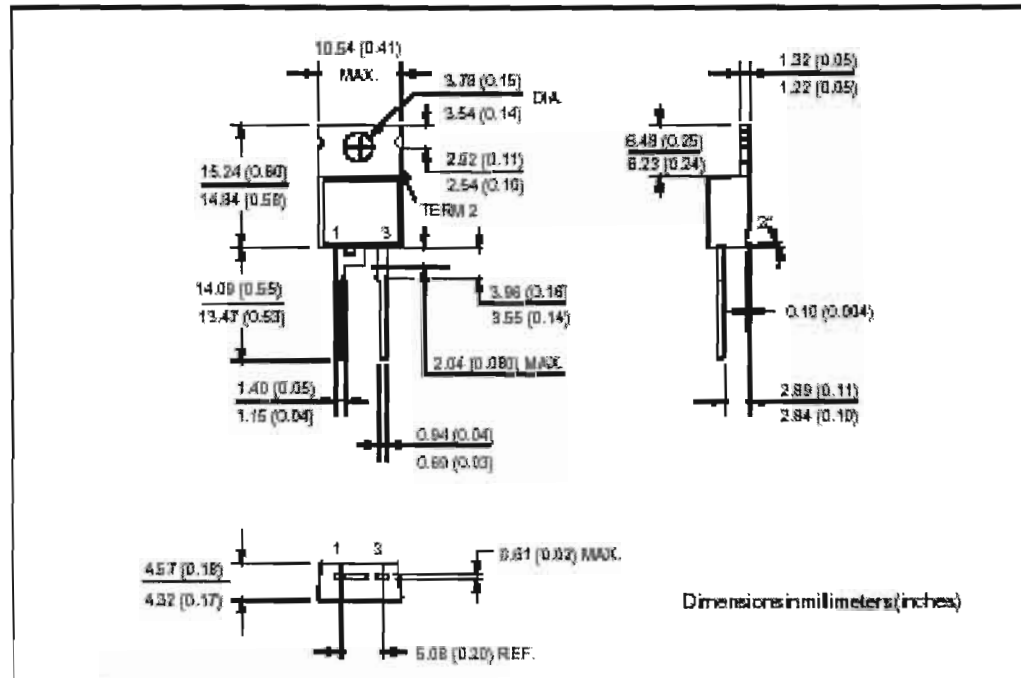
3
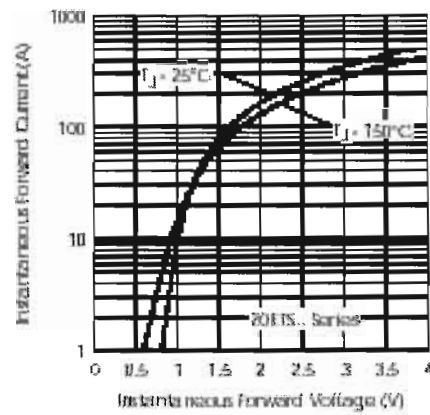
Fig. 7 - Forward Voltage Drop Characteristics
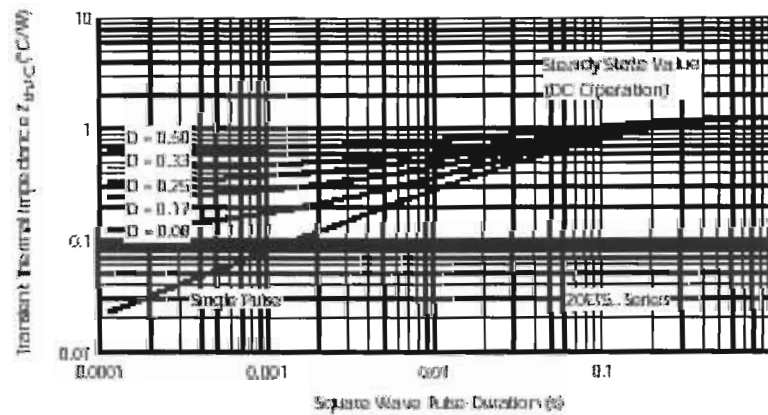
Fig. 8 - Thermal Impedance Z_{thJC} Characteristics

4

International
IGR Rectifier

20ETS.. *SAFEIR* Series
Bulletin I2101 rev. B 07/97

Outline Table

Dimensions in millimeters (inches)

Ordering Information Table

Device Code

| 20 | E | T | S | 16 |
| ① | ② | ③ | ④ | ⑤ |

1 - Current Rating

2 - Circuit Configuration:
E = Single Diode

3 - Package:
T = TO-220AC

4 - Type of Silicon:
S = Standard Recovery Rectifier

5 - Voltage code: Code x 100 = V_{RRM}

08	=	800V
12	=	1200V
16	=	1600V

BASE
CATHODE
2

1   3
CATHODE   ANODE
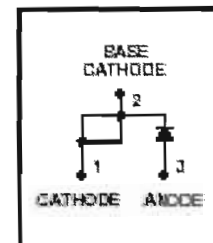
International
IЄR Rectifier

IRG4PH30KD

INSULATED GATE BIPOLAR TRANSISTOR WITH
ULTRAFAST SOFT RECOVERY DIODE

Short Circuit Rated
UltraFast IGBT

Features
- High short circuit rating optimized for motor control,
  t_{sc} =10µs, V_{CC} = 720V , T_J = 125°C,
  V_{GE} = 15V
- Combines low conduction losses with high
  switching speed
- Tighter parameter distribution and higher efficiency
  than previous generations
- IGBT co-packaged with HEXFRED™ ultrafast,
  ultrasoft recovery antiparallel diodes

Benefits
- Latest generation 4 IGBT's offer highest power density
  motor controls possible
- HEXFRED™ diodes optimized for performance with IGBTs.
  Minimized recovery characteristics reduce noise, EMI and
  switching losses
- This part replaces IRGPH30MD2 products
- For hints see design tip 97003
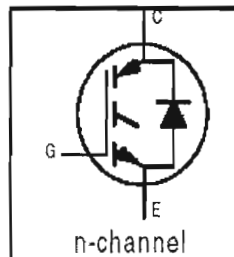
V_{CES} = 1200V

$V_{CE(on)\ typ.}$ = 3.10V

@V_{GE} = 15V, I_C = 10A

n-channel

TO-247AC
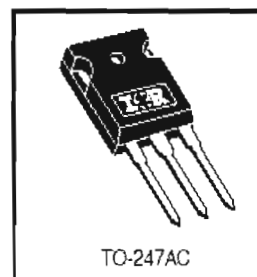
Absolute Maximum Ratings

	Parameter	Max.	Units
V_{CES}	Collector-to-Emitter Voltage	1200	V
I_C @ T_C = 25°C	Continuous Collector Current	20	
I_C @ T_C = 100°C	Continuous Collector Current	10	
I_{CM}	Pulsed Collector Current ①	40	A
I_{LM}	Clamped Inductive Load Current ②	40	
I_F @ T_C = 100°C	Diode Continuous Forward Current	10	
I_{FM}	Diode Maximum Forward Current	40	
t_{sc}	Short Circuit Withstand Time	10	µs
V_{GE}	Gate-to-Emitter Voltage	± 20	V
P_D @ T_C = 25°C	Maximum Power Dissipation	100	W
P_D @ T_C = 100°C	Maximum Power Dissipation	42	
T_J	Operating Junction and	-55 to +150	
T_{STG}	Storage Temperature Range		°C
	Soldering Temperature, for 10 sec.	300 (0.063 in. (1.6mm) from case)	
	Mounting Torque, 6-32 or M3 Screw.	10 lbf•in (1.1 N•m)	

Thermal Resistance

	Parameter	Min.	Typ.	Max.	Units
$R_{θJC}$	Junction-to-Case - IGBT	–––	–––	1.2	°C/W
$R_{θJC}$	Junction-to-Case - Diode	–––	–––	2.5	
$R_{θCS}$	Case-to-Sink, flat, greased surface	–––	0.24	–––	
$R_{θJA}$	Junction-to-Ambient, typical socket mount	–––	–––	40	
Wt	Weight	–––	6 (0.21)	–––	g (oz)

Electrical Characteristics @ T$_J$ = 25°C (unless otherwise specified)

	Parameter	Min.	Typ.	Max.	Units	Conditions	
V$_{(BR)CES}$	Collector-to-Emitter Breakdown Voltage①	1200	—	—	V	V$_{GE}$ = 0V, I$_C$ = 250μA	
ΔV$_{(BR)CES}$/ΔT$_J$	Temperature Coeff. of Breakdown Voltage	—	0.19	—	V/°C	V$_{GE}$ = 0V, I$_C$ = 1.0mA	
V$_{CE(on)}$	Collector-to-Emitter Saturation Voltage	—	3.10	4.2		I$_C$ = 10A	V$_{GE}$ = 15V
		—	3.90	—	V	I$_C$ = 20A	See Fig. 2. 5
		—	3.01	—		I$_C$ = 10A, T$_J$ = 150°C	
V$_{GE(th)}$	Gate Threshold Voltage	3.0	—	6.0		V$_{CE}$ = V$_{GE}$, I$_C$ = 250μA	
ΔV$_{GE(th)}$/ΔT$_J$	Temperature Coeff. of Threshold Voltage	—	-12	—	mV/°C	V$_{CE}$ = V$_{GE}$, I$_C$ = 250μA	
g$_{fe}$	Forward Transconductance ④	4.3	6.5	—	S	V$_{CE}$ = 100V, I$_C$ = 10A	
I$_{CES}$	Zero Gate Voltage Collector Current	—	—	250	μA	V$_{GE}$ = 0V, V$_{CE}$ = 1200V	
		—	—	3500		V$_{GE}$ = 0V, V$_{CE}$ = 1200V, T$_J$ = 150°C	
V$_{FM}$	Diode Forward Voltage Drop	—	3.4	3.8	V	I$_C$ = 10A	See Fig. 13
		—	3.3	3.7		I$_C$ = 10A, T$_J$ = 150°C	
I$_{GES}$	Gate-to-Emitter Leakage Current	—	—	±100	nA	V$_{GE}$ = ±20V	

Switching Characteristics @ T$_J$ = 25°C (unless otherwise specified)

|	Parameter	Min.	Typ.	Max.	Units	Conditions	
Q$_g$	Total Gate Charge (turn-on)	—	53	80		I$_C$ = 10A	
Q$_{ge}$	Gate - Emitter Charge (turn-on)	—	9.0	14	nC	V$_{CC}$ = 400V	See Fig.8
Q$_{gc}$	Gate - Collector Charge (turn-on)	—	21	32		V$_{GE}$ = 15V	
t$_{d(on)}$	Turn-On Delay Time	—	39	—			
t$_r$	Rise Time	—	84	—	ns	T$_J$ = 25°C	
t$_{d(off)}$	Turn-Off Delay Time	—	220	340		I$_C$ = 10A, V$_{CC}$ = 800V	
t$_f$	Fall Time	—	90	140		V$_{GE}$ = 15V, R$_G$ = 23Ω	
E$_{on}$	Turn-On Switching Loss	—	0.95	—		Energy losses include "tail"	
E$_{off}$	Turn-Off Switching Loss	—	1.15	—	mJ	and diode reverse recovery	
E$_{ts}$	Total Switching Loss	—	2.10	2.6		See Fig. 9,10,18	
t$_{sc}$	Short Circuit Withstand Time	10	—	—	μs	V$_{CC}$ = 720V, T$_J$ = 125°C	
						V$_{GE}$ = 15V, R$_G$ = 5.0Ω	
t$_{d(on)}$	Turn-On Delay Time	—	42	—		T$_J$ = 150°C. See Fig. 10,11,18	
t$_r$	Rise Time	—	79	—	ns	I$_C$ = 10A, V$_{CC}$ = 800V	
t$_{d(off)}$	Turn-Off Delay Time	—	540	—		V$_{GE}$ = 15V, R$_G$ = 23Ω.	
t$_f$	Fall Time	—	97	—		Energy losses include "tail"	
E$_{ts}$	Total Switching Loss	—	3.5	—	mJ	and diode reverse recovery	
L$_E$	Internal Emitter Inductance	—	13	—	nH	Measured 5mm from package	
C$_{ies}$	Input Capacitance	—	800	—		V$_{GE}$ = 0V	
C$_{oes}$	Output Capacitance	—	60	—	pF	V$_{CC}$ = 30V	See Fig. 7
C$_{res}$	Reverse Transfer Capacitance	—	14	—		f = 1.0MHz	
t$_{rr}$	Diode Reverse Recovery Time	—	50	76	ns	T$_J$ = 25°C See Fig.	
		—	72	110		T$_J$ = 125°C 14	I$_F$ = 10A
I$_{rr}$	Diode Peak Reverse Recovery Current	—	4.4	7.0	A	T$_J$ = 25°C See Fig.	
		—	5.9	8.8		T$_J$ = 125°C 15	V$_R$ = 200V
Q$_{rr}$	Diode Reverse Recovery Charge	—	130	200	nC	T$_J$ = 25°C See Fig.	
		—	250	380		T$_J$ = 125°C 16	di/dt = 200A/μs
di$_{(rec)M}$/dt	Diode Peak Rate of Fall of Recovery During t$_b$	—	210	—	A/μs	T$_J$ = 25°C See Fig.	
		—	180	—		T$_J$ = 125°C 17	
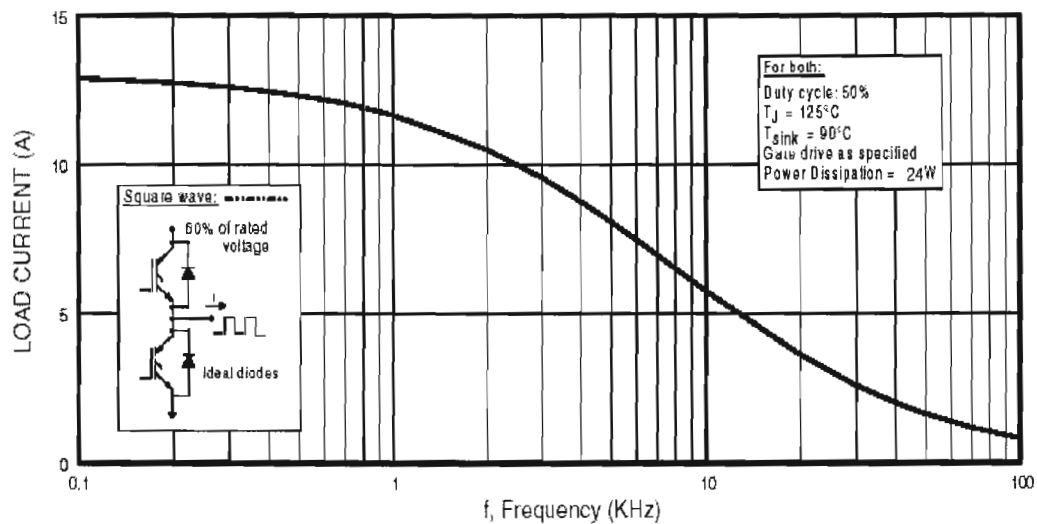
Fig. 1 - Typical Load Current vs. Frequency
(Load Current = I_{RMS} of fundamental)
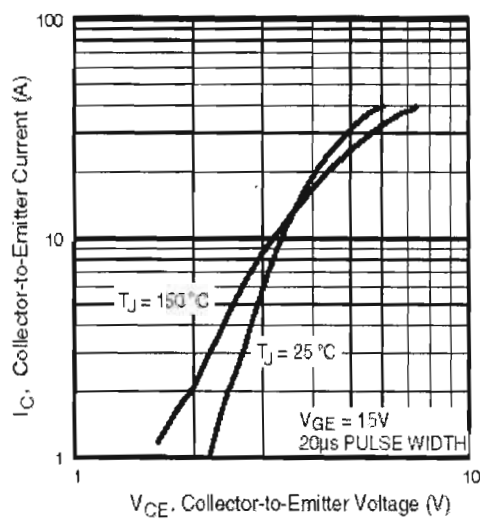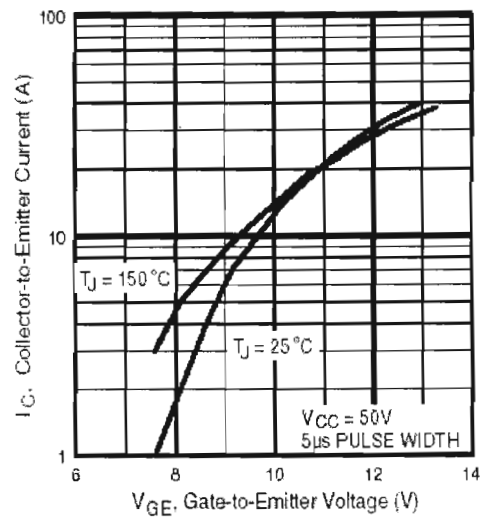

Fig. 2 - Typical Output Characteristics

Fig. 3 - Typical Transfer Characteristics
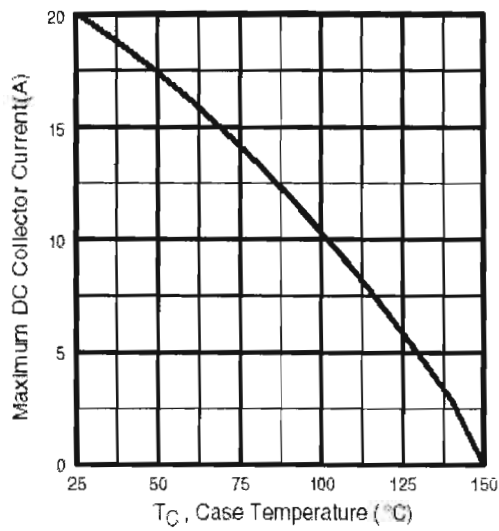
161

IRG4PH30KD

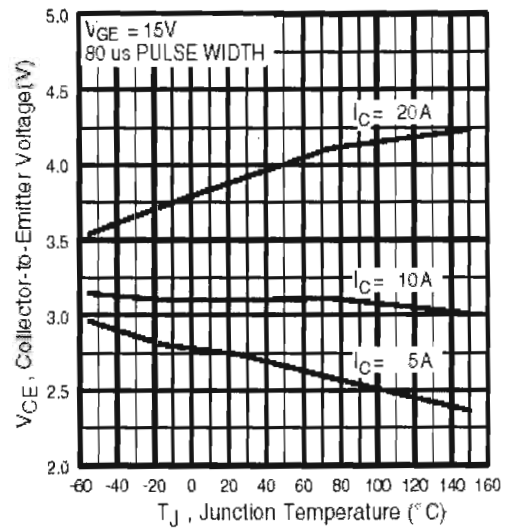**Fig. 4** - Maximum Collector Current vs. Case Temperature

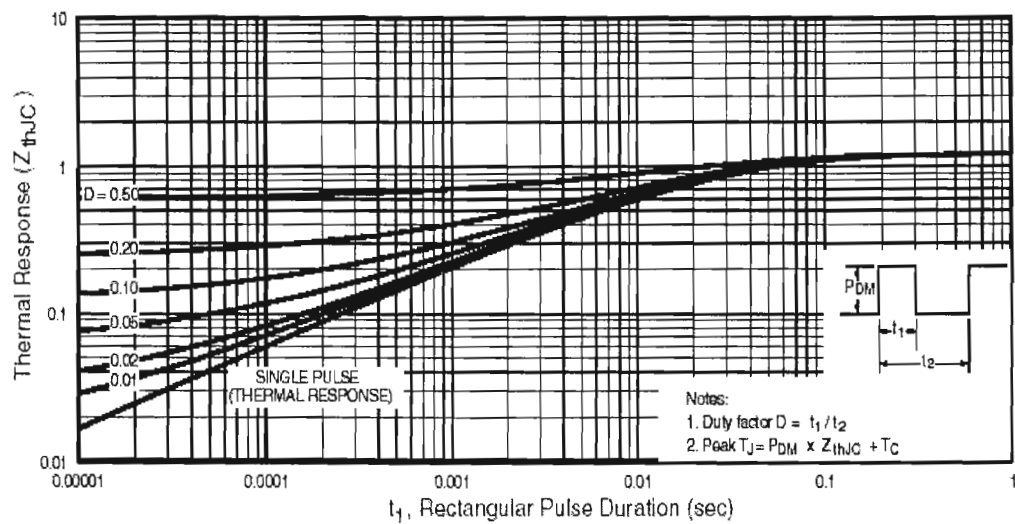**Fig. 5** - Typical Collector-to-Emitter Voltage vs. Junction Temperature

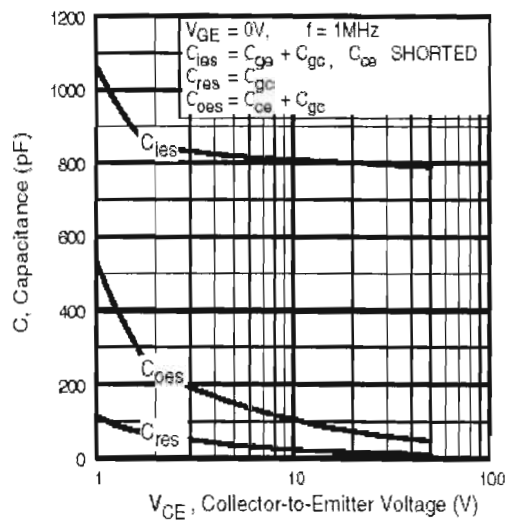**Fig. 6** - Maximum Effective Transient Thermal Impedance, Junction-to-Case

www.irf.com

IRG4PH30KD

Fig. 7 - Typical Capacitance vs.
Collector-to-Emitter Voltage
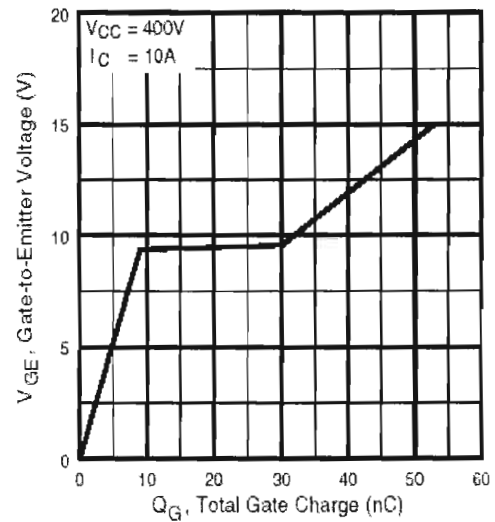
Fig. 8 - Typical Gate Charge vs.
Gate-to-Emitter Voltage
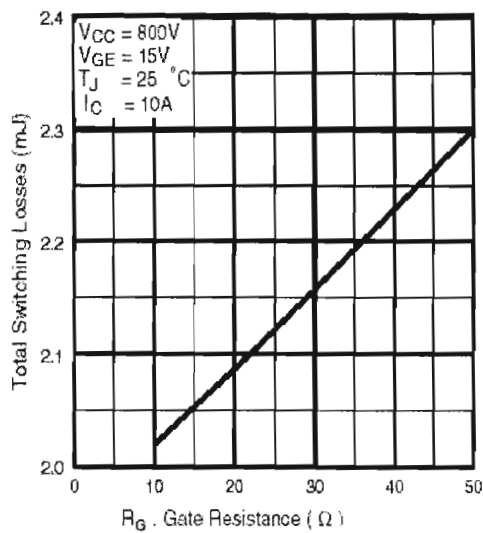
Fig. 9 - Typical Switching Losses vs. Gate
Resistance
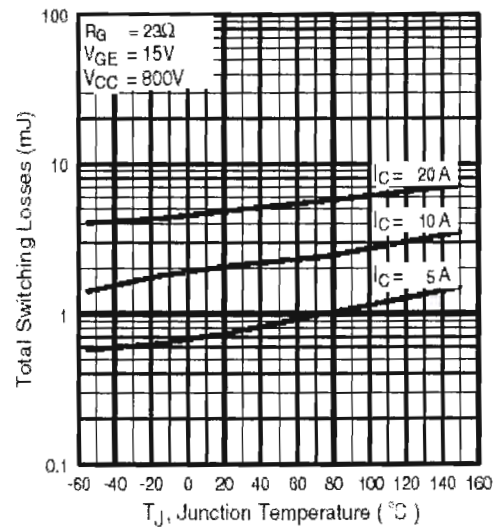
Fig. 10 - Typical Switching Losses vs.
Junction Temperature

www.irf.com
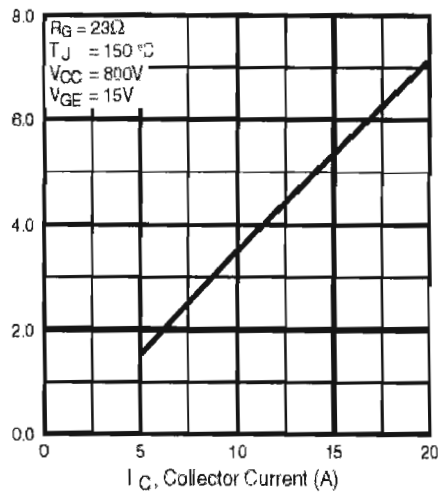
Fig. 11 - Typical Switching Losses vs.
Collector Current
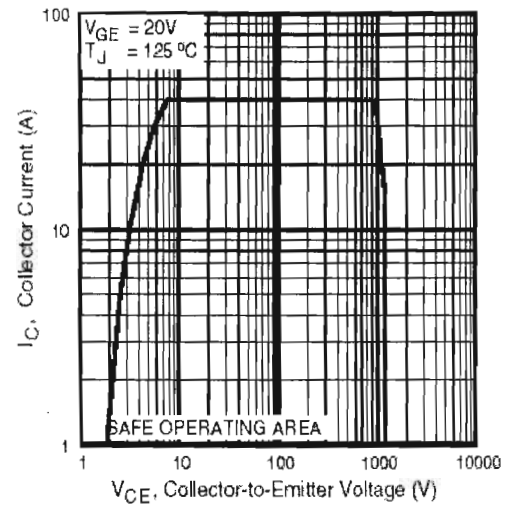
Fig. 12 - Turn-Off SOA
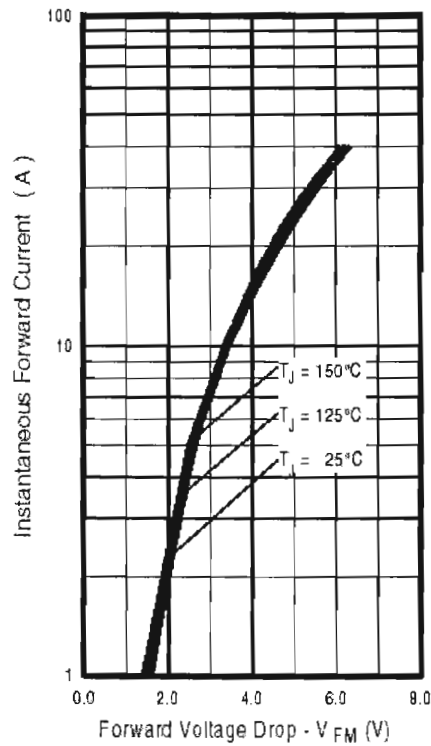
Fig. 13 - Typical Forward Voltage Drop vs. Instantaneous Forward Current
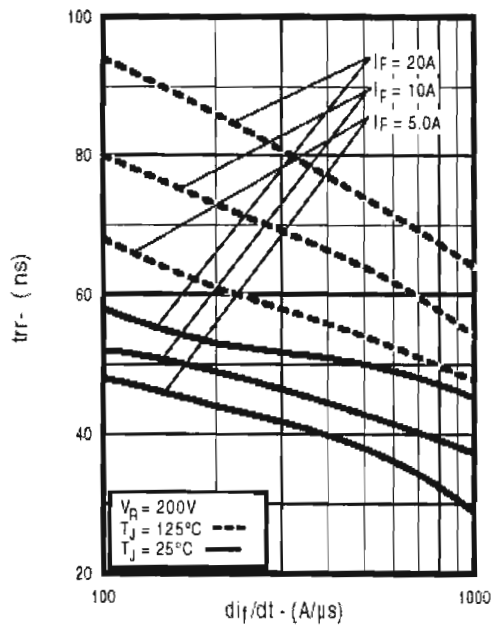
Fig. 14 - Typical Reverse Recovery vs. di$_f$/dt
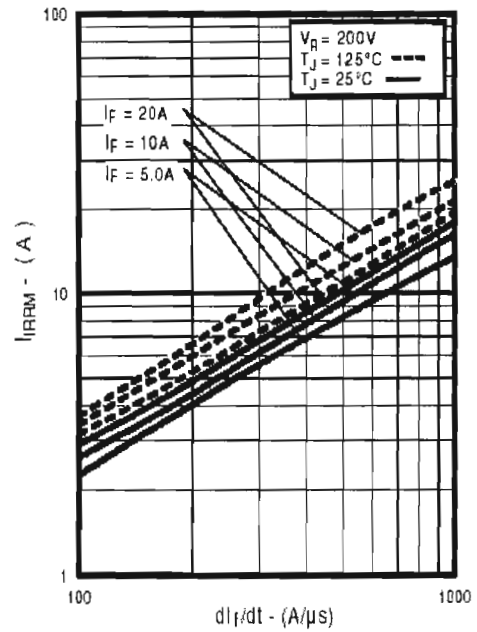
Fig. 15 - Typical Recovery Current vs. di$_f$/dt
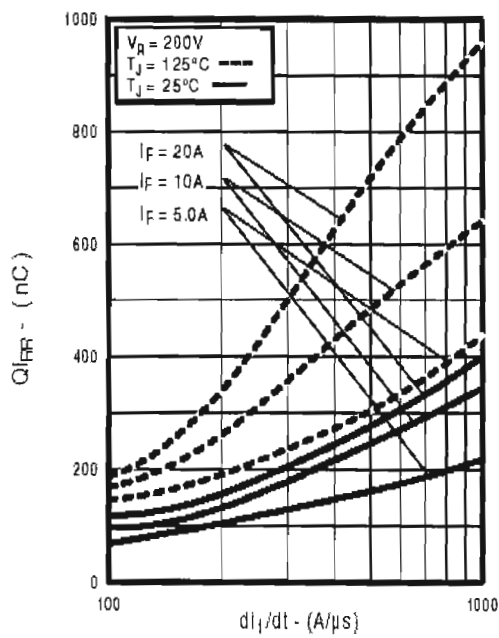
Fig. 16 - Typical Stored Charge vs. di$_f$/dt
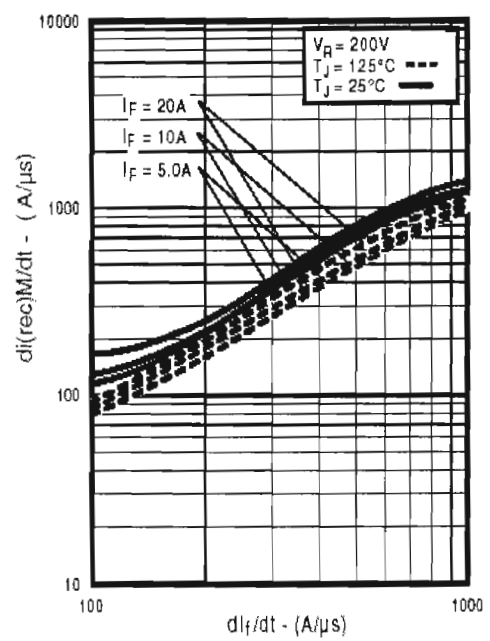
Fig. 17 - Typical di$_{(rec)M}$/dt vs. di$_f$/dt

IRG4PH30KD
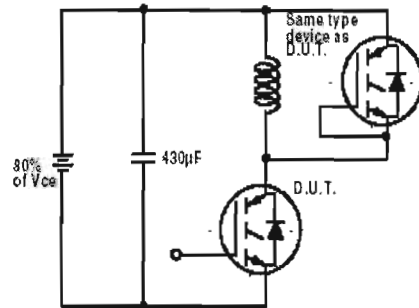
Fig. 18a - Test Circuit for Measurement of
I_{LM}, E_{on}, $E_{off(diode)}$, t_{rr}, Q_{rr}, I_{rr}, $t_{d(on)}$, t_r, $t_{d(off)}$, t_f
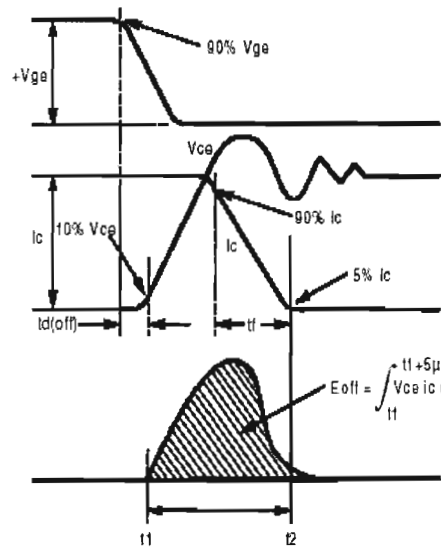
Fig. 18b - Test Waveforms for Circuit of Fig. 18a, Defining
E_{off}, $t_{d(off)}$, t_f
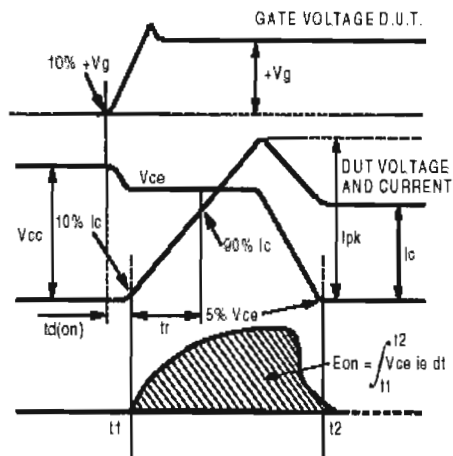
Fig. 18c - Test Waveforms for Circuit of Fig. 18a,
Defining E_{on}, $t_{d(on)}$, t_r
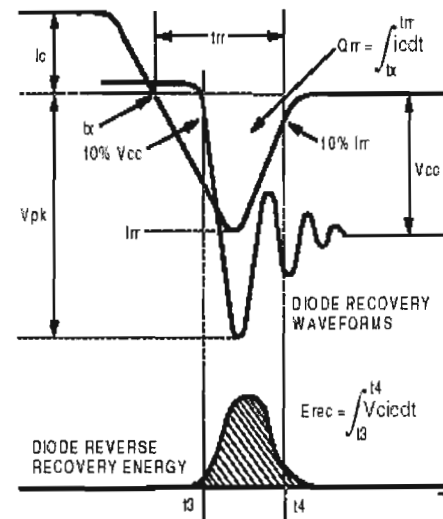
Fig. 18d - Test Waveforms for Circuit of Fig. 18a,
Defining E_{rec}, t_{rr}, Q_{rr}, I_{rr}

8
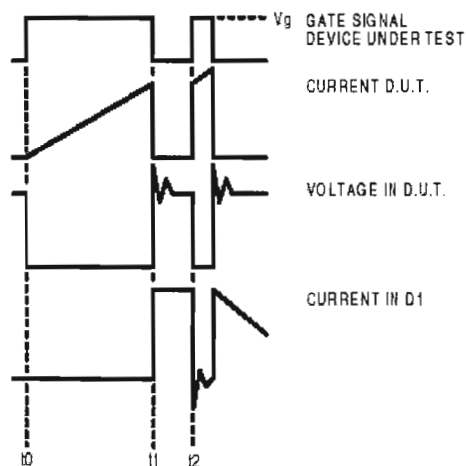
Figure 18e. Macro Waveforms for Figure 18a's Test Circuit
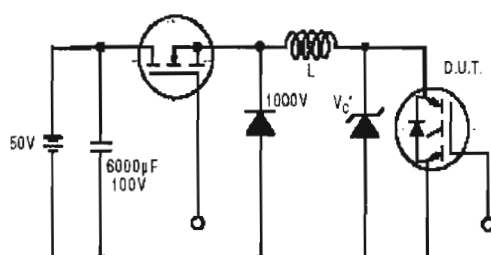
Figure 19. Clamped Inductive Load Test Circuit
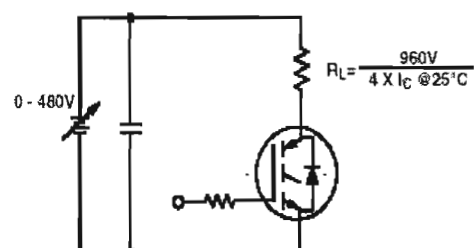
Figure 20. Pulsed Collector Current
Test Circuit

167

IRG4PH30KD

Notes:

① Repetitive rating: V_{GE}=20V; pulse width limited by maximum junction temperature (figure 20)

② V_{CC}=80%(V_{CES}), V_{GE}=20V, L=10µH, R_G=23Ω (figure 19)

③ Pulse width ≤ 80µs; duty factor ≤ 0.1%.

④ Pulse width 5.0µs, single shot.

Case Outline — TO-247AC
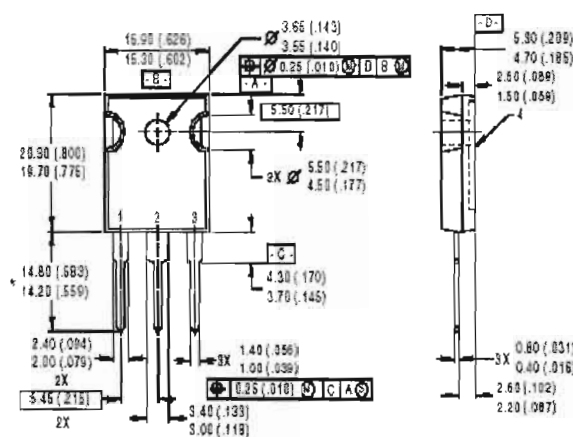
CONFORMS TO JEDEC OUTLINE TO-247AC (TO-3P)
Dimensions in Millimeters and (Inches)

www.irf.com

ANNEXURE I

ELECTRONIC DRAWINGS

Designed: DV Nicolae		ROGOWSKI COIL POWER APPLICATION	
Drawing: DV Nicolae		Static switch driver and main filter	
Checked: JFJ van Rensburg		RCPA-DW 1 / 4	Date: May 2004

Designed: DV Nicolae		ROGOWSKI COIL POWER APPLICATION	
Drawing: DV Nicolae		Control system	
Checked: JFJ van Rensburg		RCPA-DW 2 / 4	Date: May 2004

Designed: DV Nicolae		ROGOWSKI COIL POWER APPLICATION	
Drawing: DV Nicolae		Reference source (PLL)	
Checked: JFJ van Rensburg		RCPA-DW 3 / 4	Date: May 2004

Designed: DV Nicolae		ROGOWSKI COIL POWER APPLICATION	
Drawing: DV Nicolae		Auxiliary power supply	
Checked: JFJ van Rensburg		RCPA-DW 4 / 4	Date: May 2004

ANNEXURE J

ROGOWSKI COIL UNDER A DOUBLE–PARALLEL TRANSMISSION LINE

The purpose of these measurements has been the validation of the three-phase model for the Rogowski coil power application.

- To try to validate some theoretical conclusions
- To estimate what will be the voltage for a full scale coil

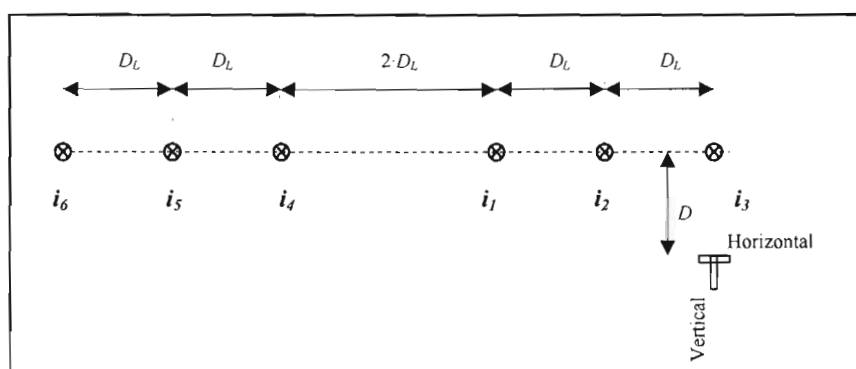An equivalent situation is illustrated in Figure 94.

Figure 94 RCPA under a double-parallel transmission line

The coil has been placed at half distance between two consecutive towers therefore the curve of lines has a minimum influence.

Geometrical parameters were determined by telemetry:
- Distance between towers = 246 m.
- Distance between lines and position of the coil $D = 8,5$ m

Evaluation of the voltage induced into the Rogowsky coil:

$$e = e_1 + e_2 + e_3 + e_4 + e_5 + e_6$$

Let us consider that phase sequence for the second parallel line is the same as the first:

$$i_1(t) = I_1 \sin\left(\omega t - 120^0\right)$$

$$i_2(t) = I_1 \sin\left(\omega t\right)$$

$$i_3(t) = I_1 \sin\left(\omega t + 120^0\right)$$

$$i_4(t) = I_2 \sin\left(\omega t + 120^0\right)$$

$$i_5(t) = I_2 \sin\left(\omega t\right)$$

$$i_6(t) = I_2 \sin\left(\omega t - 120^0\right)$$

NOTE:

- The currents in the lines are not known.
- The only assumption that could be done is the same amplitude of the currents:
  $$I_1 = I_2 = I$$
- A possible method for evaluation regardless of the line currents is to do the ratio $\mathcal{E}_h / \mathcal{E}_v$ between voltages measured for horizontal and vertical position

Then applying (6.12) to (6.18) to this particular situation the result is:

$$k = 2 \cdot \pi \cdot 50 \cdot 200 \cdot 2 \cdot I \cdot 10^{-7} = 12,57 \cdot I \cdot 10^{-7}$$

$$e_{h3}(t) = 0$$

$$e_{h2}(t) = -k \cdot \ln \frac{(8,5+0,43)^2 + 8,5^2}{(8,5-0,43)^2 + 8,5^2} \cos(\omega t)$$

$$= -1,2712 \cdot I \cdot 10^{-3} \cos(\omega t)$$

$$e_{h1}(t) = -k \cdot \ln \frac{(2 \cdot 8,5 + 0,43)^2 + 8,5^2}{(2 \cdot 8,5 - 0,43)^2 + 8,5^2} \cos\left(\omega t - 120^o\right)$$

$$= -1,0175 \cdot I \cdot 10^{-3} \cos\left(\omega t - 120^o\right)$$

$$e_{h4}(t) = -k \cdot \ln \frac{(4 \cdot 8,5 + 0,43)^2 + 8,5^2}{(4 \cdot 8,5 - 0,43)^2 + 8,5^2} \cos\left(\omega t + 120^o\right)$$

$$= -0,5985 \cdot I \cdot 10^{-3} \cos\left(\omega t + 120^o\right)$$

$$e_{h5}(t) = -k \cdot \ln \frac{(5 \cdot 8,5 + 0,43)^2 + 8,5^2}{(5 \cdot 8,5 - 0,43)^2 + 8,5^2} \cos(\omega t)$$

$$= -0,4892 \cdot I \cdot 10^{-3} \cos(\omega t)$$

$$e_{h6}(t) = -k \cdot \ln \frac{(6 \cdot 8,5 + 0,43)^2 + 8,5^2}{(6 \cdot 8,5 - 0,43)^2 + 8,5^2} \cos\left(\omega t - 120^o\right)$$

$$= -0,4125 \cdot I \cdot 10^{-3} \cos\left(\omega t - 120^o\right)$$

$$e_h = -\left(0,518 \cdot I \cdot 10^{-3}\right) \cos\left(\omega t + 43,7^0\right) \qquad \mathcal{E}_{h(rms)} = 0,366 \cdot I \cdot 10^{-3}$$

$$e_{v3}(t) = -2 \cdot k \cdot \ln \frac{8,5 + 0,43}{8,5 - 0,43} \cos\left(\omega t + 120^0\right)$$

$$= -2,5457 \cdot I \cdot 10^{-3} \cos\left(\omega t + 120^0\right)$$

$$e_{v2}(t) = -k \cdot \ln \frac{(8,5)^2 + (8,5+0,43)^2}{(8,5)^2 + (8,5-0,43)^2} \cos(\omega t)$$

$$= -1,2712 \cdot I \cdot 10^{-3} \cos(\omega t)$$

$$e_{v1}(t) = -k \cdot \ln \frac{(2 \cdot 8,5)^2 + (8,5+0,43)^2}{(2 \cdot 8,5)^2 + (8,5-0,43)^2} \cos(\omega t - 120^o)$$

$$= -0,5085 \cdot I \cdot 10^{-3} \cos(\omega t - 120^o)$$

$$e_{v4}(t) = -k \cdot \ln \frac{(4 \cdot 8,5)^2 + (8,5+0,43)^2}{(4 \cdot 8,5)^2 + (8,5-0,43)^2} \cos(\omega t + 120^o)$$

$$= -0,1496 \cdot I \cdot 10^{-3} \cos(\omega t + 120^o)$$

$$e_{v5}(t) = -k \cdot \ln \frac{(5 \cdot 8,5)^2 + (8,5+0,43)^2}{(5 \cdot 8,5)^2 + (8,5-0,43)^2} \cos(\omega t)$$

$$= -0,0978 \cdot I \cdot 10^{-3} \cos(\omega t)$$

$$e_{v6}(t) = -k \cdot \ln \frac{(6 \cdot 8,5)^2 + (8,5+0,43)^2}{(6 \cdot 8,5)^2 + (8,5-0,43)^2} \cos(\omega t - 120^o)$$

$$= -0,0687 \cdot I \cdot 10^{-3} \cos(\omega t - 120^o)$$

$$e_v = -\left(0,927 \cdot I \cdot 10^{-3}\right) \cos\left(\omega t - 98,2^0\right) \qquad E_{v(rms)} = 0,655 \cdot I \cdot 10^{-3}$$

$\mathcal{E}_{h(rms)}$ / $\mathcal{E}_{v(rms)}$ = 0,559

The first measurement has been done with the coil positioned horizontally and then vertically under the far-right line (under i_3) for a minimal influence of the parallel transmission line; the measured values are:

$\mathcal{E}_h$ = 0,360 V

$\mathcal{E}_v$ = 0,615 V

$\mathcal{E}_{h(rms)}$ / $\mathcal{E}_{v(rms)}$ = 0,585

COMMENTS:

 a. The determined through measurements ratio $\mathcal{E}_{h(rms)}$ / $\mathcal{E}_{v(rms)}$ differs to the estimated value; the error is 4,7 percent.

 b. Probably the amplitude of the currents in the two parallel lines are not the same.

 c. The measurements for horizontal and vertical have not been done simultaneously and this could explain part of the error.

 d. Overall, it can be concluded that the measurements validate the theoretical model.

 e. The electrostatic potential at 2m height above the ground is around 1kV.

ANNEXURE K

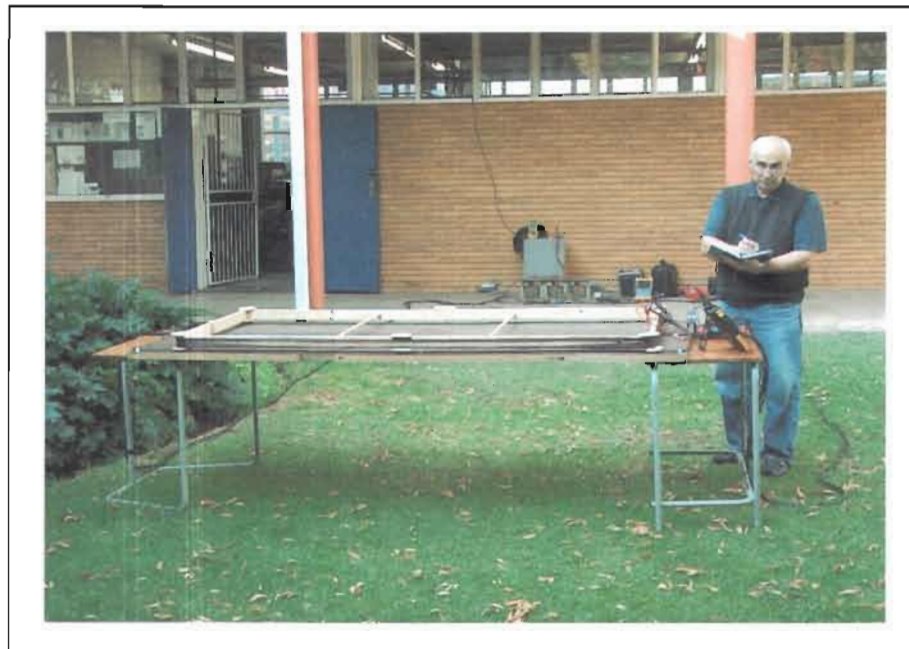## EXPERIMENTAL WORK – PHOTOGRAPHS

The two coils
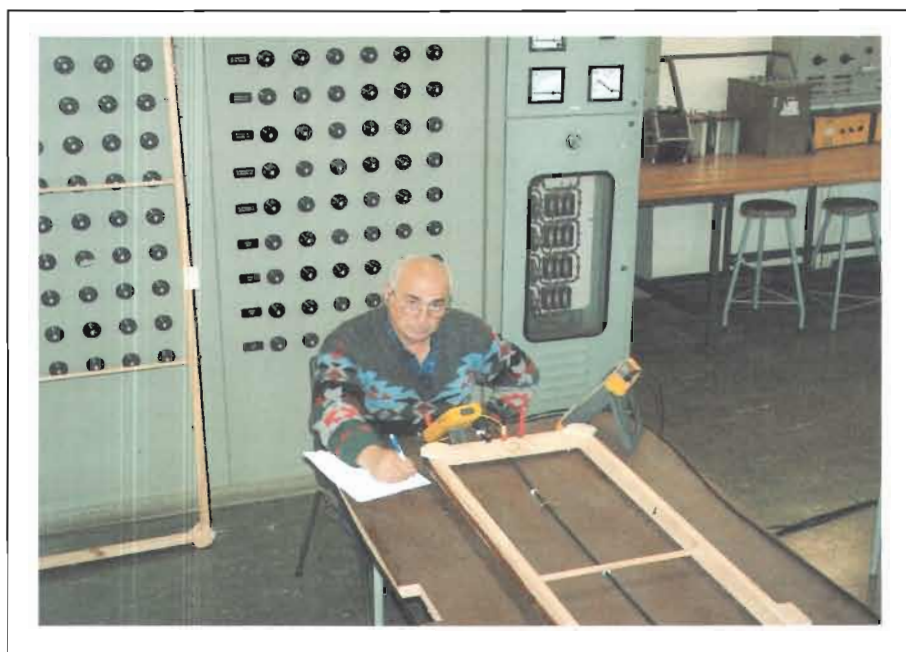
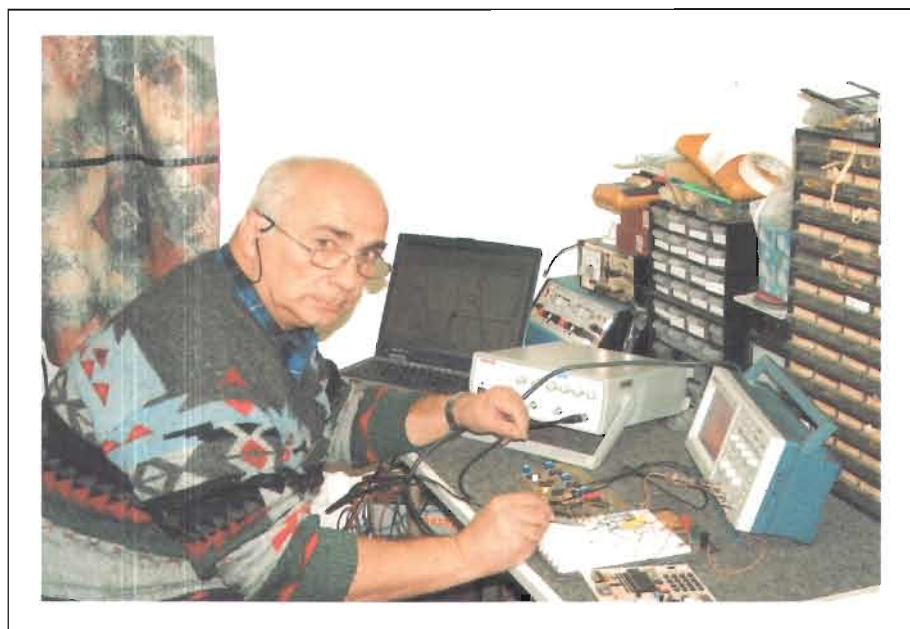Measurements with small coil for single-phase

Setup for three-phase currents

Recording data: three-phase horizontal

Recording data: three-phase vertical

Testing the electronics